

**Sakonnet River Bridge
Rehabilitation or Replacement Project**

**DRAFT ENVIRONMENTAL
IMPACT STATEMENT
& SECTION 4(f) STATEMENT**

Volume IIb

**Hydrodynamic and Sediment
Transport Modeling**

Prepared for:

Marine Research, Inc.
141 Falmouth Heights Road
Falmouth, MA 02540

Hydrodynamic and Sediment Transport Modeling at the Sakonnet River Bridge

ASA Report 99-175

Draft Final Report

May 2001

Prepared by:

Hyun-Sook Kim
J. Craig Swanson



Applied Science Associates, Inc.
70 Dean Knauss Drive
Narragansett, RI 02882

TABLE OF CONTENTS

EXECUTIVE SUMMARY.....	ii
LIST OF FIGURES.....	iv
LIST OF TABLES.....	viii
1. Introduction.....	1
2. Hydrodynamic Modeling.....	3
2.1 Velocity Observations and Comparisons.....	3
2.1.1 ADCP Observations.....	3
2.1.2 BFHYDRO Model Properties.....	13
2.1.3 Model-Data Comparisons.....	15
2.2 Hydrodynamic Simulations.....	16
2.3 Evaluation of Causeway Effects.....	26
3. Sediment Transport Modeling.....	27
3.1 Bottom Sediment Samples.....	27
3.2 Settling Velocity.....	28
3.3 Sediment Deposition Distribution.....	29
3.4 Sediment Transport.....	45
4. Conclusions and Summary.....	58
5. References.....	61
APPENDIX A.....	62

EXECUTIVE SUMMARY

This study presents results of hydrodynamic simulations and sediment transport modeling for the Sakonnet River and lower Mt. Hope Bay. The objective of the study was to evaluate potential impacts that five bridge construction alternatives will have in the area. The hydrodynamic scenarios were differentiated by the existence of the causeways in two configurations (present and completely removed), and the sediment transport scenarios were further discriminated by the locations of sediment release (east and west river shore, and middle of river). The hydrodynamics were simulated using the ASA WQMAP BFHYDRO model, and the sediment transport and deposition simulations were performed using the BFMASS model.

The currents in the area are driven by semi-diurnal tides, having a pattern consisting of two floods and single ebb over a tidal cycle. The configuration with the railroad causeways in place resulted in the highest speed (> 1.5 m/s [3 kt]) at the opening waterway, with the magnitude decreasing closer to shore. A conspicuous result from the hydrodynamic simulation for the scenario without the causeways was a drastic decrease in speed to a range between 20 cm/s (0.4 kt) and 50 cm/s (1 kt) on average. Nonetheless, the same current pattern was persistently observed in both the simulations.

Analysis of the sediment samples indicated that sand was the dominant size fraction surrounding the causeways, with 66% of the total composition. However, the assessment of the sediment transport and deposition was focused on three grain sizes (very fine sand, silt and clay), because the fate of larger size particles was much shorter than the smaller sizes. A common result from the sediment transport and deposition simulations was that their distributions formed an elongated plume whose axis was aligned with the river axis. Over 5-day simulations with a continuous sediment release at a rate of 1 ton/day, the maximum sediment layer thicknesses were found at the release site in range between 0.01 mm (4×10^{-4} in) and 0.4 mm (1.6×10^{-2} in). This estimate excluded the contribution by the grain sizes greater than very fine sand. The layer thickness by the larger grain sizes was estimated to be 0.75 mm (~ 0.03 in) after 5-day simulation for a continuous release of 1-ton/day, assuming that it settled in the bottom area of a $1,620 \text{ m}^2$ ($17,400 \text{ ft}^2$).

The distribution pattern and the range of sediment layer thickness varied depending on the location of the sediment release. When the release was to the north of the west causeway, higher accumulation was observed to the north of the causeway whereas little deposition occurred to the south of the causeway. Similar results were observed when the release was south of the east causeway. The reason for the asymmetric distribution patterns was that the causeway tends to keep the sediment on the same side as the release site. However, the areal coverage of the deposition was larger for the release at the east causeway than at the west causeway. Without the causeways, the release location made little difference on the resulting sediment deposition. However, the pattern was symmetric with similar extents to the north and south.

The sediment transport simulations showed that the suspended sediment was advected by the tidal currents in a form of an elongated plume, similar to the sediment deposition distribution. During the flood tide, high sediment concentrations greater than 0.5 mg/L were observed to the north of the release site, similarly to the south during ebb tide. The finest grain particles (clay) could theoretically travel to Spar Island, 5.19 km (3.23 miles) to the north and Sapowet Point, 6.04 km (3.75 miles) to the south, but the concentrations at those locations were very small $O(1 \mu\text{g/L})$. The range of more significant concentrations ($> 0.1 \text{ mg/L}$) was limited to the area adjacent to the release sites, or less than 640 m ($\sim 2,100 \text{ ft}$) for flood and 1.06 km (0.66 miles) for ebb. The maximum concentrations in the water column were found in the near field with values in the range between 0.12 mg/L and 0.55 mg/L. Compared to available total suspended solids (TSS) observations in Mt. Hope Bay, the suspended sediment concentration caused by the bridge construction are small, only 6% of the TSS observations at maximum.

The sediment suspended concentrations are observed to be, in general, lower without the causeways than with the causeways. The values may be further reduced, depending on the final bathymetry. The water depths with no causeways are defined at the same level as the surroundings, which resulted in a speed decrease of 40%. If dredging is required to open the navigation channel wider, the resultant current speed would be even smaller. The impact to sediment transport by the currents would therefore be less than the results that are presented in this study.

It should be noted that the estimate of transport and deposition was based on a hypothetical, unit load of 1-ton/day. Actual suspended volume, however, is most likely going to be less than this amount. To obtain a corresponding estimate for the actual load, the simulation results can be scaled by a more definitive value of the load. Also, reduction of the load can be assumed if the construction work occurs only in daytime.

LIST OF FIGURES

Figure 2.1a. The ADCP velocity profile observations for the first observation period between 31 August and 8 September 2000. Speed and direction for each velocity component are color-coded: red (positive) for the east/north components represents high speed and eastward/northward, while blue (negative) is a strong current toward the west/south.....	5
Figure 2.1b. The ADCP velocity profile observations for the second observation period between 8 September and 2 October 2000 (first week: 8-15 September).....	6
Figure 2.1c. The ADCP velocity profile observations for the second observation period between 8 September and 2 October 2000 (second week: 16-22 September).....	7
Figure 2.1d. The ADCP velocity profile observations for the second observation period between 8 September and 2 October 2000 (third week: 23-29 September).....	8
Figure 2.1e. The ADCP velocity profile observations for the second observation period between 8 September and 2 October 2000 (fourth week: 30 September-2 October).	9
Figure 2.2a. Depth-averaged velocity in a vector plot format.	11
Figure 2.2b. Line plots of depth-average velocity components: u- and v-component are east and north currents.....	12
Figure 2.3. Power spectrum density for the ADCP north velocity observations. X-axis is CPH (cycle per hour), and y-axis is energy per CPH.....	14
Figure 2.4. Model domain and its boundary fitted grids of the study area. Open boundary cells are in blue.....	15
Figure 2.5. Time series of the north velocity components. The BFHYDRO simulation is in red and the ADCP data are in blue.....	17
Figure 2.6. Details of the model grids around the Sakonnet River Bridge: top panel) with the present structure and the railroad causeways; bottom panel) without the causeways. A star symbol represents the ADCP location.....	19
Figure 2.7. Details of the depths around the Sakonnet River Bridge: top panel) with the present structure and the railroad causeways; bottom panel) without the causeways. A star represents the ADCP location.	20
Figure 2.8a. Simulated velocity fields at maximum flood for the present condition with the causeways.....	21

Figure 2.8b. Simulated velocity fields at maximum flood for a condition without the causeways.....	22
Figure 2.9a. Simulated velocity fields at maximum ebb for the present condition with the causeways.....	23
Figure 2.9b. Simulated velocity fields at maximum ebb for a condition without the causeways.....	24
Figure 2.10. Time series of simulated north-south velocity component for the scenarios with and without causeways. Both the data are taken at the ADCP site.....	25
Figure 2.11. Changes in speed due to increase in the waterway cross-section area. A point at (0,0) represents the present configuration of the causeways.....	26
Figure 3.1. Locations of bottom sediment sampling site surrounding the Sakonnet River railroad causeways.	28
Figure 3.2. Sediment grain size composition analysis results for the eight bottom samples. Values shown at the bottom are weights of the three fractions in percent.....	29
Figure 3.3a. Locations of the sediment release (cross) sites for scenarios 1, 2, and 3 (with the causeways).....	31
Figure 3.3b. Locations of the sediment release (cross) sites for scenarios 4, 5, and 6 (without the causeways).....	32
Figure 3.4a. Deposition distribution (μm) of clay particles with settling velocity of 0.05 m/d (1×10^{-6} kt) at simulation-day 5. The BFMASS grids include the causeways (the present condition), and the sediment source is located to the south of the east causeway. Deposition units conversion is $1 \mu\text{m} = 0.00004$ in.....	34
Figure 3.4b. Deposition distribution (μm) of clay particles with settling velocity of 3.32 m/d (7.7×10^{-5} kt) at simulation-day 5. The BFMASS grids include the causeways (the present condition), and the sediment source is located to the south of the east causeway. Deposition units conversion is $1 \mu\text{m} = 0.00004$ in.....	35
Figure 3.4c. Deposition distribution (μm) of clay particles with settling velocity of 53.32 m/d (1.2×10^{-3} kt) at simulation-day 5. The BFMASS grids include the causeways (the present condition), and the sediment source is located to the south of the east causeway. Deposition units conversion is $1 \mu\text{m} = 0.00004$ in.....	36
Figure 3.5. Deposition distribution (μm) after 5-day simulation for scenario 1. This is a super position of the individually weighted results shown in Figures 3.4a, 3.4b and 3.4c.	

The sediment release site is south of the east causeway. Deposition units conversion is $1 \mu\text{m} = 0.00004 \text{ in.}$ 39

Figure 3.6. Deposition distribution (μm) after 5-day simulation for scenario 4. The sediment release site is at the east side of river. Deposition units conversion is $1 \mu\text{m} = 0.00004 \text{ in.}$ 40

Figure 3.7. Deposition distribution (μm) after 5-day simulation for scenario 2. The sediment release site is north of the west causeway. Deposition units conversion is $1 \mu\text{m} = 0.00004 \text{ in.}$ 41

Figure 3.8. Deposition distribution (μm) after 5-day simulation for scenario 5. The sediment release site is at the west side of river. Deposition units conversion is $1 \mu\text{m} = 0.00004 \text{ in.}$ 42

Figure 3.9. Deposition distribution (μm) after 5-day simulation for scenario 3. The sediment release site is at the opening waterway. Deposition units conversion is $1 \mu\text{m} = 0.00004 \text{ in.}$ 43

Figure 3.10. Deposition distribution (μm) after 5-day simulation for scenario 6. The sediment release site is at the middle of river. Deposition units conversion is $1 \mu\text{m} = 0.00004 \text{ in.}$ 44

Figure 3.11a. Sediment concentration in the water column at maximum flood for scenario 1. The sediment release site is south of the east causeway. 46

Figure 3.11b. Sediment concentration in the water column at maximum flood for scenario 4. The sediment release site is at the east side of river..... 47

Figure 3.12a. Sediment concentration in the water column at maximum ebb for scenario 1. The sediment release site is south of the east causeway. 48

Figure 3.12b. Sediment concentration in the water column at maximum ebb for scenario 4. The sediment release site is at the east side of river..... 49

Figure 3.13a. Sediment concentration in the water column at maximum flood for scenario 2. The sediment release site is north of the west causeway. 50

Figure 3.13b. Sediment concentration in the water column at maximum flood for scenario 5. The sediment release site is at the west side of river. 51

Figure 3.14a. Sediment concentration in the water column at maximum ebb for scenario 2. The sediment release site is north of the west causeway. 52

Figure 3.14b. Sediment concentration in the water column at maximum ebb for scenario 5. The sediment release site is at the west side of river. 53

Figure 3.15a. Sediment concentration in the water column at maximum flood for scenario 3. The sediment release site is at the opening waterway..... 54

Figure 3.15b. Sediment concentration in the water column at maximum flood for scenario 6. The sediment release site is at the opening waterway..... 55

Figure 3.16a. Sediment concentration in the water column at maximum ebb for scenario 3. The sediment release site is at the opening waterway..... 56

Figure 3.16b. Sediment concentration in the water column at maximum ebb for scenario 6. The sediment release site is in the middle of river..... 57

LIST OF TABLES

Table 1-1. Five rehabilitation/replacement alternatives for the Sakonnet River Bridge.....	1
Table 2-1. Mean and standard deviation of east and north velocity component profiles. Values in highlighted cells are the mean and standard deviation of the data observed during the period of high water level. Values in the first column are depth below the water level. Direction is in degrees clockwise from True North.	10
Table 2-2. Result of harmonic analysis with 8 tidal constituents.	13
Table 2-3. Comparison of the harmonic analysis results between the predicted and observed north velocity components.....	16
Table 2-4. Statistics of the simulated currents between the scenarios with and without the causeways. The time series of data are at the ADCP site.	18
Table 3-1. Sediment sizes, settling velocity and travel time for vertical distance of 10 m. The velocity is estimated using Stokes law (Allen, 1985).	30
Table 3-2. Sediment deposition scenarios, causeway configuration, sediment release sites and relation to rehabilitation/replacement alternatives.	30
Table 3-3. Average composition fractions and sediment particles.	37
Table 3-4. Maximum north and south extends of $2\ \mu\text{m}$ (8×10^{-5} in) layer from the release site at simulation-day 5.	38
Table 3-5. Maximum suspended sediment concentrations (mg/L) at a release site and six sediment transport scenarios.	58

1. Introduction

The work presented here documents the results of hydrodynamic and sediment transport modeling at the head of the Sakonnet River in Rhode Island. This is part of the environmental impact study (EIS) for the rehabilitation or replacement of the Sakonnet River Bridge. There are five alternative scenarios that have been proposed for the Bridge repair/replacement. They are listed in Table 1-1.

Table 1-1. Five rehabilitation/replacement alternatives for the Sakonnet River Bridge.

Alternative	Option	Details
1	No build	Railroad causeways remain.
2	Bridge rehabilitation	Railroad causeways are removed.
3	New bridge along the existing alignment	Temporary bridge over widened causeways.
4	New bridge to north of existing alignment	Railroad causeways are removed.
5	New bridge to south of existing alignment	Railroad causeways are removed.

The goal of this modeling and field study is first, to precisely resolve current and current patterns under various alternatives, and second, to estimate the deposition and transport of suspended or re-suspended sediments that would be generated from the bridge construction activities.

The currents in the study area are governed by semi-diurnal tides, but they have a peculiar character of a double-flood pattern consisting of two floods and single ebb in a semi-diurnal tidal cycle (12.42 hr). The flood currents have slightly longer duration by an average of about 1 hour than the ebb, of which the second flood peak is slightly smaller than the first and occurs immediately after the first. The cause of this pattern is attributed to the strength of the harmonics M_4 and M_6 , overtides to the semi-diurnal M_2 tide. The effect is furthermore enhanced by the natural oscillatory period of Narragansett Bay [5.72 hr] (Haight, 1936) that falls between the M_4 (6.21 hr) and M_6 (4.14 hr) periods.

In general, the hydrodynamics at the head of the Sakonnet River is sensitive to the river morphological structure, particularly since this long, narrow river has the highest current [> 1.5 m/s (3.0 kt)] (Haight, 1936) found in all of Narragansett Bay and Mt Hope Bay. About 45 m (148 ft) to the north of the Sakonnet River Bridge is a railroad bridge with a swinging component over an opening between an east and west causeway. These causeways extend into the river approximately three quarters of its width, and leave an opening of about 66 m (217 ft) wide, where the strongest current exists. Thus, removal of

the causeways as proposed in alternatives 2, 4, and 5 is expected to have a significant influence on the velocity distribution.

A river configuration with and without the causeways was represented in a hydrodynamic model grid that was fitted to the boundaries of the study area. The hydrodynamic simulation based on the grid used the ASA WQMAP (Water Quality Mapping and Analysis Package) BFHYDRO (boundary fitted hydrodynamic) model (Spaulding et al, 1999). The current results were then used in a companion model to assess the transport and deposition of suspended sediment. The sediment model used for the study was BFMASS (boundary fitted mass transport model), another module WQMAP. BFMASS was run separately from WQMAP BFHYDRO but used the BFHYDRO predicted currents.

The hydrodynamic simulation results will be discussed in Section 2, followed by the assessment of sediment deposition and transport in Section 3. Overall conclusions are presented in Section 4. References are listed in Section 5.

2. Hydrodynamic Modeling

The most influential factor affecting the currents in the area is the existence of the railroad causeways that restrict the flow. Without the causeways, the current speeds would be much lower because the waterway would be almost three times wider than the present configuration. This is much more important than the highway bridge piers which have an insignificant effect on the currents. Therefore, the presentation in this section focuses on the hydrodynamic simulation results for just two scenarios: with and without the causeways.

Prior to the hydrodynamic simulations without the causeways, the tidally dominant currents are simulated for the present configuration of the area, and a calibration made to the velocity observations that have been collected at a location between the causeways. This section includes two parts. Results of the current measurement analysis and comparisons between the observed and simulated currents are presented in the first part, followed by a detailed analysis of the hydrodynamic simulations for the two scenarios.

2.1 Velocity Observations and Comparisons

2.1.1 ADCP observations

Velocity data were measured at a location ($41^{\circ}38.33'N$, $71^{\circ}12.80'W$) between the west causeway and the swing bridge of the Sakonnet River railroad bridge. The instrument used for the measurement was a 600 kHz convex BroadBand ADCP. It was moored at the bottom, where the mean water depth is about 10.3 m (33.8 ft), and it collected currents throughout the water column every 5 minutes at 0.5 m (1.6 ft) intervals (bins) in the vertical, for two consecutive periods from 29 August to 2 October 2000. The first data period lasted almost 9 days between 30 August and 8 September 2000, and the second period extended approximately 24 days from 8 September to 2 October 2000.

The ADCP is set up so that it sends out a ping every 2 seconds. It collects a set of returning sound speeds for 150 pings, equivalent to 5 minutes, averages the ensemble, and then converts the mean speed to a water velocity profile using the Doppler effect. The instrument used for this study is a convex 4-beam transducer. Each beam is oriented 20° from the vertical and is divided into 30 bins (depth-cells) in the vertical with a bin-size of 0.5 m (1.6 ft) with the first bin closest to the transducer. Accordingly, this instrument can measure water velocity up to 15 m (49 ft) deep.

The quality of data collected was found good and very consistent throughout the period, judging from the echo intensity and correlation profile data from each ensemble. However, the first and last several ensembles generally were bad because of inaccurate heading and tilting until the instrument became steady. After deleting the end-ensembles from the record, we corrected for magnetic heading offset, and removed the first and last bin from each ensemble because they were generally over weighted or contaminated by

large backscatter as a result of surface waves, respectively. The number of the last bins (close to the water surface) to be removed varied because the water level changed over the tidal cycle. Finally, we removed velocity profiles flagged by an error velocity beyond its threshold (200 cm/sec for this study, error velocity is the difference in vertical velocity estimates measured for each pair of beams), and removed spurious data occasionally found due to either high error velocity or low correlation values.

The processed ADCP velocity profiles for the first and second observation periods are shown in Figures 2.1a through 2.1e. The east and north components (top two panels) are color-coded with red for positive and high speed and with blue for negative and high speed, whereas the total speed (bottom panel) is blue for null speed and red for high speed. The vertical excursion of the water level is also shown in the figure, which varies over the top five bins at maximum depending on the time of the diurnal cycle and the spring-neap tidal cycle. Toward the end of the first period, the currents are driven by neap (smaller) tides. The color contrast is less significant and the water level is relatively higher than at the beginning of the period. At the beginning of the period the tides are at spring (larger) resulting in a larger current range.

Both the east and north velocity components in the area show little variations in the vertical. In other words, the flow is barotropic. The current pattern for the north component is such that ebb currents (in blue) always occur during high water-level periods, whereas flood currents (in red) exist for either low water level or the time between low and high levels. Though it is difficult to tell from Figure 2.1a, the east component shows similar behavior except it is mostly westward and eastward during low and high water levels, respectively. The same observations are true for the data collected for the second period, 8 September to 2 October (Figures 2.1b through 2.1e).

Table 2-1 shows mean and standard deviation of the velocity component profile data over the 33-day observation period. Average currents range from 128.4 cm/s (2.56 kt) at the surface layer to 4.1 cm/s (0.08 kt) at the bottom layer, with the mean mid-layer currents varying between 2.9 cm/s (0.06 kt) and 4.4 cm/s (0.09 kt). The direction also changes from southeastward near the surface, northwestward at mid-depths to southwestward near the bottom. The cause of the large difference between the surface and mid-layer is simply the bias of using data in the top four bins only during high water levels, during which the current is predominantly ebbing. Changes in the current speed and direction seen in the lowest two bins above the bottom appear real, since their

Figure 2.1a. The ADCP velocity profile observations for the first observation period between 31 August and 8 September 2000. Speed and direction for each velocity component are color-coded: red (positive) for the east/north components represents high speed and eastward/northward, while blue (negative) is a strong current toward the west/south.

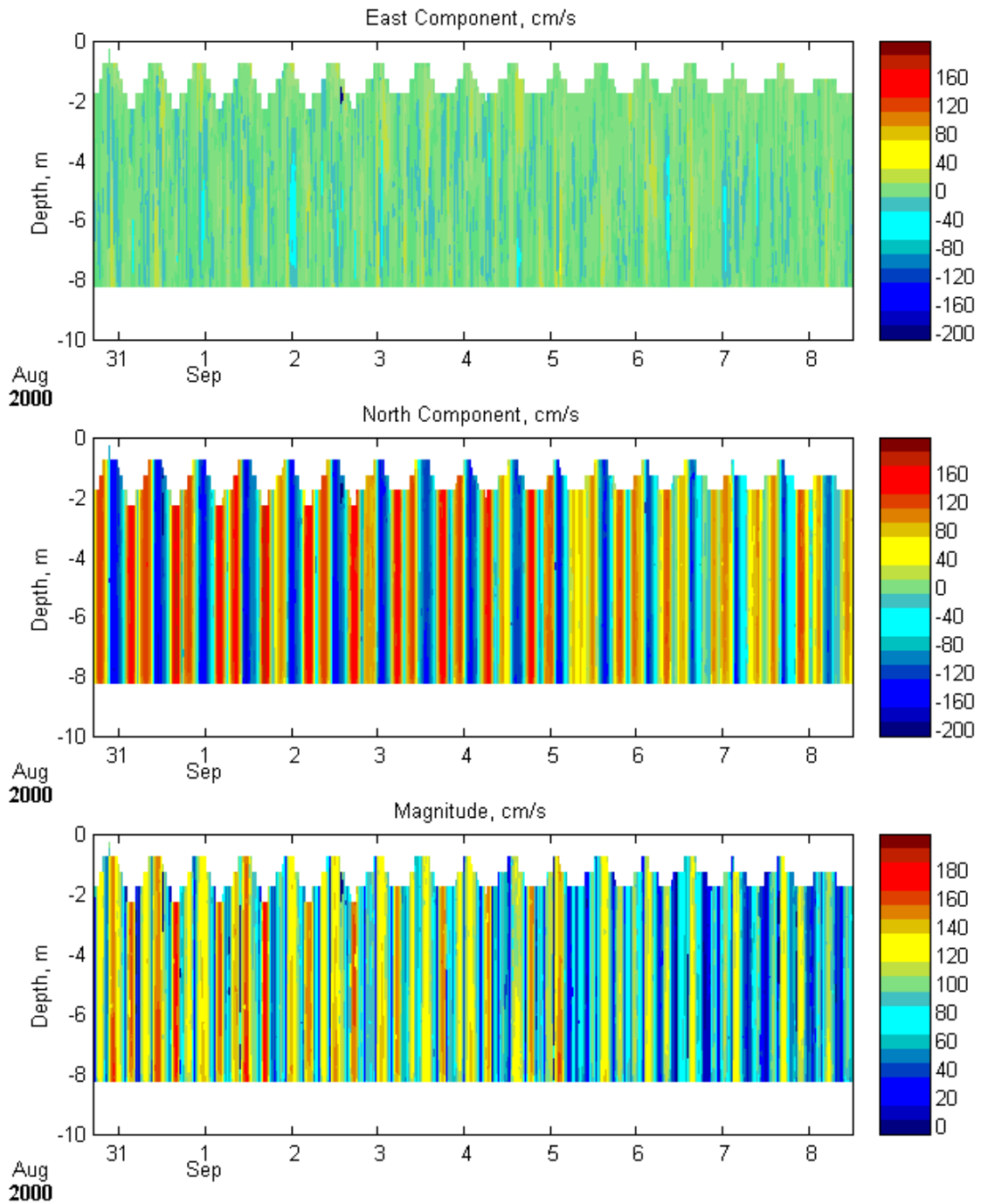


Figure 2.1b. The ADCP velocity profiles for the second observation period between 8 September and 2 October 2000 (first week: 8-15 September).

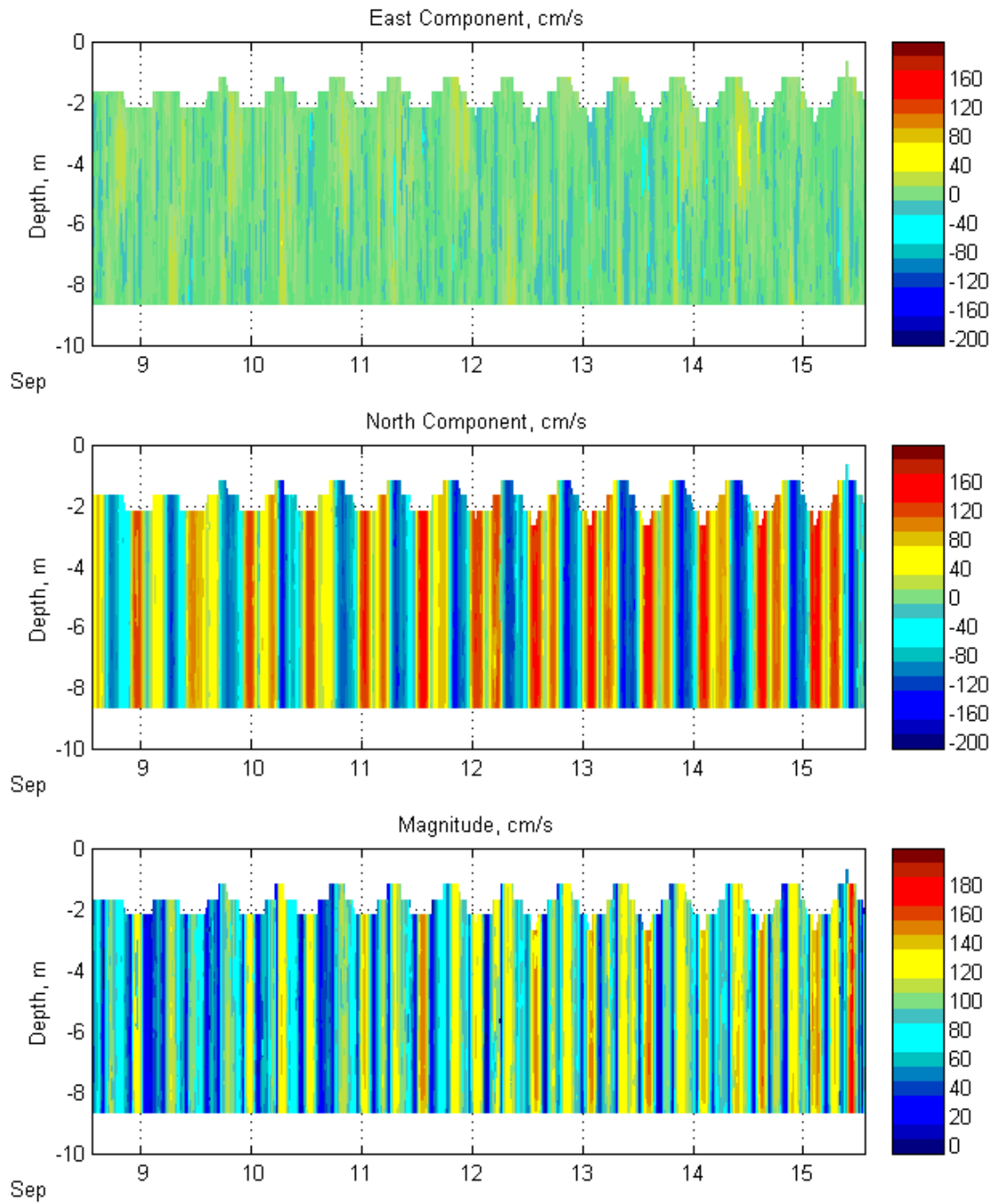


Figure 2.1c. The ADCP velocity profiles for the second observation period between 8 September and 2 October 2000 (second week: 16-22 September).

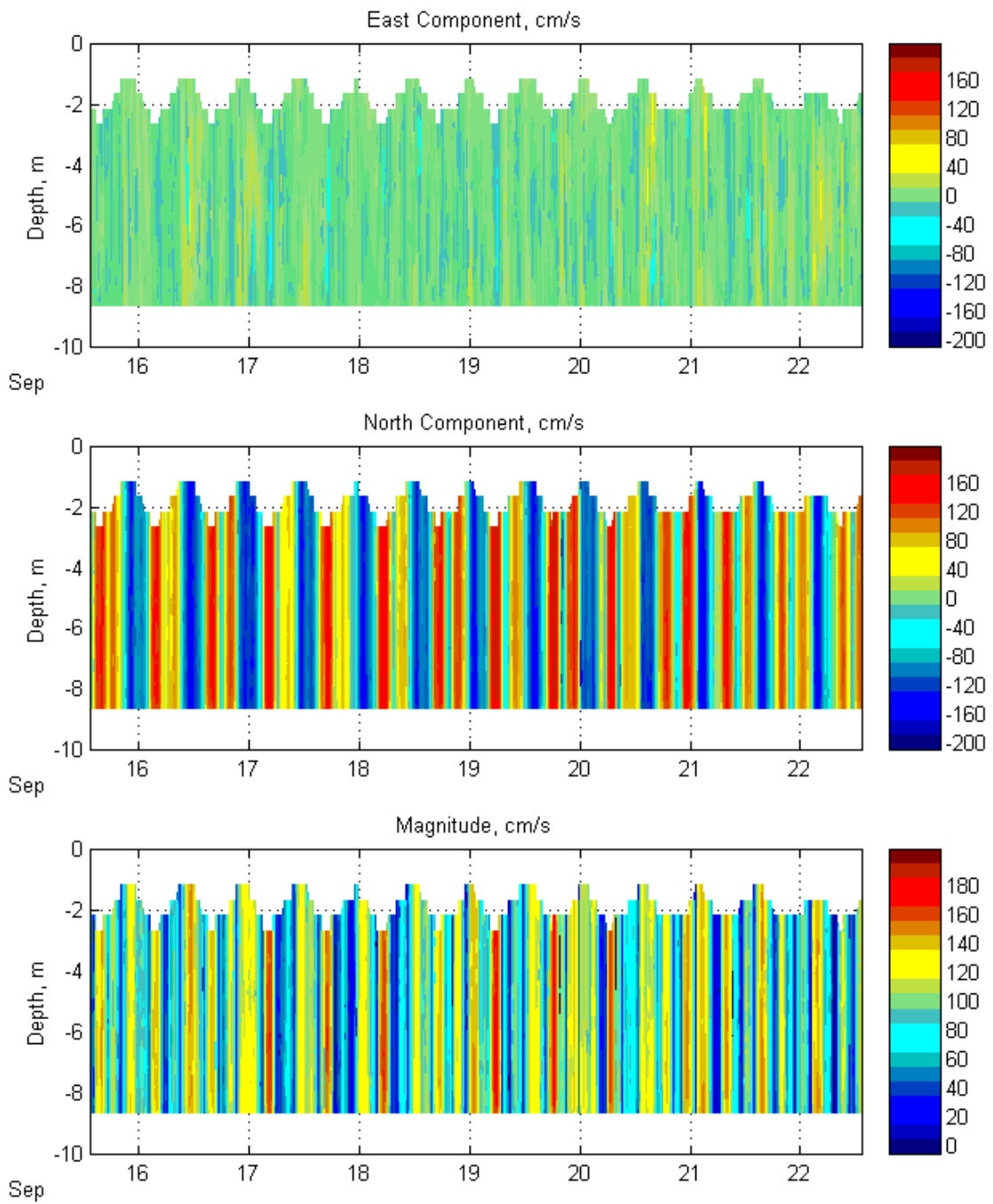


Figure 2.1d. The ADCP velocity profiles for the second observation period between 8 September and 2 October 2000 (third week: 23-29 September).

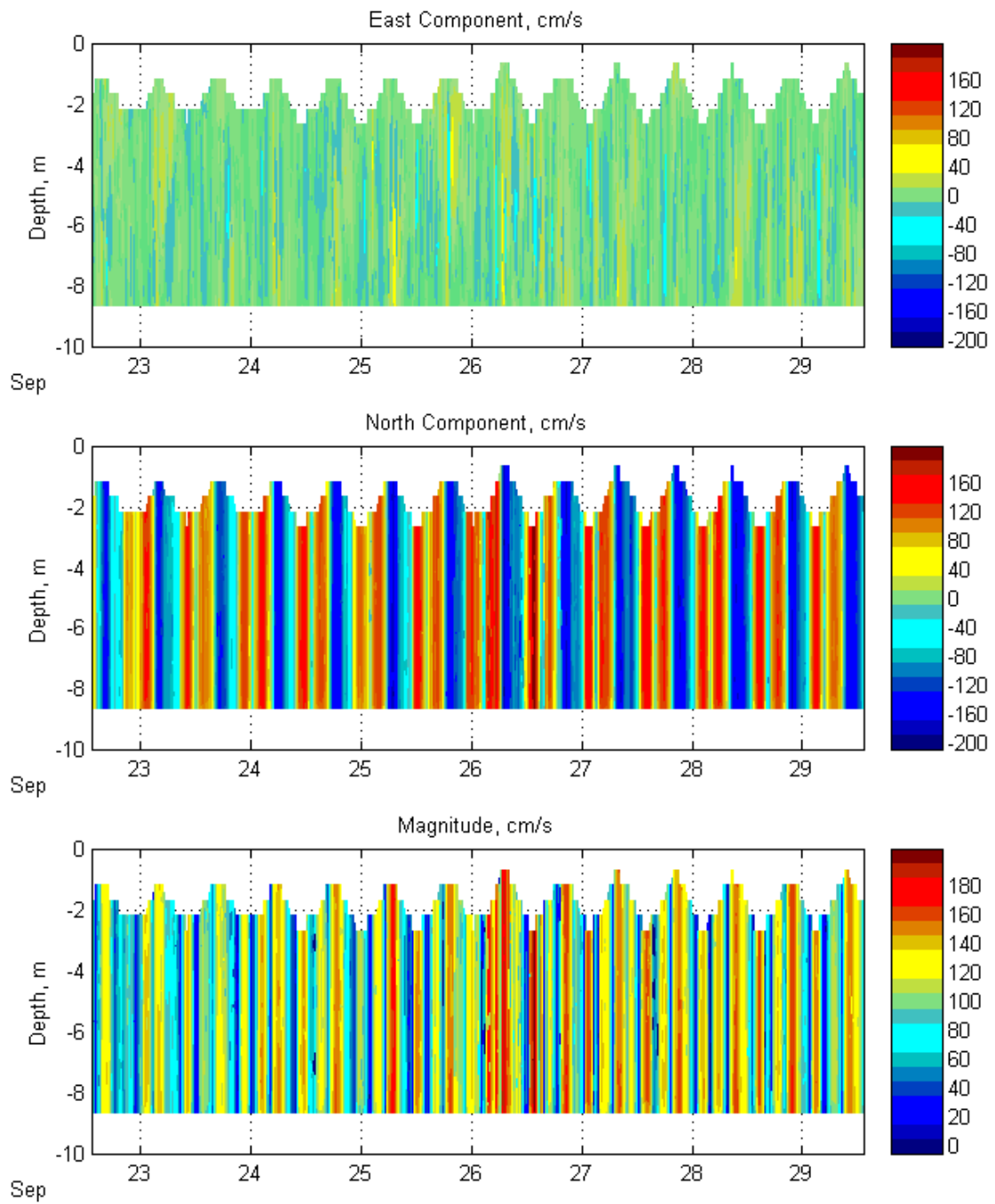
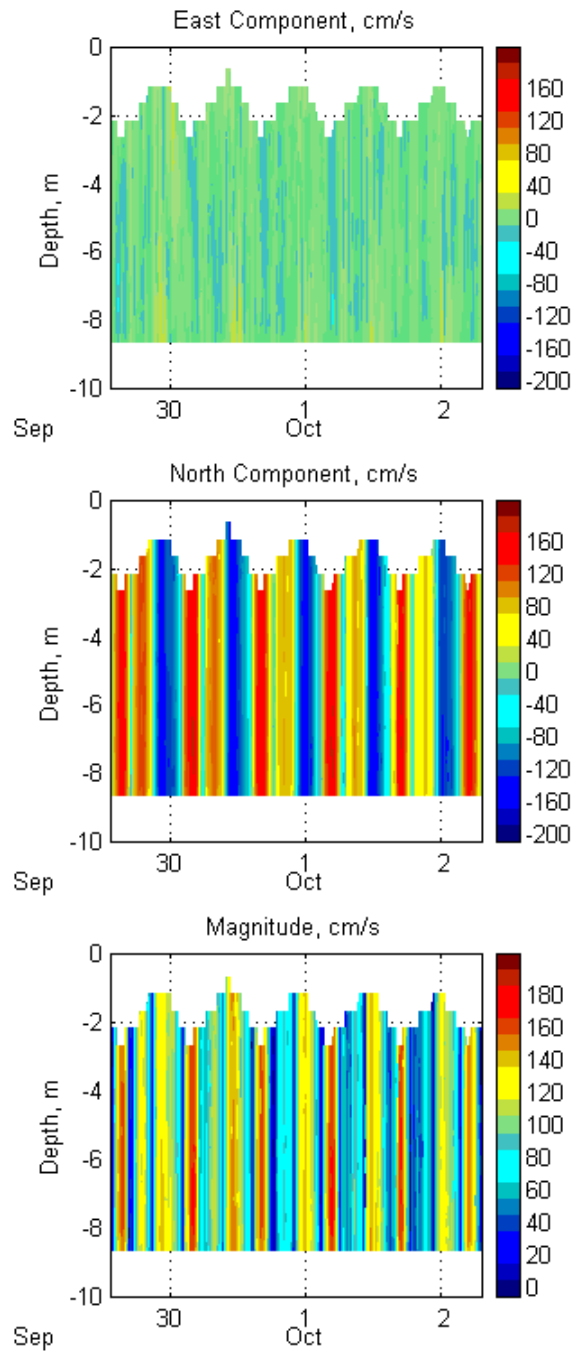


Figure 2.1e. The ADCP velocity profiles for the second observation period between 8 September and 2 October 2000 (fourth week: 30 September – 2 October).



standard deviations are consistently smaller than the values in the bins above, and may result from the bottom boundary effects.

The current over the water column varies, but the change is minor: the difference in speed in the mid water column is only 1.48 cm/s (0.03 kt) The top four bins (shaded in Table 2-1) are biased because the prevailing ebb current near high water contributes to the high speed in the bins.

Table 2-1. Mean and standard deviation of east and north velocity component profiles. Values in highlighted cells are the mean and standard deviation of the data observed during the period of high water level. Values in the first column are depth below the water level. Direction is in degrees clockwise from True North.

Bin Center-Depth m	Mean, cm/s				Standard Deviation, cm/s		# of data points
	East	North	Speed	Direction (°T)	East	North	
-0.8	5.2	-128.3	128.43	182.34	8.79	39.92	80
-1.3	2.4	-81.0	81.01	181.70	9.05	67.92	2102
-1.8	0.7	-39.1	39.11	181.01	8.81	89.98	4847
-2.3	-1.0	-10.8	10.82	174.71	8.70	88.11	8496
-2.8	-2.1	2.0	2.90	45.71	9.42	93.46	9379
-3.3	-2.3	2.2	3.15	46.82	9.63	93.47	9379
-3.8	-2.6	2.2	3.43	49.79	9.81	93.54	9379
-4.3	-2.9	2.2	3.61	53.09	9.96	93.65	9379
-4.8	-3.2	2.2	3.88	55.91	10.08	93.89	9379
-5.3	-3.5	2.1	4.10	58.62	10.19	94.14	9379
-5.8	-3.8	2.0	4.30	61.56	10.24	94.67	9379
-6.3	-3.9	1.9	4.36	64.17	10.39	95.06	9379
-6.8	-4.0	1.7	4.38	67.15	10.54	95.45	9379
-7.3	-4.1	1.4	4.34	71.74	10.67	95.71	9379
-7.8	-4.2	0.8	4.24	79.06	10.70	95.80	9379
-8.3	-4.1	-0.2	4.06	92.34	10.54	95.29	9379
-8.8	-3.4	-2.4	4.17	125.20	9.61	92.63	9379

Figure 2.2 shows depth-averaged currents as a time series in vector plot format (a), and in line plot format (b). Generally, the currents are south southwestward during ebb, and north northwestward during flood, having two flood peaks separated by a lull or even a small, short duration ebb. The flood and ebb current pattern is solely governed by the north component dynamics, and the degree of double flooding varies depending on the spring and neap tides. For example, large two-flood peaks and a large ebb trough are found during spring tide (e.g., around 1 September 2000) whereas both the flood peak and ebb trough weaken during neap tide, for example 7 September 2000.

Figure 2.2 implies that there is a very strong north and south excursion of the current in the Bridge opening. Maximum depth-averaged south and north speeds are

Figure 2.2a. Depth-averaged velocity in a vector plot format.

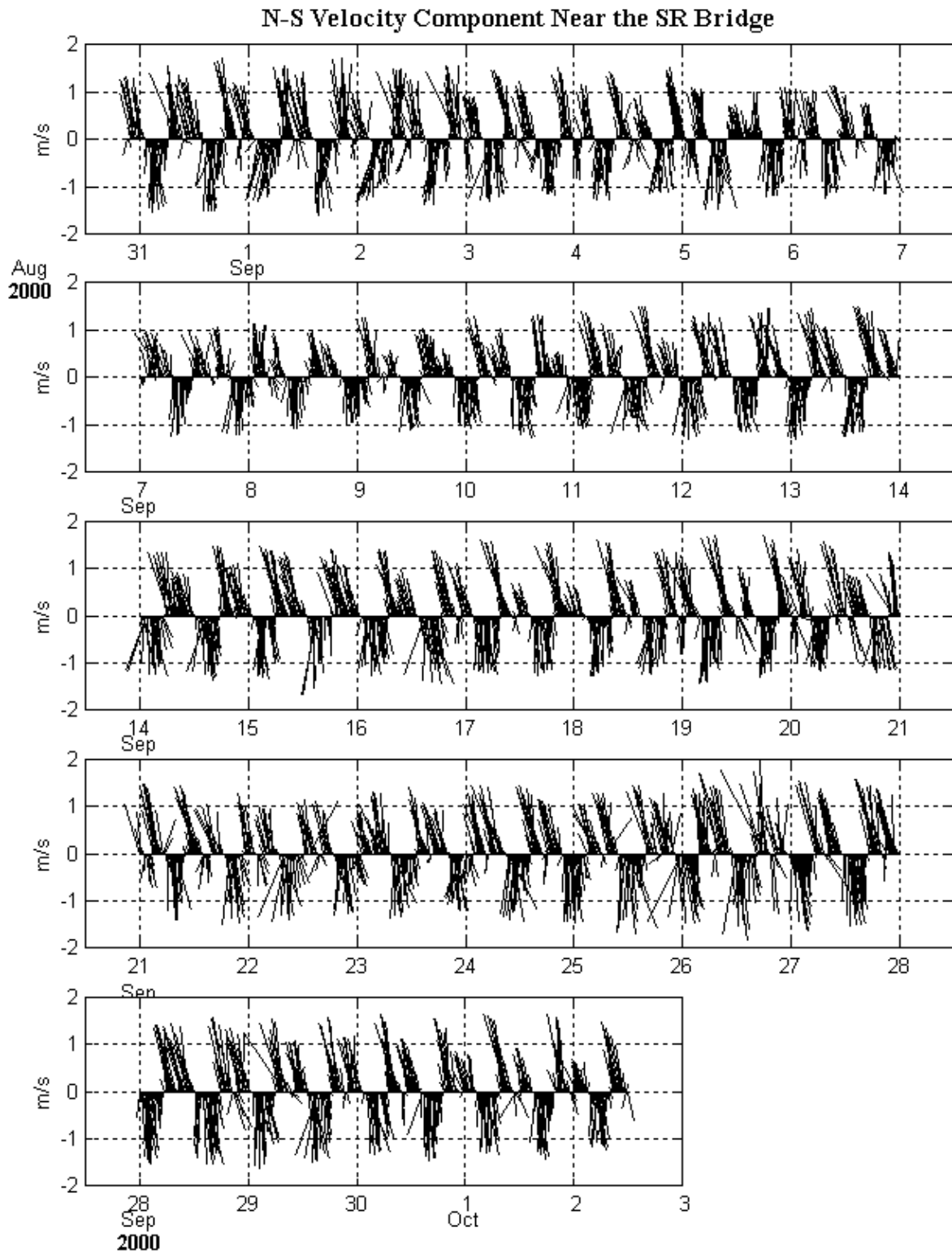
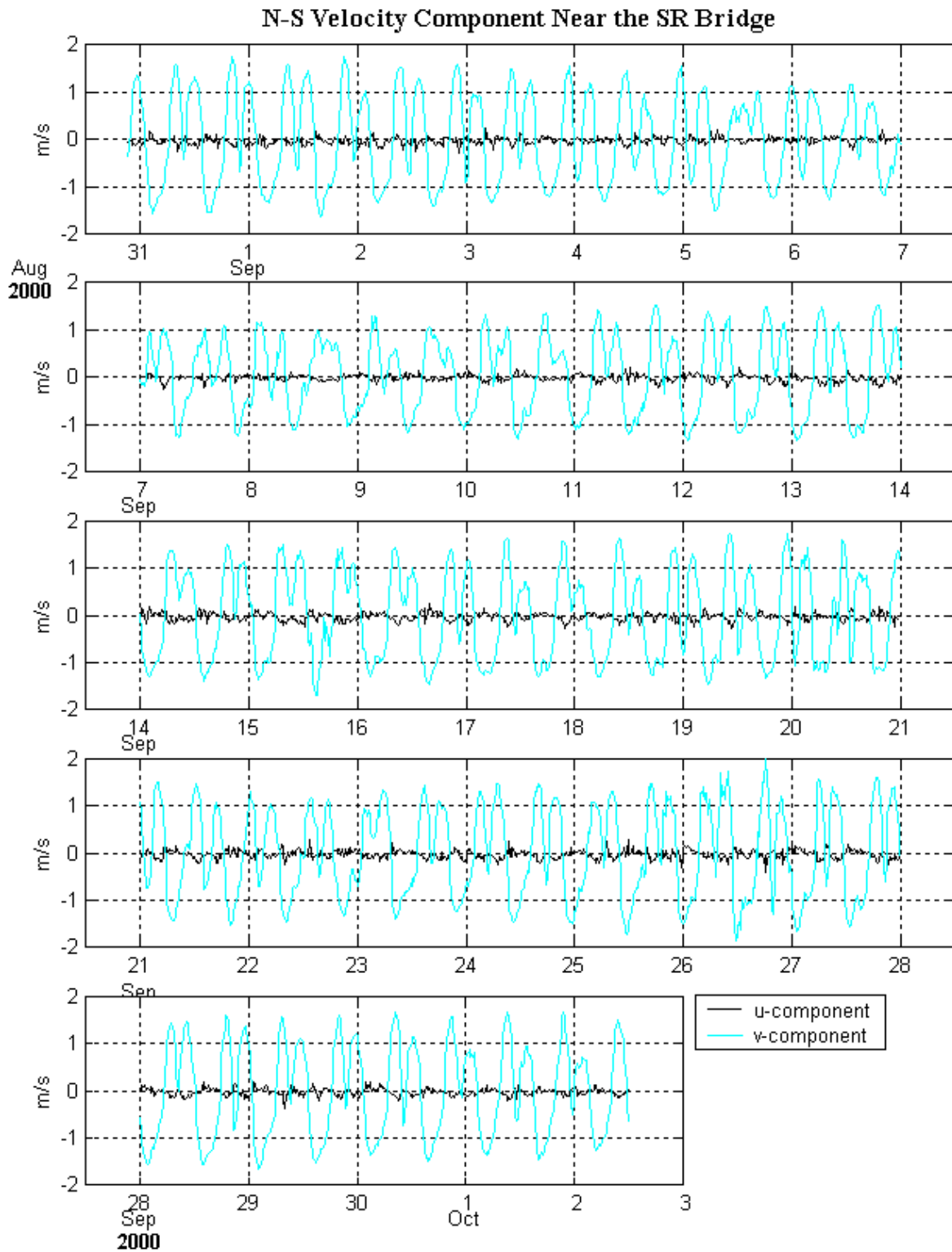


Figure 2.2b. Line plots of depth-average velocity components: u- and v-component are east and north currents.



1.93 m/s (3.86 kt) and 2.14 m/s (4.28 kt), respectively. The mean value over the total observation period is 0.015 m/s (0.03 kt) with a standard deviation of ± 0.94 m/s (1.88 kt), indicating a slight northerly residual flow.

Figure 2.3 shows a power spectrum density (PSD) plot of the vertically averaged ADCP north velocity component. The PSD is a useful tool to detect signals (here constituents) based on the energy distribution as a function of frequency. Most energy in the ADCP data exists at the M_2 , M_4 and M_6 tidal frequencies, 0.08, 0.16, and 0.25 cycles per hour (CPH), respectively. Low frequency variations with periods longer than 12 hours are small. In other words, there is not much energy derived from the forcing whose period is longer than semi-diurnal.

Harmonic tidal analysis using 8 constituents provides a similar result, presented in Table 2-2. The harmonic analysis resolves the semi-diurnal constituent M_2 as the dominant constituent, followed by the M_4 , M_6 , and S_2 constituents. The energy from the diurnal tides O_1 and K_1 is very small. This is the reason that they do not appear in the PSD distribution. The S_2 and M_2 constituents are too close in frequency to exist as two separate peaks in the PSD. They rather appear as one peak around the semi-diurnal frequency.

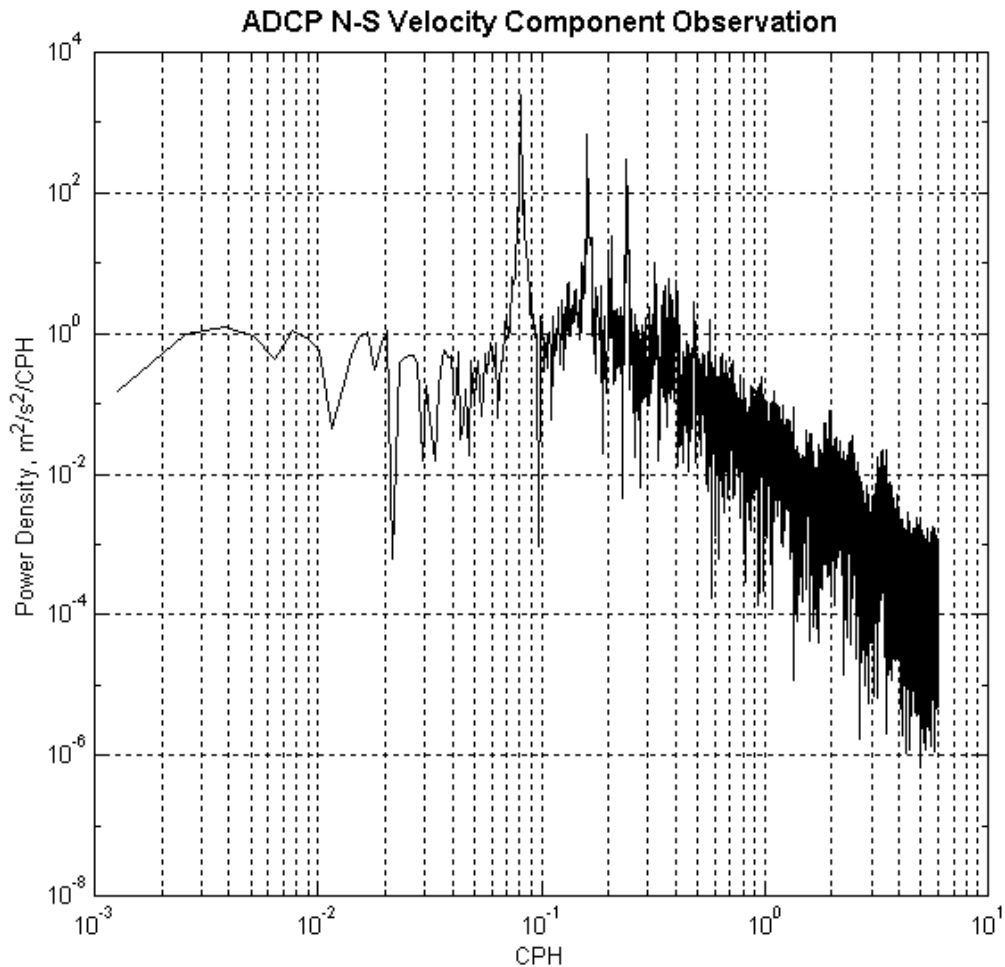
Table 2-2. Result of harmonic analysis with 8 tidal constituents.

Tidal Constituent	Tidal Frequency, CPH	ADCP North Component	
		Amplitude, m/s	Phase, °
Z_0	0.0000	0.018	0.00
O_1	0.0387	0.009	123.86
K_1	0.0417	0.019	50.62
M_2	0.0805	0.924	243.95
S_2	0.0833	0.225	266.20
M_4	0.1610	0.502	317.66
M_6	0.2415	0.332	228.13
M_8	0.3220	0.060	52.65

2.1.2 BFHYDRO Model Properties

The BFHYDRO model in two-dimensional and vertically averaged mode was applied to simulate currents that are primarily governed by the tides. Boundary friction at the surface and bottom layers is the only non-linear process included in the model. The simulations covered the full spring-neap tidal cycle, about 32 days. The period modeled

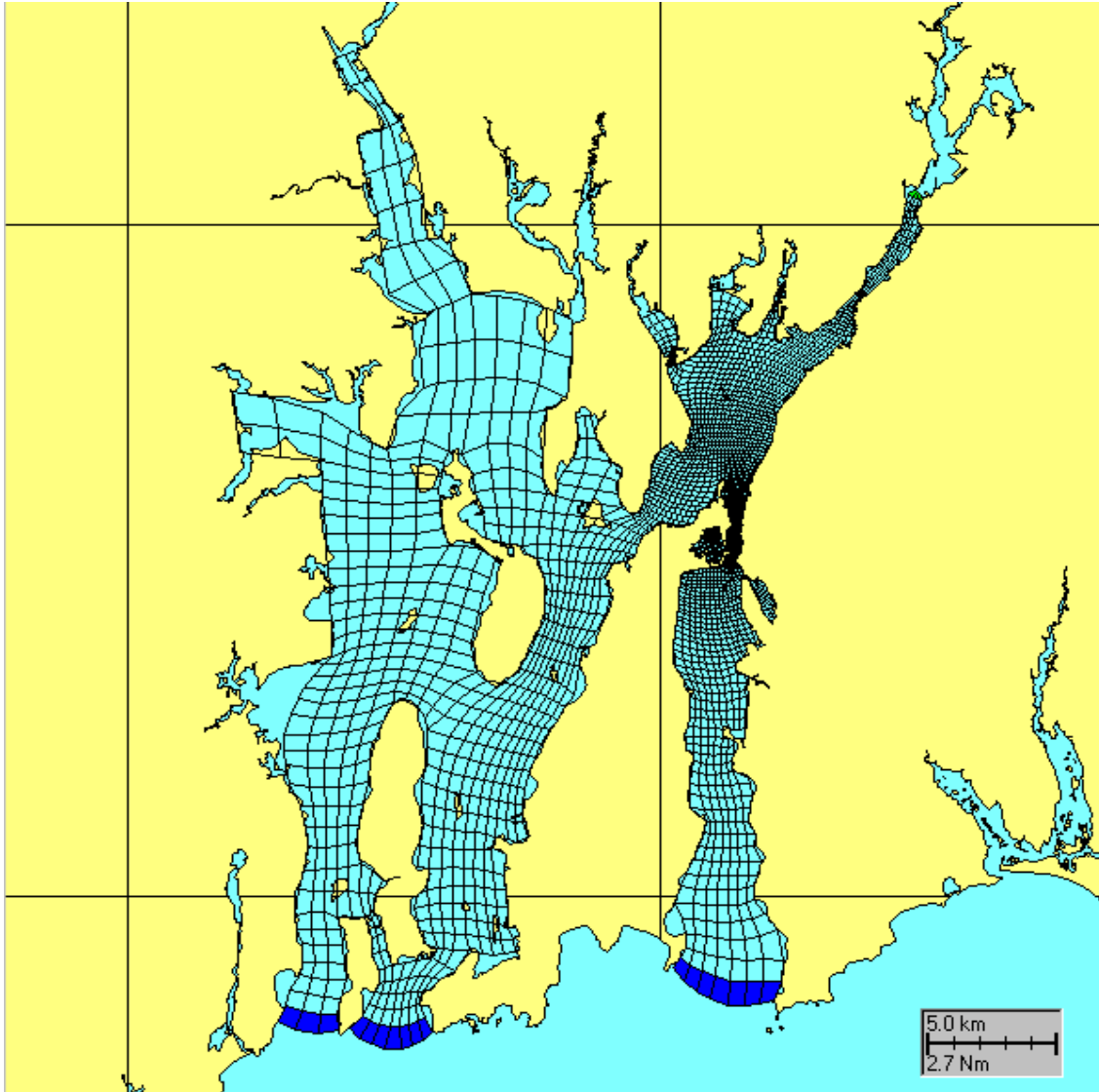
Figure 2.3. Power spectrum density for the ADCP north velocity observations. X-axis is CPH (cycle per hour), and y-axis is energy per CPH.



was from 30 August to 1 October 2000, approximately the same as the ADCP velocity measurement duration. We applied wind data collected at the T.F. Green Airport in Warwick, and the actual NOAA Newport tidal elevation along the open boundary. Additional details about the model can be found in Spaulding et al., (1999) and Muin and Spaulding (1997).

The model grid domain (Figure 2.4) is centered at the Sakonnet River Bridge and extends south to Rhode Island Sound. It also includes Mt. Hope Bay and part of the Taunton River to the north, and the whole of Narragansett Bay to the west. The total surface area of the domain is 338 km^2 (130 mi^2) and the average depth is approximately 7.4 m (24.28 ft). Bathymetric data was obtained from the NOAA National Ocean Service digital depth data on CD. The model grid conforms to the boundaries, *i.e.*, a boundary fitted grid, where each cell is not necessarily rectangular or square. The grid consists of 4028 cells, including 17 cells for the open boundary at Rhode Island Sound to the south

Figure 2.4. Model domain and its boundary fitted grids of the study area. Open boundary cells are in blue.



and 8 river cells at the Taunton and Providence Rivers to the north. Grid cells in the waterway between the railroad causeways are very fine (approximately 8.78 by 9.84 m [28.80 by 32.28 ft]), compared to those in the area away from the Bridge. The finest cells are used in the waterway to resolve currents better in the area. The cells in Narragansett Bay are especially coarse (1.61 by 1.16 km [1.00 by 0.72 mi]). The reason for their inclusion is to maintain the influence of bay-wide dynamics to this study area.

2.1.3 Model- Data Comparisons

It was found during the course of model calibration that the velocity is most sensitive to the frictional coefficient of the bottom boundary layer. We conducted a

sensitivity study on the friction, using a set of four different coefficients (0.0015, 0.003, 0.005 and 0.01). In general, the larger the coefficient value used, the smaller the amplitude of current variations. Nevertheless, the BFHYDRO model resolved the tidal current patterns with a range of coefficient values. The mean velocity difference between the coefficients 0.0015 and 0.01 was 1.3 cm/s (0.03 kt), and the standard deviation for the smallest coefficient was almost twice that of the largest. The best calibration determined from the study used the frictional coefficient 0.005.

Figure 2.5 shows time series of the calibrated currents superimposed on the ADCP observations. Occasionally the BFHYDRO model poorly predicts random behavior such as seen on 15 and 26 September, but the agreement between the simulated and observed data is usually excellent. The simulation exactly behaves like the observation: double peaks during flood and one trough during ebb. The simulation of the two flood peaks is less dramatic than the observation, but the trough between the two always exists in the same manner as observed. The second flood peak follows the first about 4.5 hour later, and it is either the same amplitude as or smaller than the first, depending on the spring-neap cycle.

Table 2-3 compares the major tidal components found in the simulated and observed current data. The results were determined from a harmonic analysis using 8 tidal constituents. The dominant tide in both data sets is the M_2 semi-diurnal, followed by M_4 , M_6 , S_2 , M_8 , K_1 and O_1 . The difference in amplitude between the model results and observations varies from -0.07 m/s to 0.09 m/s. The maximum phase difference is found to be about 40° for the M_6 tide, and the minimum difference is -7° for the M_8 tide. The differences in both amplitude and phase are minor, and therefore the ability of the model to predict currents is excellent.

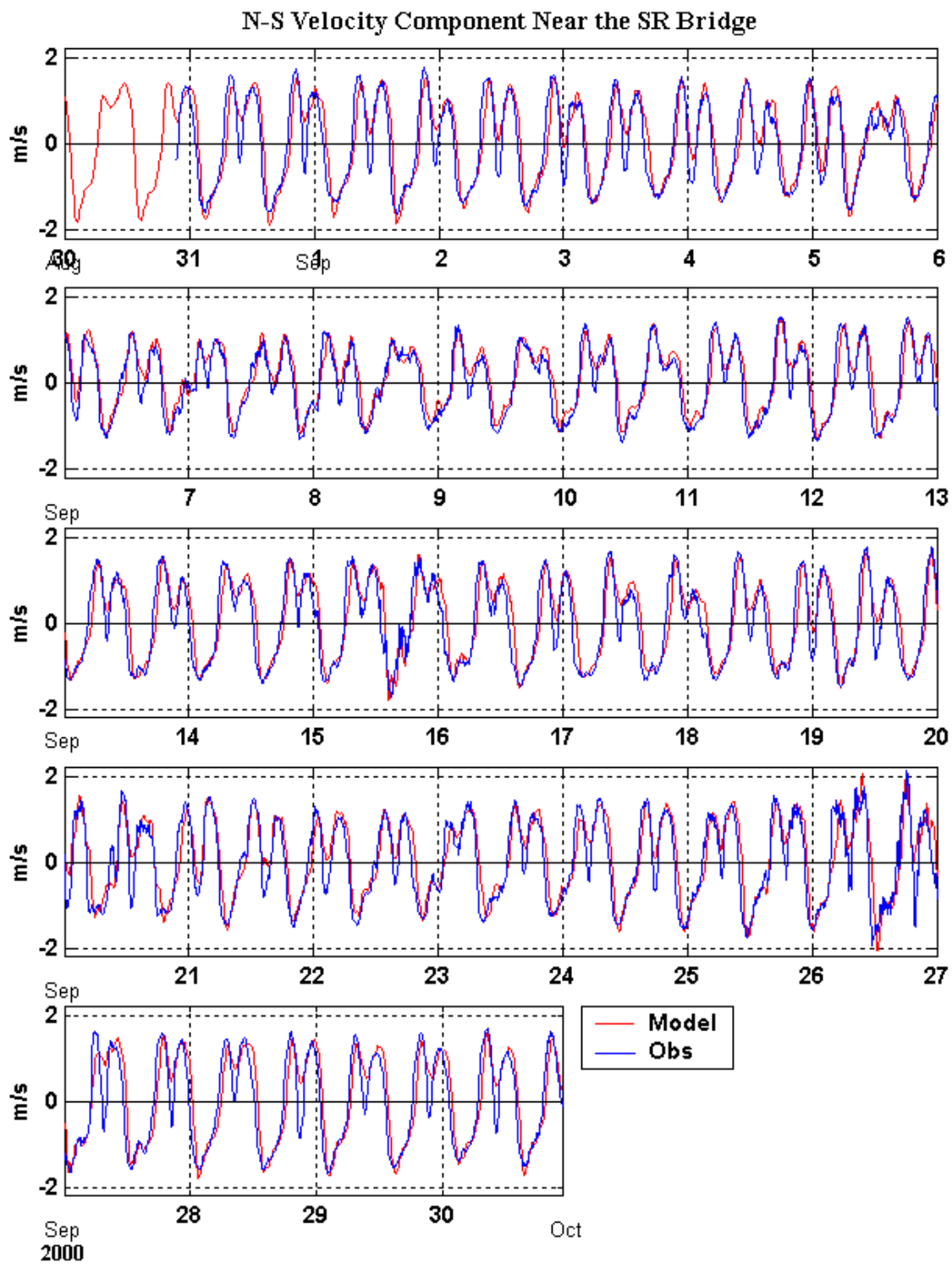
Table 2-3. Comparison of the harmonic analysis results between the predicted and observed north velocity components.

Tidal Constituent	ADCP		Model	
	Amplitude, m/s	Phase, °	Amplitude, m/s	Phase, °
Z_0	0.018	0.00	0.109	0.00
O_1	0.009	123.86	0.020	143.26
K_1	0.019	50.62	0.030	69.46
M_2	0.924	243.95	0.978	261.51
S_2	0.225	266.20	0.233	292.97
M_4	0.502	317.66	0.425	328.47
M_6	0.332	228.13	0.272	268.16
M_8	0.060	52.65	0.103	45.61

2.3 Hydrodynamic Simulations

Under the Sakonnet River Bridge Environmental Impact Study (EIS), five alternatives are considered in relation to the Bridge construction. Among them, four include the removal of the Sakonnet River railroad causeways, which are located north of

Figure 2.5. Time series of the north velocity components. The BFHYDRO simulation is in red and the ADCP data are in blue.



the Bridge. Thus, we combined the alternatives into two separate scenarios based on the configuration of the river. They are with the causeways (scenario 1), which is the present condition, and without the causeways (scenario 2). The model grid for the scenario 1 was exactly the same as the one used for the calibration simulation. However, the second scenario required two major modifications. First, removal of the causeways was accomplished by expanding the waterway to both sides of the riverbank. The final model grid is shown in Figure 2.6 in a close-up view at the railroad bridge. The top panel shows the grid for the present condition (scenario 1), and the bottom panel is for scenario 2. The second modification is to the depths, which is done by generally defining depths at the same level as the surroundings, in a range between 2.0 and 12.5 meters below the mean water level (Figure 2.7). The second modification can be varied depending on details of the construction and the extent of causeway removal. For instance, if the removal of the causeways included extensive dredging to smooth the bathymetry longitudinally, or to widen the channel laterally, then the currents in the area would diminish.

The most substantial difference between the two simulations is the current distribution in the area where the causeways presently exist. Figures 2.8 and 2.9 show typical maximum flood currents and ebb currents in the upper Sakonnet River, respectively. With the causeways remaining, the currents at the waterway exhibit a bell shape, having a maximum speed in the middle. Without the causeways, the shape flattens out, having almost the same speed ($O[0.25 \text{ m/s (0.50 kt)]}$) across the river except near the west shore. At both flood and ebb, relatively large speeds observed at the area close to the west shore appear due to a sill in the depths used to simulate the bathymetry after causeway removal. The currents, however, in the far field away from the bridge are almost identical between the two simulations. Therefore, the influence on currents due to the removal of the causeways is limited to the near field.

Figure 2.10 shows a comparison between two sets of model-predicted time series data taken at the ADCP location. The currents without the causeways show the same pattern (double flood, single ebb) as those with the causeways. However, the flood and ebb peaks from scenario 2 simulation decrease in speed to only 40% of scenario 1. Averages over the simulation period are about same (see Table 2-4), but the standard deviation and the velocity range for scenario 2 drops to about 0.4 times that for scenario 1.

Table 2-4. Statistics of the simulated currents between the scenarios with and without the causeways. The time series of data are at the ADCP site.

Scenario	Causeways	Mean, m/s	Standard deviation, m/s	Maximum ebb, m/s	Maximum flood, m/s
1	with	-0.001	0.89	-2.20	1.98
2	without	0.008	0.35	-0.82	0.79

Figure 2.6. Details of the model grids around the Sakonnet River Bridge: top panel) with the present structure and the railroad causeways; bottom panel) without the causeways. A star symbol represents the ADCP location.

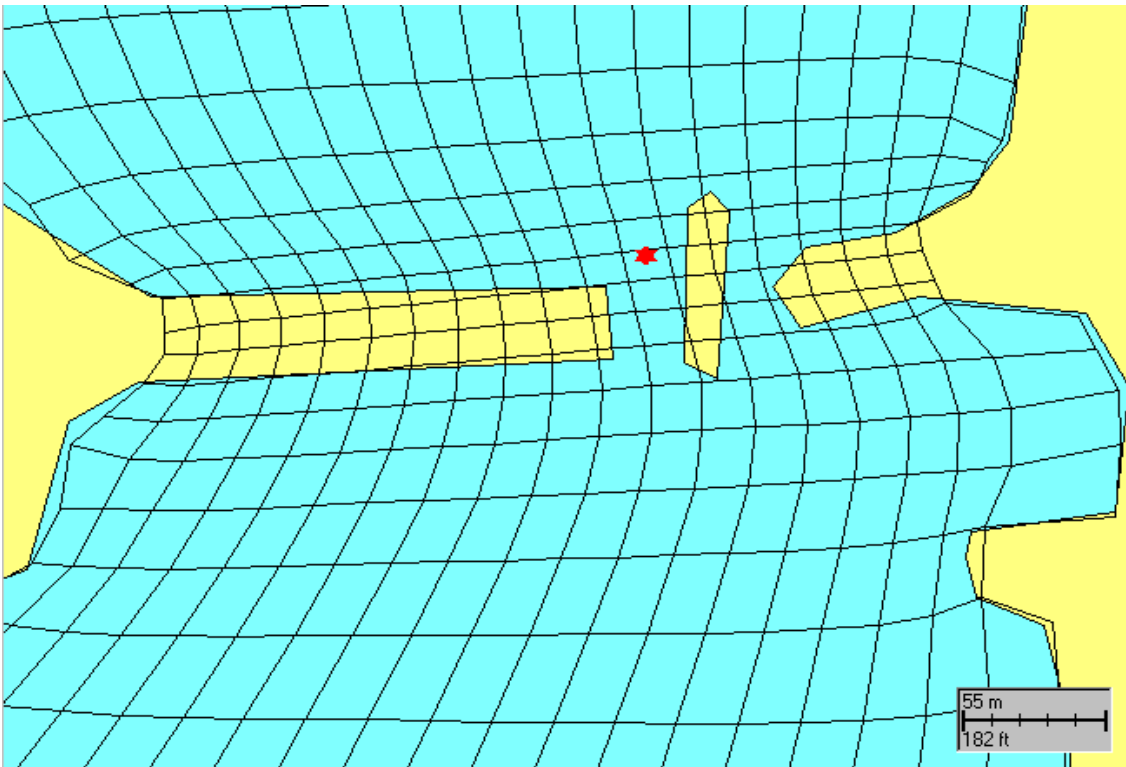
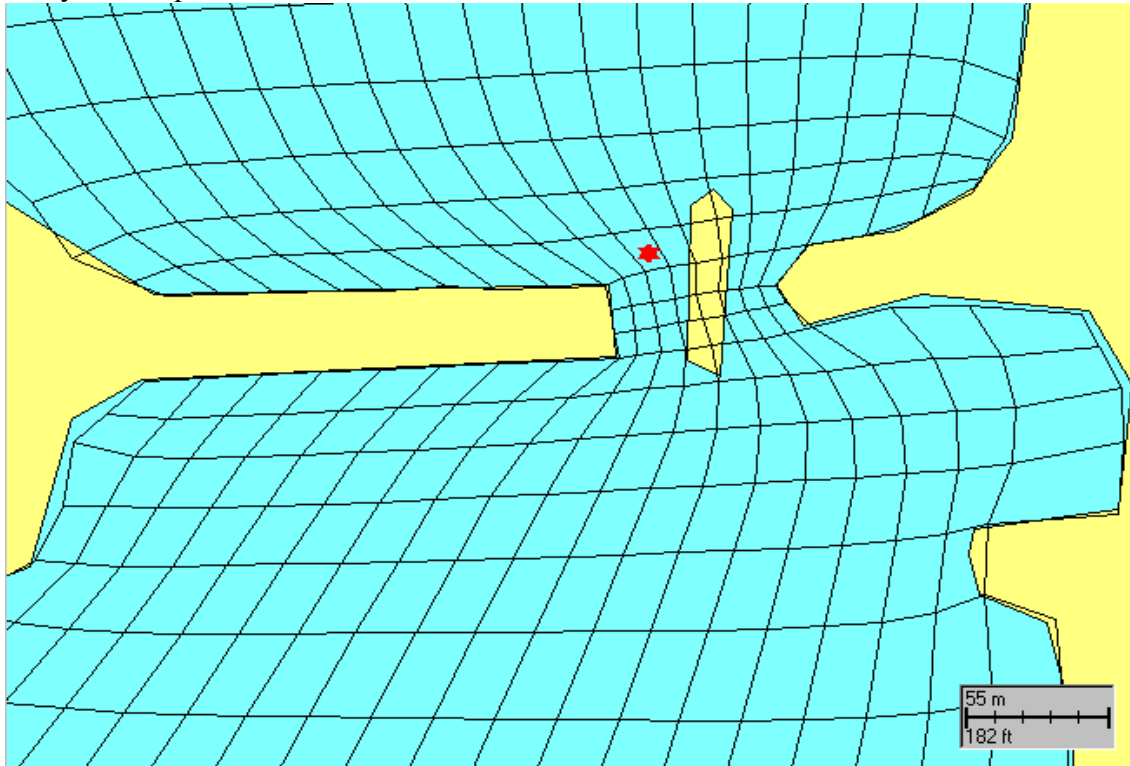


Figure 2.7. Details of the depths around the Sakonnet River Bridge: top panel) with the present structure and the railroad causeways; bottom panel) without the causeways. A star represents the ADCP location.

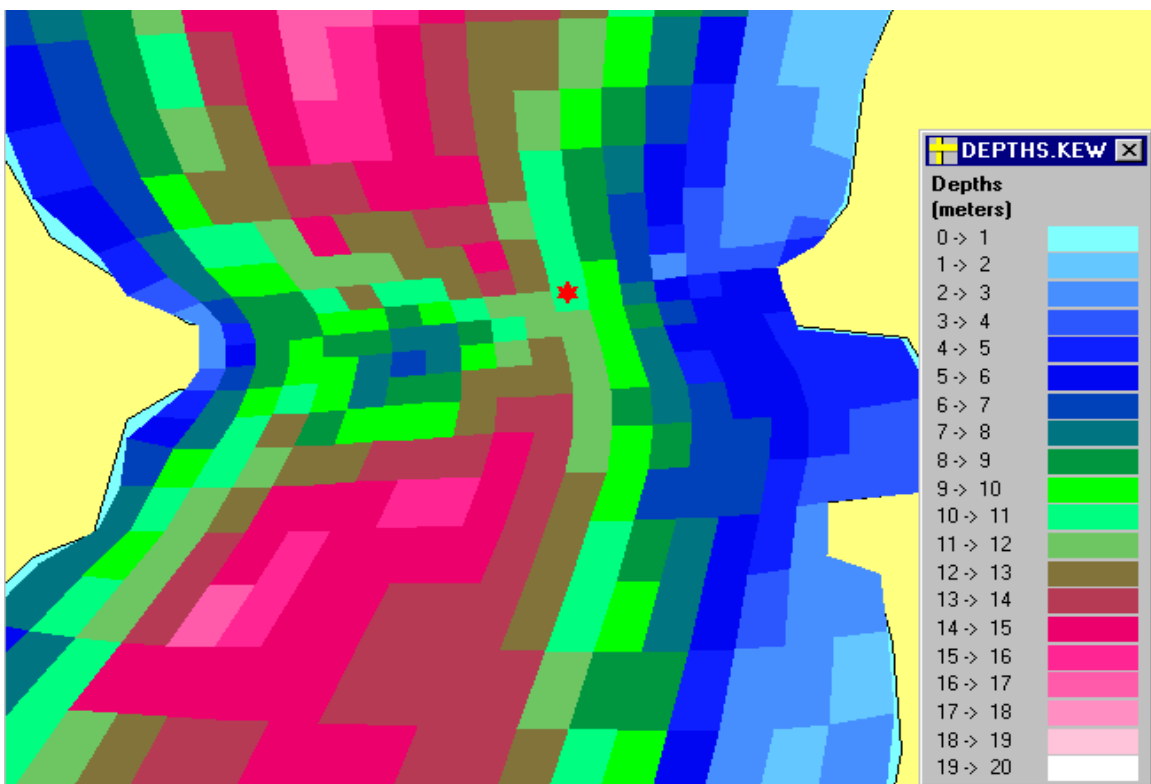
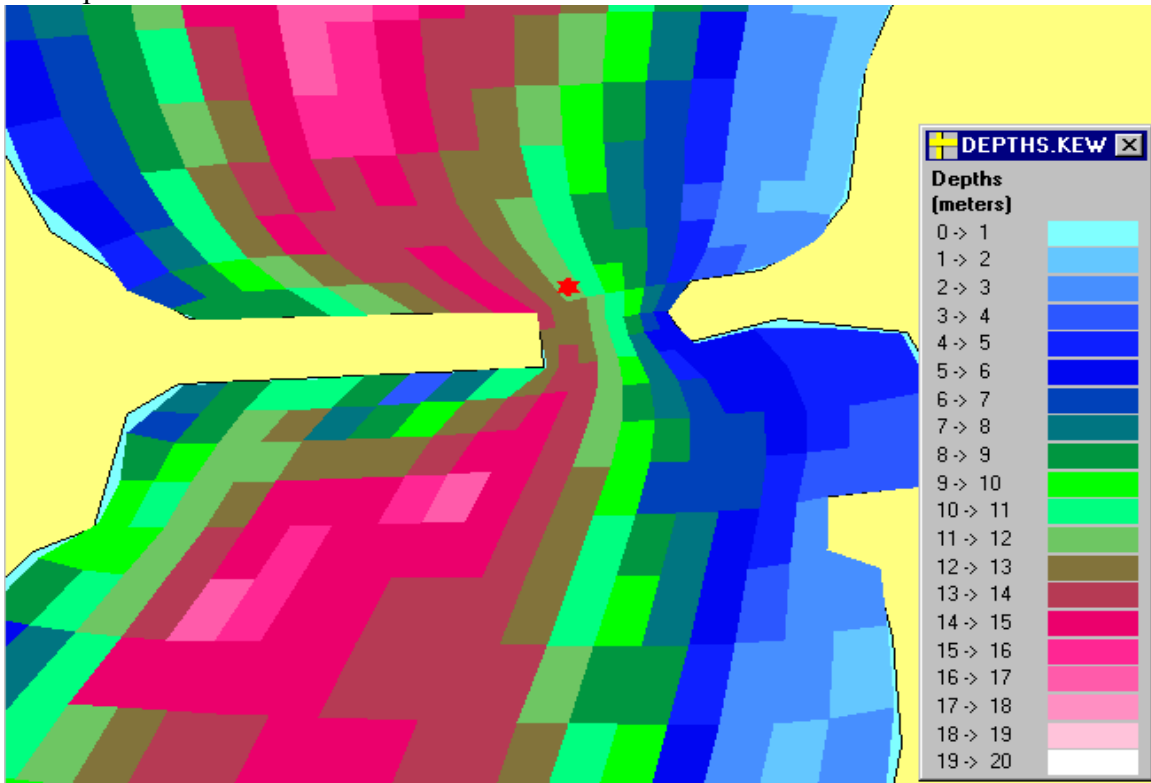


Figure 2.8a. Simulated velocity fields at maximum flood for the present condition with the causeways.

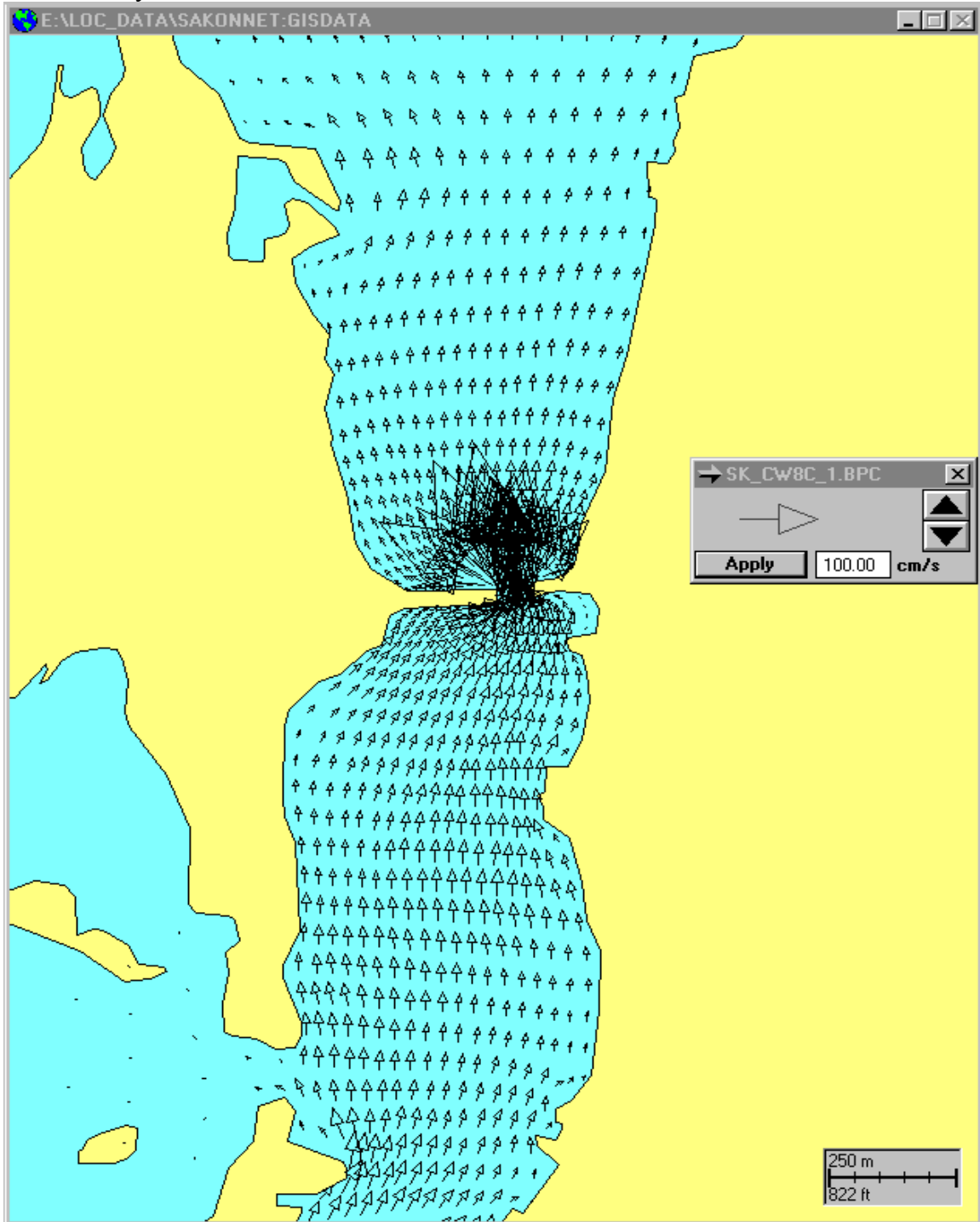


Figure 2.8b. Simulated velocity fields at maximum flood for a condition without the causeways.

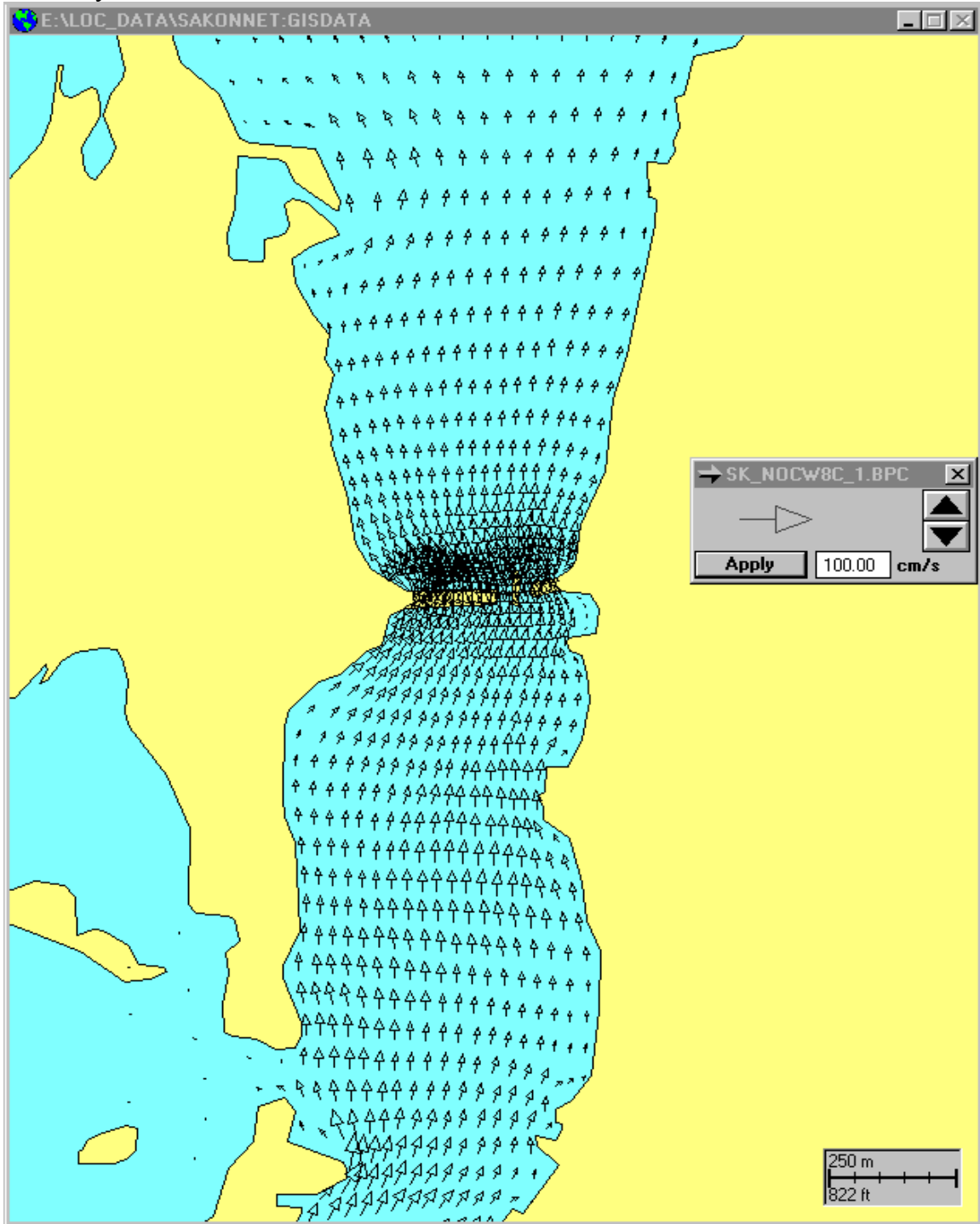


Figure 2.9a. Simulated velocity fields at maximum ebb for the present condition with the causeways.

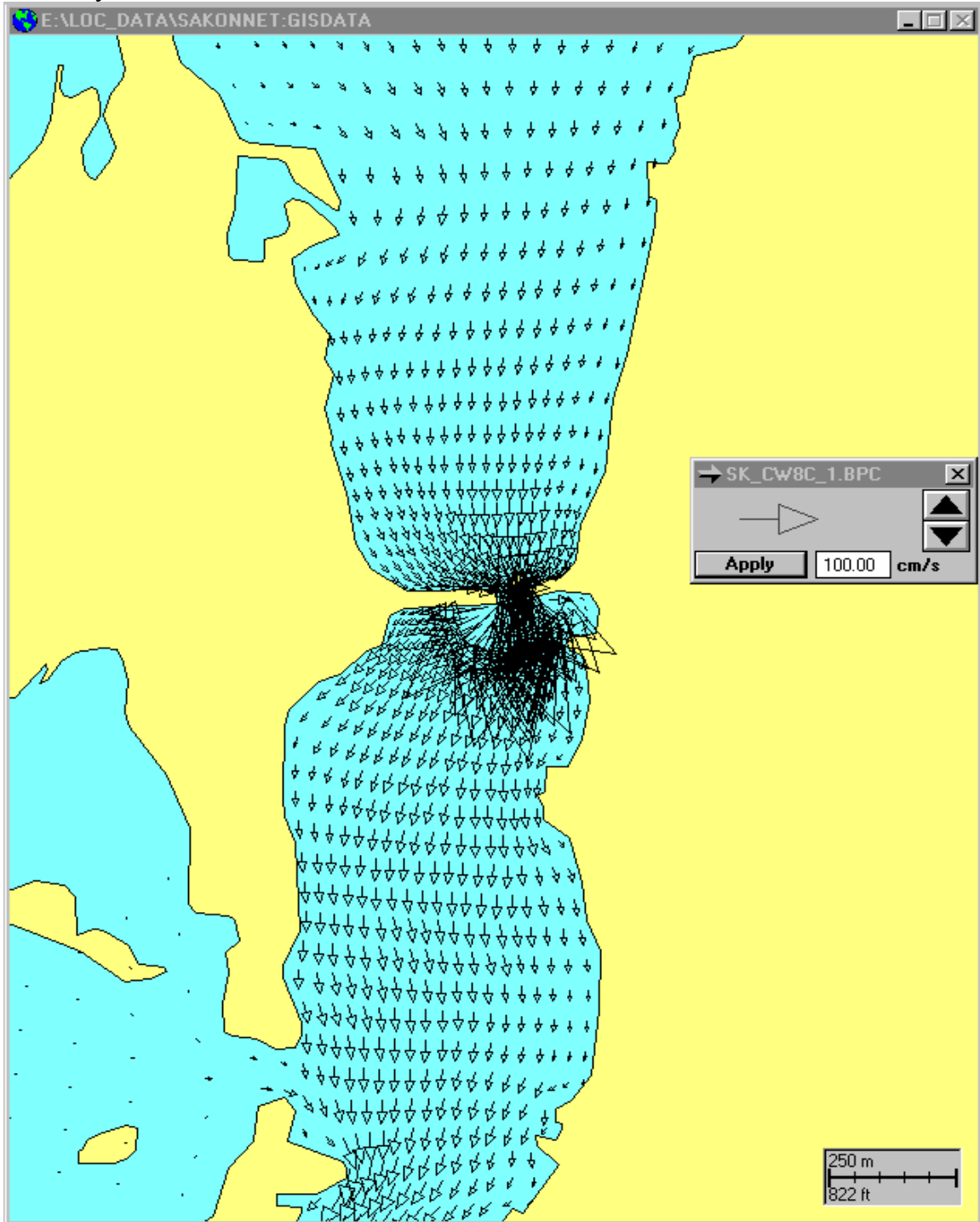


Figure 2.9b. Simulated velocity fields at maximum ebb for a condition without the causeways.

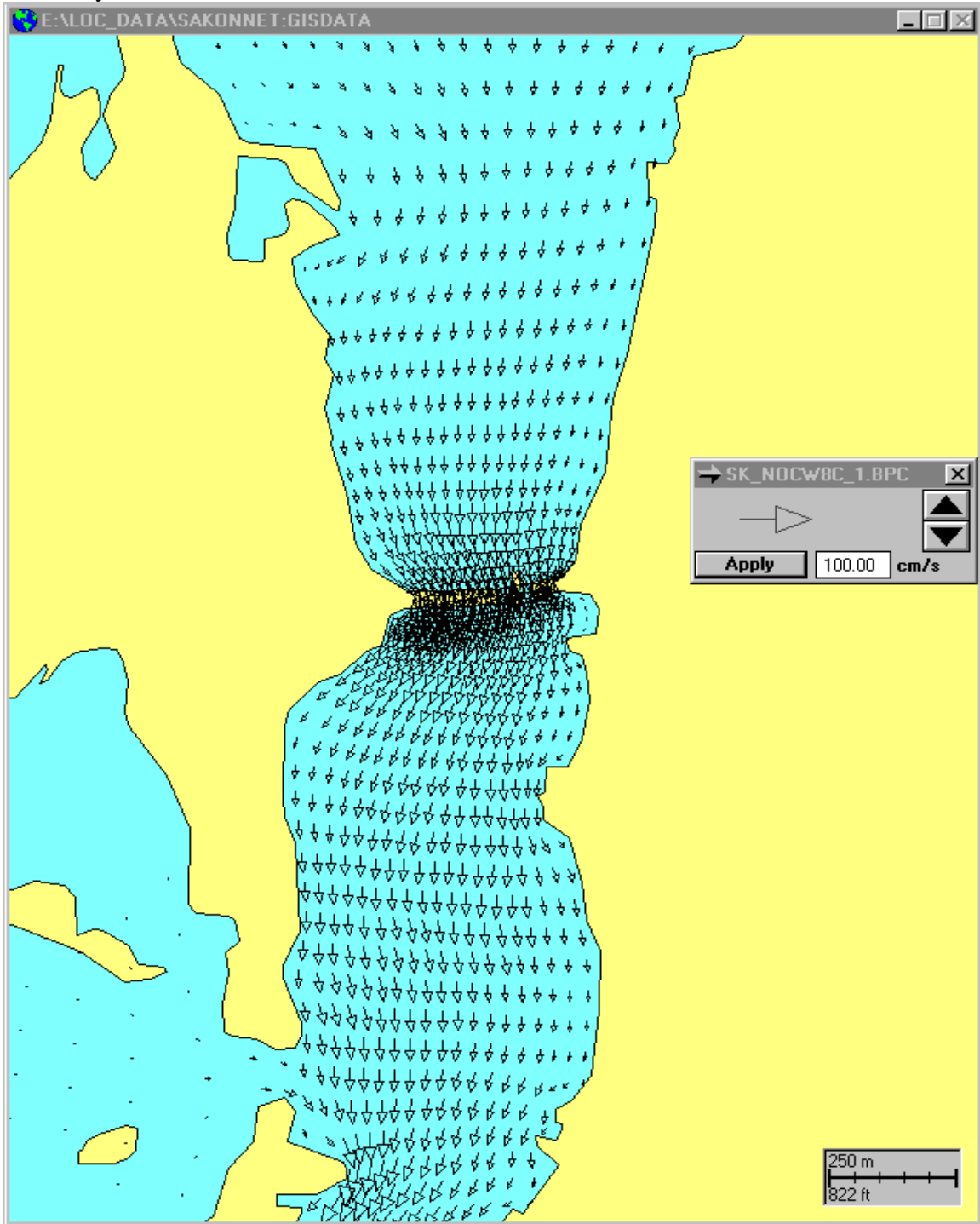
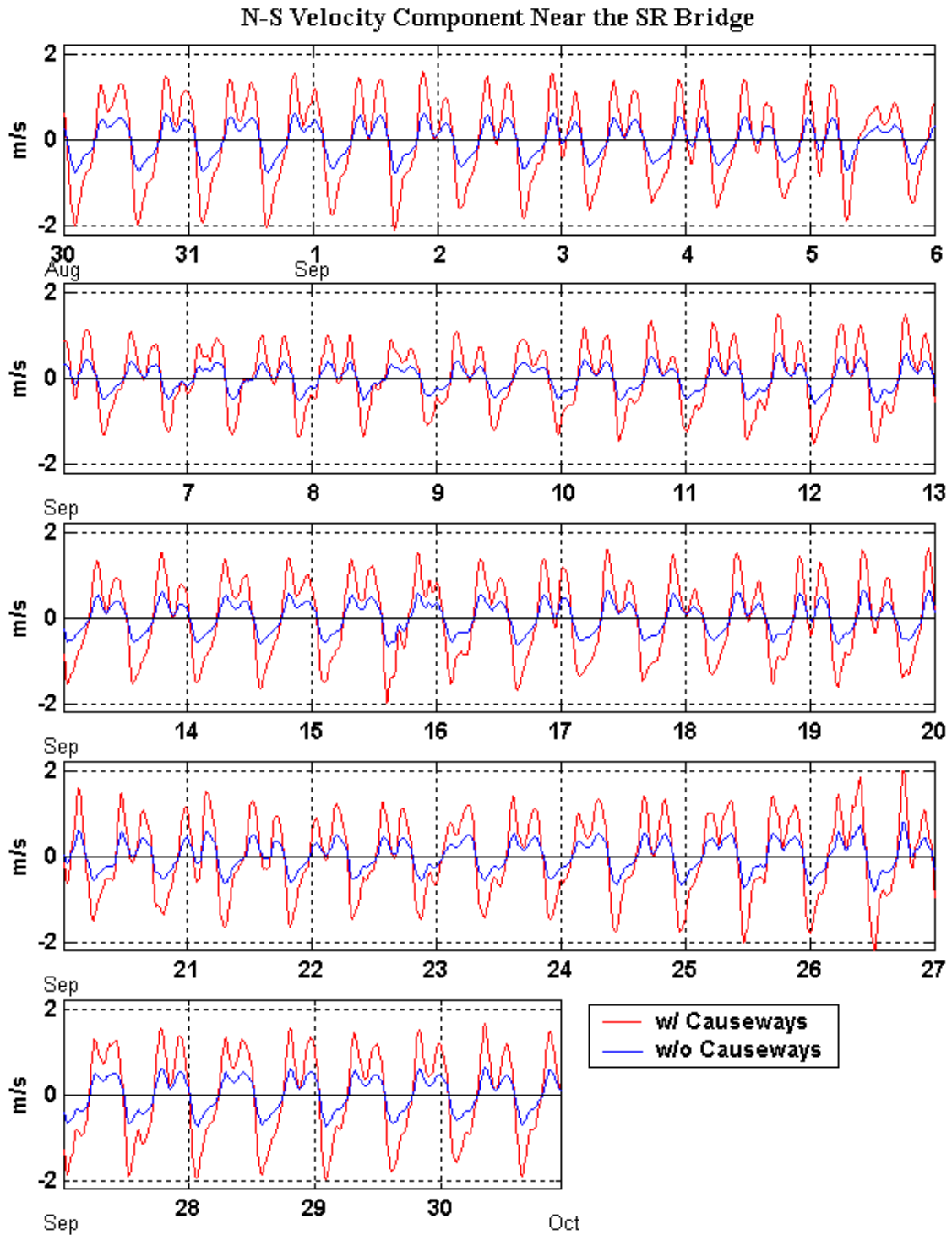


Figure 2.10. Time series of simulated north-south velocity component for the scenarios with and without causeways. Both the data are taken at the ADCP site.

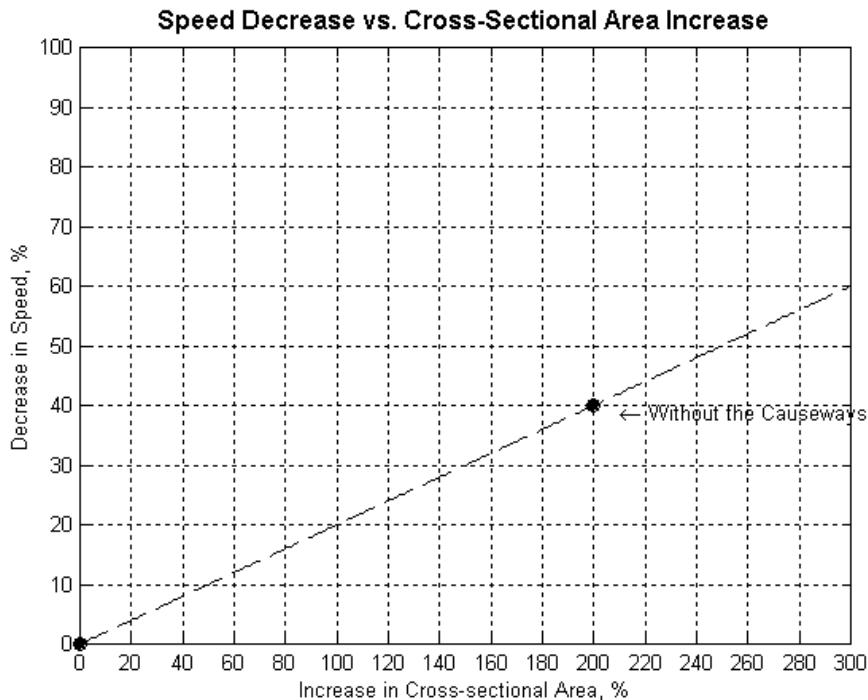


2.3 Evaluation of Causeway Effects

The total length of the causeways extends across about three quarters of the river width, and leaves an open waterway of approximately 670 m^2 ($7,211.82 \text{ ft}^2$) in cross-sectional area. Depending on which alternative is ultimately chosen, the removal of the causeways increases the waterway cross-sectional area. In this hydrodynamic simulation, a scenario chosen involved complete removal of the causeways and the water depth defined to the same level as the surroundings. This results a doubling of waterway area, and about a 40% decrease in speed. The speed decrease compensates for the amount of the area increase.

Based on the simulation results, one may try to estimate speeds in proportion to increment of the waterway cross-sectional area, assuming mass conservation and the linear relationship between the speed and area. The scenarios that have been simulated are two extreme cases. In a plot of area increase vs. speed decrease (Figure 2.11), scenario 1 is at the origin (0%,0%) and scenario 2 is at (200%,40%). The line connecting these two points indicates possible speed changes for a cross-sectional area change. For example, an increase in cross-sectional area to 150% would decrease speed to 30%. The line beyond the point (200%,40%) implies the depth increase only, for example, by dredging the waterway. Overall, this method provides only a bulk estimate. To get an accurate speed for a specific configuration, the hydrodynamic model should be used.

Figure 2.11. Changes in speed due to increase in the waterway cross-section area. A point at (0,0) represents the present configuration of the causeways.



3. Sediment Transport Modeling

All the proposed alternatives except #1 involve a series of construction activities such as removal of causeways, pile driving, dredging, etc, that may disturb the underlying sediments. The transport and eventual deposition of suspended or re-suspended sediments were simulated for each alternative using the ASA boundary fitted mass transport model (BFMASS). The exact amount and composition of suspended sediment will vary depending on the location and activity. The primary parameters governing the fate of suspended sediment are 1) the sinking velocity related to the particular type and size distribution of the sediment, and 2) the current patterns in the area.

The background currents were generated by the ASA BFHYDRO (boundary fitted hydrodynamic) model, and were calibrated to the present condition. The currents predicted at the waterway were greater than 1.5 m/s (3.0 kt) and had a double-flood pattern over the tidal cycle, consistent with the ADCP observations. The alternatives were involved two configurations, with and without the causeways, and the corresponding velocities were assessed. The removal of the causeways resulted in a significant change in current, for instance, a decrease in speed at the waterway by a factor of 2.6, because of the cross-sectional area increase. However, the double-flood pattern in the area and the current speed along the riverbanks, O (0.05 m/s [0.1 kt]), remained the same. The water depth with no causeways can be further refined corresponding to actual dredging details.

The substrate characteristics in the area consist of sand, silt/clay and gravel, averaging 66%, 26% and 8% of the total sediment composition, respectively. Gravel and sand fall back to the bottom immediately after suspension. For this modeling study, grain sizes less than O (0.1 mm [0.004 in]) encompassing particles of very fine sand, silt and clay were simulated. The objective of this sediment simulation was to assess the transport and deposition of sediment from construction activities. The approach was first to produce a series of simulations for each single particle size fraction, with the results then combined by weighting each fraction by its percentage of the total to simulate the actual sediment deposition.

The location of sediment sources will and perhaps simultaneously change during bridge construction activities which in turn cause changing deposition and concentration in the water column. However, this study is simplified so that the sediment release occurs only at one site at a time. Three release locations are considered separately for both configurations: with and without the causeways. A continuous sediment release, constant during the 8-day simulation period, was chosen to simulate the construction activities.

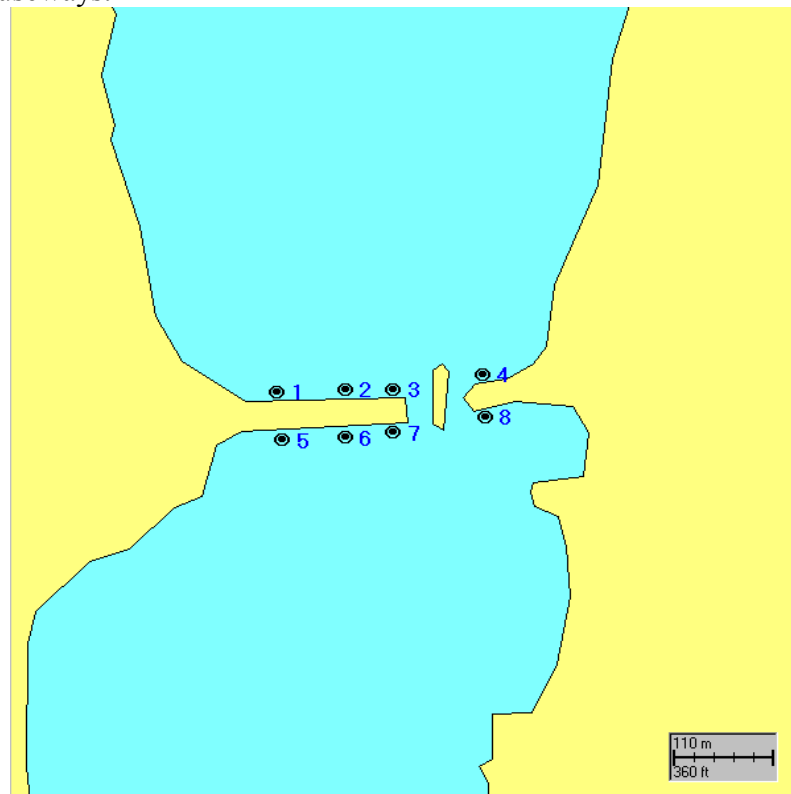
3.1 Bottom Sediment Samples

Bottom sediment samples were collected at eight locations, four each north (station 1 – 4) and south (station 5 – 8) of the causeways (Figure 3.1). The grain size analysis indicated that the dominant size fraction of the sediment in the area is sand, composing more than 66% on average of the total composition. It is followed by silt/clay

and gravel, respectively having 26% and 8% on average of the total composition fraction. The pattern of sand distribution is similar both north and south of the causeways, but the distribution is asymmetric in the east-west direction (Figure 3.2). More sand is found toward the east, with the highest amount observed at station 8 while the lowest fraction was detected at station 5.

The grain size for sand can be further divided into 5 sizes: very fine, fine, medium, coarse and very coarse sand. The average fraction with respect to the total composition was approximately 11, 20, 18, 10, 7%, in ascending order of size.

Figure 3.1. Locations of bottom sediment sampling site surrounding the Sakonnet River railroad causeways.



3.2 Settling Velocity

Each individual model run in a series of sediment simulations was generated assuming that the sediment was composed of a single particle size. The BFMAS model uses settling velocity to differentiate the particle types. Sediment particle size and its velocity are related in form of

$$V = \frac{1}{18} (d_1 - d_2) gr^2 / \mu \quad (\text{Allen, 1985}).$$

The equation above is Stokes law, in which d_1 and d_2 are the densities of the particle and water, respectively, g is gravity, r is the radius of the particle, and μ is the viscosity of water.

Figure 3.2. Sediment grain size composition analysis results for the eight bottom samples. Values shown at the bottom are weights of the three fractions in percent.

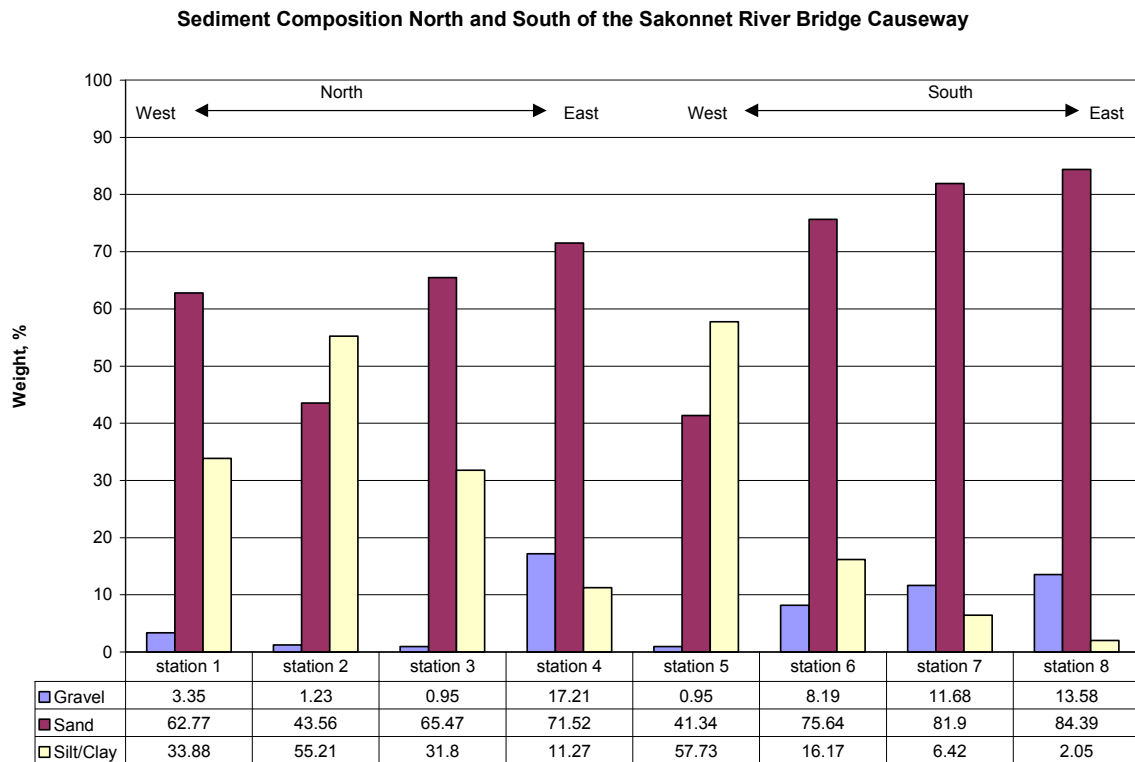


Table 3-1 shows the settling velocity for various types (sizes) of sediment particles. The velocity is estimated from Stokes law, using $\mu = 1.4 \times 10^{-3} \text{ kg/m s}$ ($9.4 \times 10^{-4} \text{ lb/ft s}$), $d_1 = 2650 \text{ kg/m}^3$ (164.30 lb/ft^3) and $d_2 = 1025 \text{ kg/m}^3$ (63.55 lb/ft^3). The table also shows the travel time for a vertical fall through 10 m of water. After release at the water surface, very coarse sand, which has large settling velocity (about 14000 m/d [0.32 kt]), takes only one minute to reach the bottom, and correspondingly it does not travel far horizontally. However, the finest grains travel the farthest distance in the horizontal before settling to the bottom layer. The range of particle grain sizes that we simulated is between very fine sand and clay.

3.3 Sediment Deposition Distribution

Analysis of the deposition distributions was made based on the two different configurations with correspondingly different model grids (with and without causeways) (Figure 2.6). Each case is further explored using different sediment releases. Table 3-2 lists the cases, the release site, and relation to the proposed alternatives for the Sakonnet River Bridge. There are three release locations considered for each configuration

alternative (Figures 3.3a and 3.3b). The first three scenarios include the existing causeway scenario. The last three scenarios include no causeway and the release sites are located in the general vicinity where the piers for the new bridge would be located. The amount of released material will vary with different construction activities. For the sake of simplicity, we used 11.6 g/s (0.026 lb/s), which is equivalent to 1 ton/day. This is a unit load to make computation simple. It can be scaled up and down to simulate actual loads.

Table 3-1. Sediment sizes, settling velocity and travel time for vertical distance of 10 m. The velocity is estimated using Stokes law (Allen, 1985).

Sediment Type	Radius (μm)	Settling Velocity (m/d)	Time for vertical fall through 10 m of water (day)
Clay	2	0.05	183.1502
Silt	15.6	3.32	3.0104
Very fine sand	100	53.32	0.1875
Fine sand	150	307.13	0.0326
Medium sand	300	1228.50	0.0081
Coarse sand	600	4914.00	0.0020
Very coarse sand	1000	13650.00	0.0007

Table 3-2. Sediment deposition scenarios, causeway configuration, sediment source locations and relation to rehabilitation/replacement alternatives.

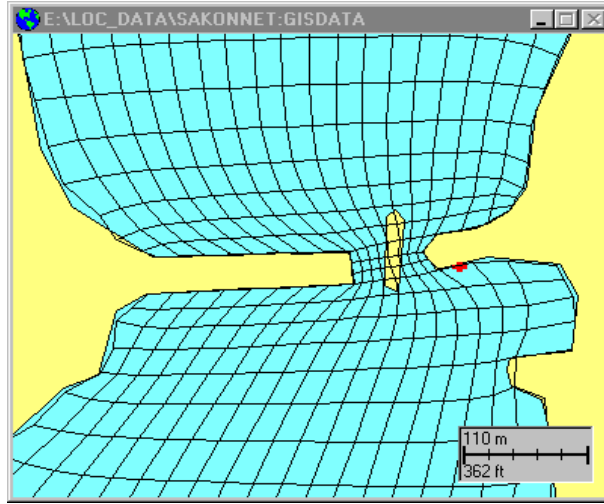
Scenario	Causeways	Location of sediment release	Related to the five alternatives
1	Yes	South of east causeway	1
2	Yes	North of west causeway	1
3	Yes	Waterway between causeways	1
4	No	East side of river	2, 3, 4, 5
5	No	West side of river	2, 3, 4, 5
6	No	Middle of the river	2, 3, 4, 5

Resultant deposition simulations are presented as predictions of thickness of the sedimentation layer, in units of micrometers, or equivalently, 4×10^{-5} inches. The raw BFMAS output of the simulation is particle concentration defined in mass per area units, and a conversion was applied to find the sediment thickness T:

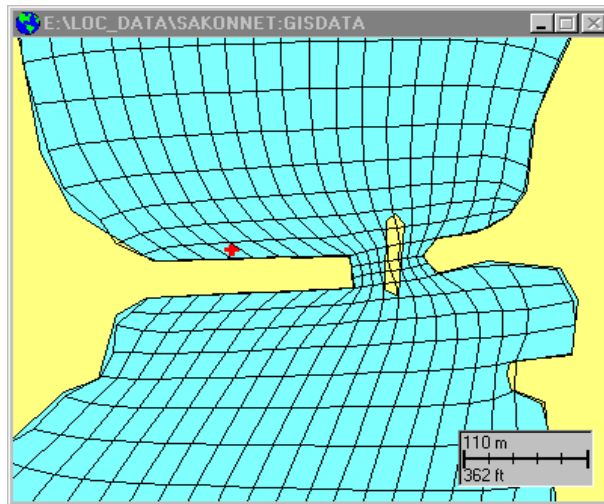
$$T = \frac{C_s}{C_b},$$

Figure 3.3a. Locations of the sediment release (cross) sites for scenarios 1, 2, and 3 (with the causeways).

Scenario 1



Scenario 2



Scenario 3

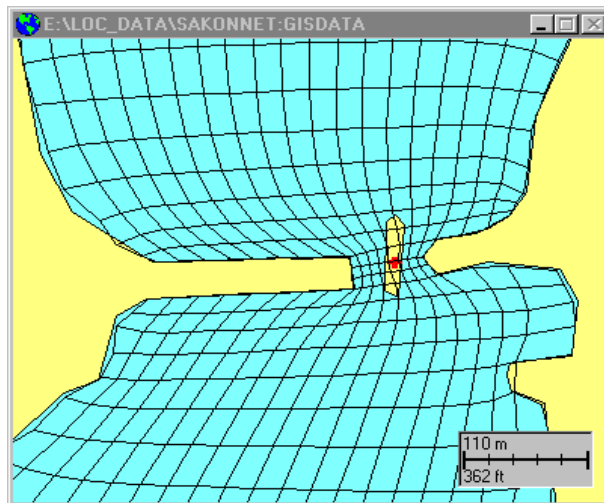
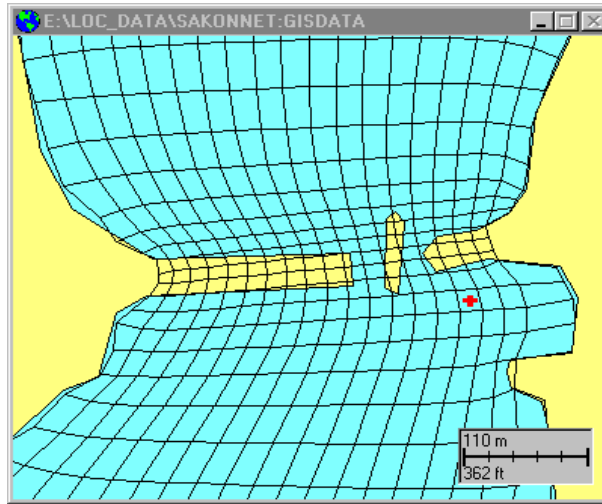
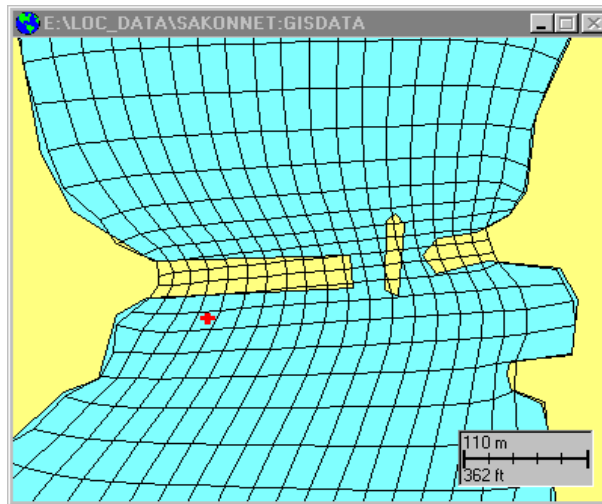


Figure 3.3b. Locations of the sediment release (cross) sites for scenarios 4, 5, and 6 (without the causeways).

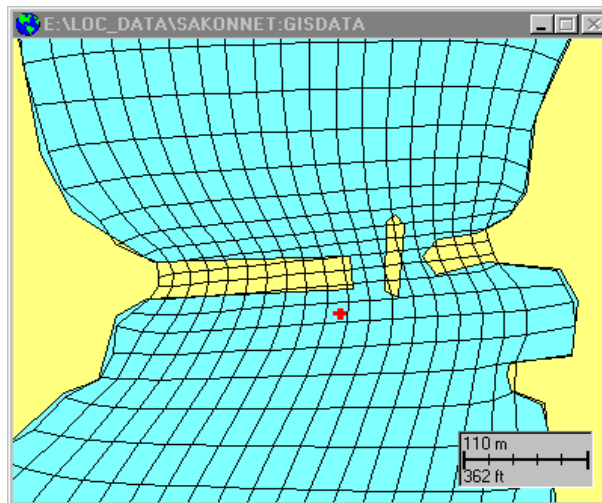
Scenario 4



Scenario 5



Scenario 6



where C_s is the particle concentration in mg/m^2 and C_b is the bulk density in mg/m^3 . A value of $1.84 \times 10^{-9} \text{ mg}/\text{m}^3$ ($0.114 \times 10^{-15} \text{ lb}/\text{ft}^3$) was used for the bulk density (Allen, 1985).

A common result in all the simulations is the occurrence of deposition immediately to the north and south of a release site. The deposition of the released materials depends on the tidal cycle: accumulation occurs to the north side during flood and to the south side during ebb. The currents observed in the study area have the double-flood pattern over one tidal cycle, regardless of the existence of the causeways. Consequently, there are different rates of transport and deposition to the north and south of the site.

There is another common result among all the simulations. The slower the particle settling velocity, the further it travels. However, clay particles do not travel the farthest even though they have the slowest settling velocity. The reason is that the clay particles are caught in the returning tidal flow since the period of the tidal flow is too short for the small particles to settle all the way to the bottom. The particles are instead carried back and forth by the tidal flow.

The current pattern is an important component in the deposition distribution. If the location is close to the shore, where the current is low, the deposition is expected to be higher in the shallow areas. Conversely, in the middle of the river where the currents are the fastest, it is expected that the particles will be carried away from the source ultimately settle in shallower areas. However, we observed higher deposition near the site and less away from the source. This can be explained by the continuous load that we used. The general pattern of the distribution is an elongated plume shape whose axis is parallel to the river. The distribution across the river is much shorter than the river axial direction. Another component controlling the shape is the horizontal dispersion. In general, the value of this parameter is not well defined. For this study, we used a median value of $0.1 \text{ m}^2/\text{s}$ ($1.08 \text{ ft}^2/\text{s}$)

Figure 3.4 shows a series of the BFMASS deposition simulations related to scenario 1. They show individual particle size results that are later added to estimate the total accumulation. Each figure presents a layer thickness of a single particle size at simulation-day 5. The day 5 is arbitrarily chosen. However, the deposition rate is generally linear with time. The accumulation for a desired period can be estimated by scaling these results to the appropriate length of time. The sediment source location is to the south of the east causeway (Figure 3.3a-(a)) with a 1-ton/day load, and is the same for all particle sizes. More deposition occurs at the south of the east causeway, which is very conspicuous for relatively larger particles (Figure 3.4b and 3.4c). It should be noted that these deposition thicknesses are very small, $0.5 \mu\text{m}$ is 2×10^{-5} in and $500 \mu\text{m}$ is 2×10^{-2} in.

For the total thickness of mixtures of the three particle sizes, we scaled the individual simulations to the exact fraction and then added them together. Table 3-3 lists the fractions in percent, which are determined as the average from the bottom sediment samples collected around the causeways. The remainder of the sediment, coarse sand

Figure 3.4a. Deposition distribution (μm) of clay particles with settling velocity of 0.05 m/d (1×10^{-6} kt) at simulation-day 5. The BFMASS grids include the causeways (the present condition), and the sediment source is located to the south of the east causeway. Deposition units conversion is $1 \mu\text{m} = 0.00004$ in.

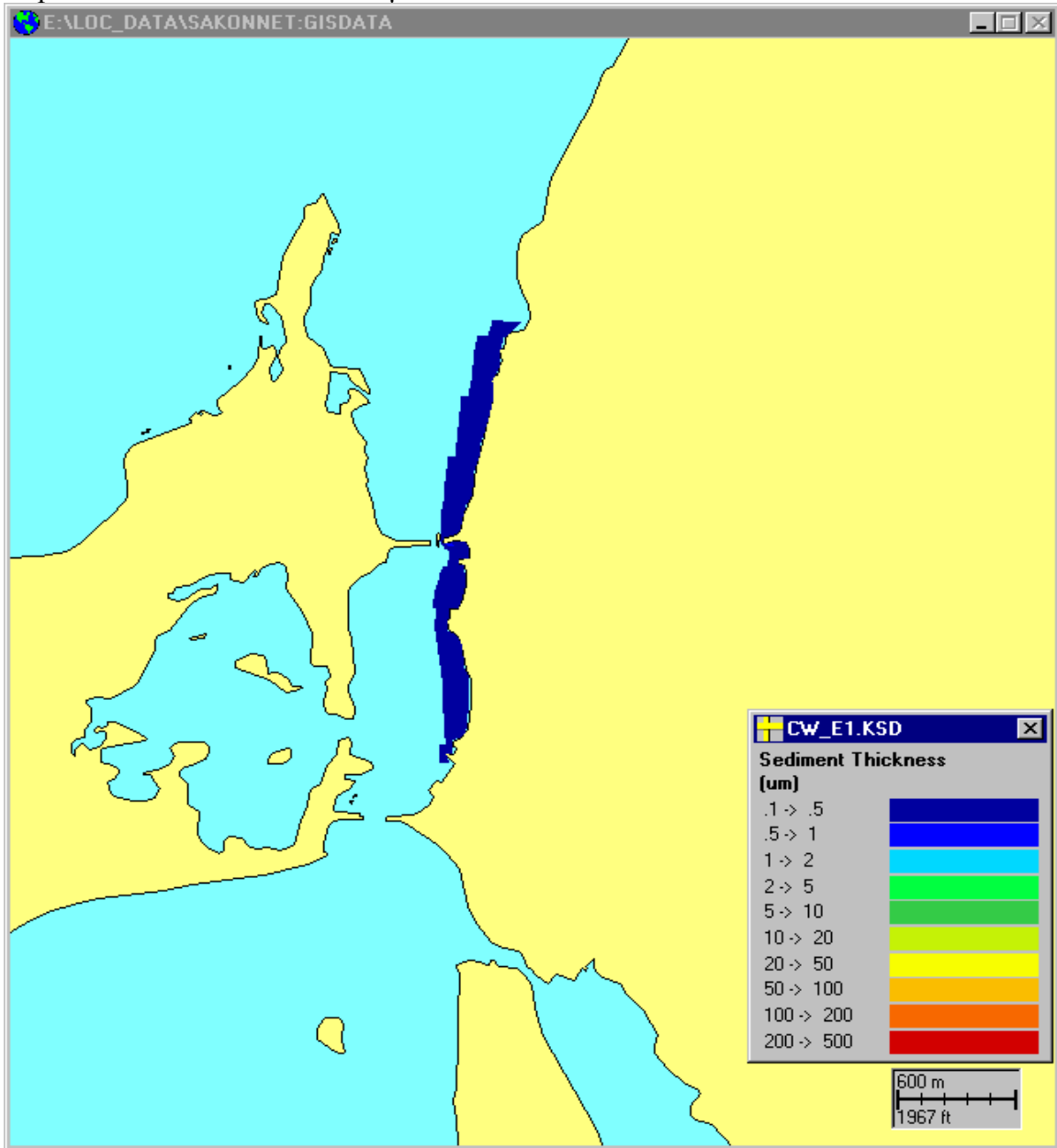


Figure 3.4b. Deposition distribution (μm) of clay particles with settling velocity of 3.32 m/d (7.7×10^{-5} kt) at simulation-day 5. The BFMASS grids include the causeways (the present condition), and the sediment source is located to the south of the east causeway. Deposition units conversion is $1 \mu\text{m} = 0.00004$ in.

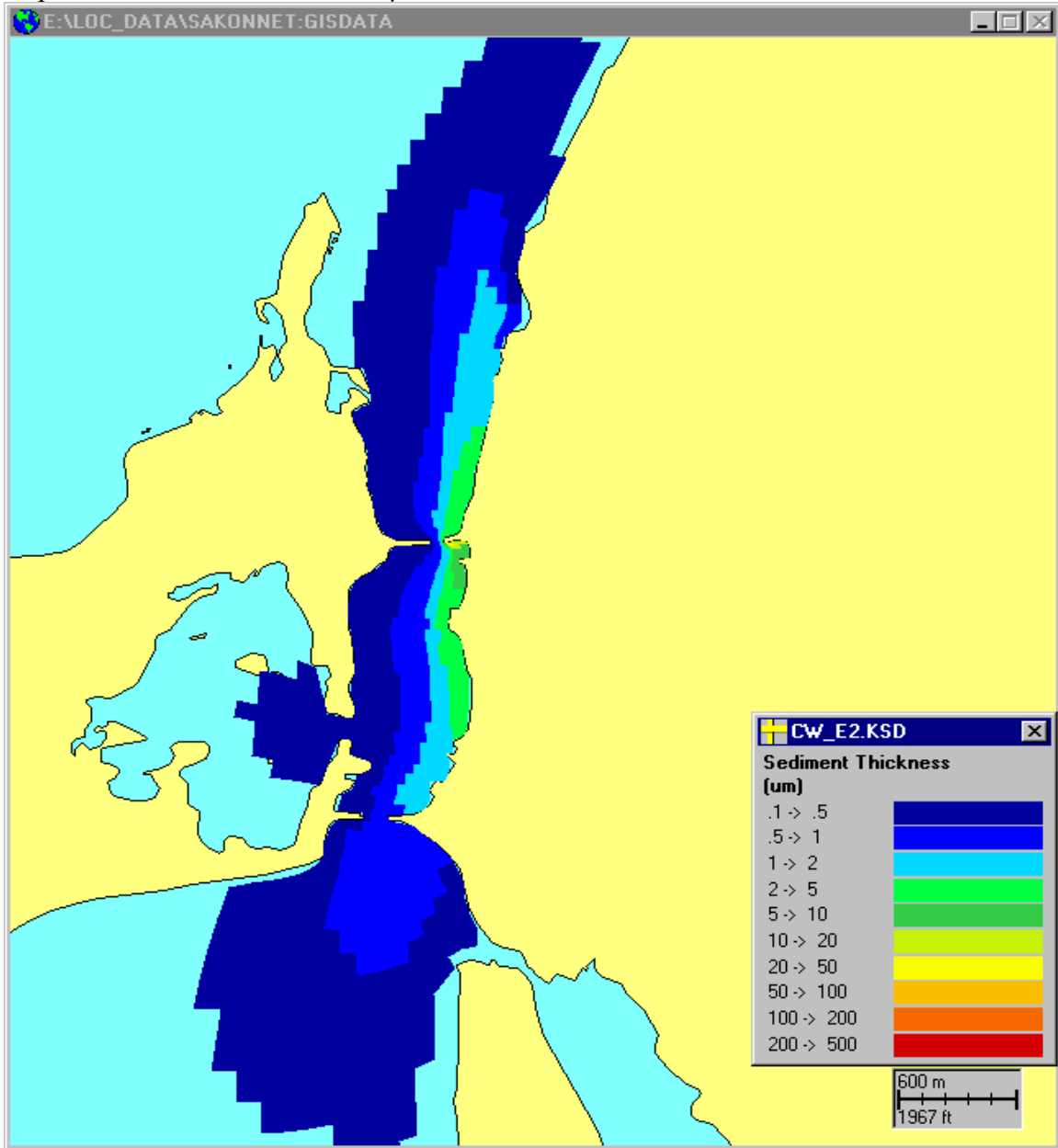
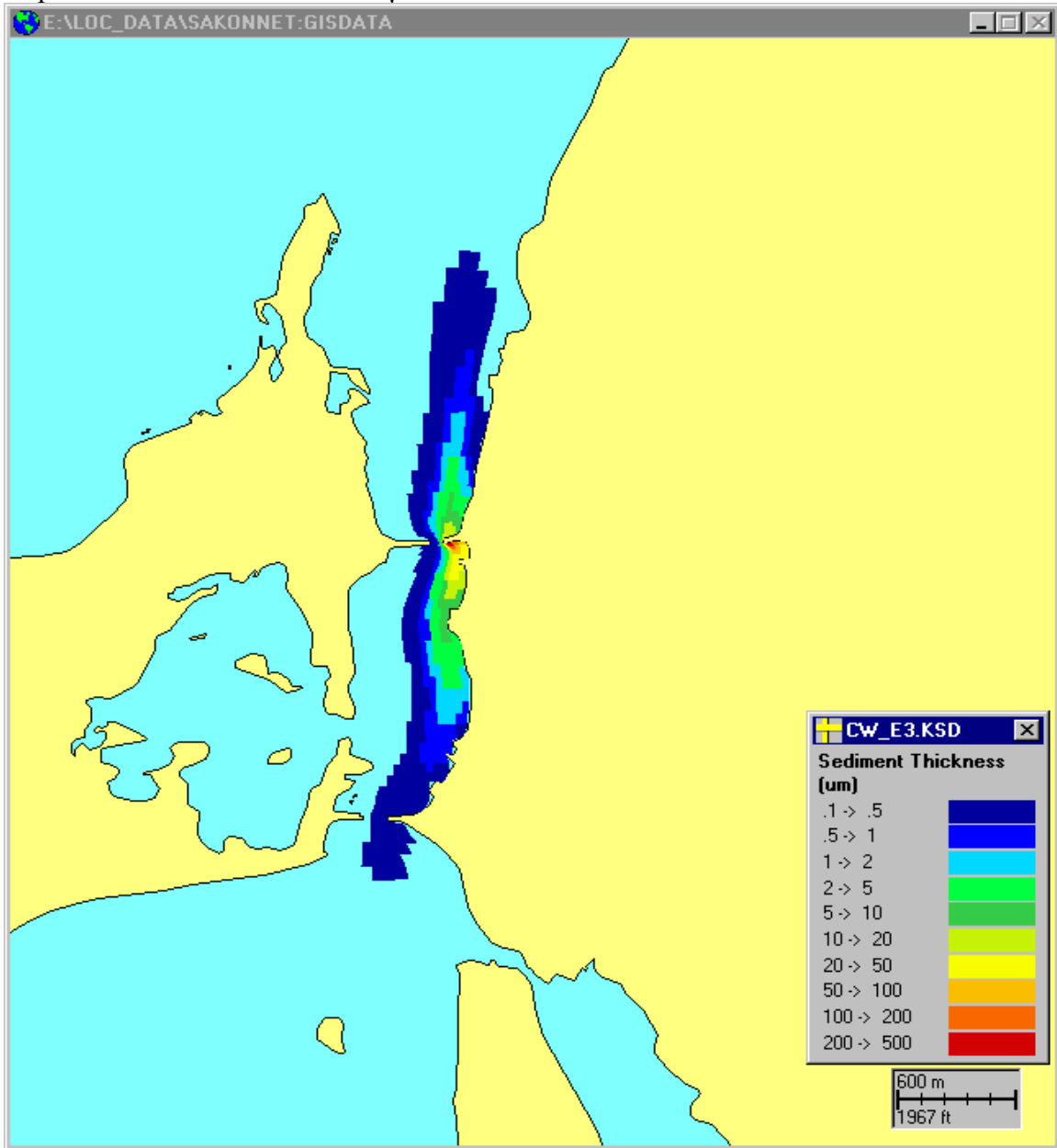


Figure 3.4c. Deposition distribution (μm) of clay particles with settling velocity of 53.32 m/d (1.2×10^{-3} kt) at simulation-day 5. The BFMAS grids include the causeways (the present condition), and the sediment source is located to the south of the east causeway. Deposition units conversion is $1 \mu\text{m} = 0.00004$ in.



(55%) and gravel (8%), will fall immediately to the bottom at the source location because of their higher fall velocities.

The sedimentation rate of the large particle sizes can be estimated by dividing the load by an appropriate area and the bulk density. Through a 10-m (32.81 ft) water column, a large grain size such as coarse sand will take 3 minutes to fall to the bottom. However, before it reaches the bottom it would be advected by the ambient currents. For typical waterway speeds of 0.5 m/s (1.0 kt) in the north-south direction and 0.1 m/s (0.2 kt) to the east-west direction, the particles would cover an area of 1,620 m² (17,437.53 ft²). Assuming that when a large grain size release of 1-ton/day accumulates in the area and the bulk density for the particles is 2 g/cm³ (124 lb/ft³), the accumulation of these particles is 0.03 cm (9.9×10⁻⁴ ft) per day. In the bottom sediment samples, the large size particles constitute 51.6% of the total composition. Accordingly, the accumulation rate by the larger size grains is 0.015 cm/day (4.9×10⁻⁴ ft/day). This estimate is somewhat larger than the deposition by the smaller size particles (clay, silt and very fine sand).

Table 3-3. Average composition fractions and sediment particles.

Particle classification	Composition fraction, %
Very fine sand	11.1
Silt	21.5
Clay	5.7

Results of the fine grain combination are shown in Figure 3.5. The total accumulation distribution in the near field is mostly the sand fraction (scaled down from Figure 3.3c), because its bulk density is larger than the two smaller grain sizes (silt and clay). The far field distribution is similar to the silt fraction distribution (scaled down from Figure 3.3b). The thickest layer is 340 μm (0.013 in), located at the release site. A rate of the layer decrease in space is higher in the direction perpendicular to than along the river axis. The suspended material, mainly silt, can reach about 0.88 km (2887.14 ft) to the north (from the release site to the 2 μm (8×10⁻⁵ in) contour, which is almost two order of magnitude smaller than the maximum) and 1.18 km (3871.39 ft) to the south after 5 days.

Figure 3.6 shows the combined results for scenario 4, with the causeways removed. Compared to the results in Figure 3.5, there is no significant difference in terms of the distribution pattern: deposition in the shallower areas, dissimilar travel distances to the north and south, and a general elongated pattern in the axial direction. The exceptions are that the thickest layer is 390 μm (0.015 in) at the release site, and the deposition in the near field is symmetric. With the same amount of load, the scenario without the causeways results in more accumulation to the north and the distribution extends farther to the north and south. The distance from the site to the 2 μm (8×10⁻⁵ in) layer front is 1.42 km (4,658.79 ft) and 1.27 km (4166.67 ft) to the north and south, respectively.

Analysis of the sediment deposition for the rest of the scenarios is as follows: Figures 3.7 to 3.10 present the layer distribution at simulation-day 5 for scenarios 2 through 6, respectively. The main difference between the scenarios with and without the causeways is the longitudinal extent of the deposition distribution. The broader and longer extent is found for the scenarios without the causeways, relative to the condition with the causeways. Table 3-4 lists the north and south extents from the release site, defined as the distance from the site to the $2 \mu\text{m}$ (8×10^{-5} in) contour, and maximum layer thicknesses at the release site.

Table 3-4. Maximum north and south extents of $2 \mu\text{m}$ (8×10^{-5} in) layer from the release site at simulation-day 5.

Scenario	Maximum layer thickness μm	North Extent		South Extent	
		km	ft	km	ft
1	345	0.88	2887.14	1.18	3871.39
2	40	0.78	2559.06	0.28	918.64
3	13	0.52	1706.04	0.37	1213.91
4	390	1.42	4658.79	1.27	4166.67
5	120	1.08	3543.31	1.33	4363.52
6	105	1.44	4724.41	1.29	4232.28

When the sediment release occurs to the north of the west causeway, the particles are not transported to the south of the causeway (Figure 3.7). This is evident in the north and south extents listed in Table 3-4. A similar result is expected when the release site is south of the causeway. On the other hand, with the release site at the east causeway, more deposition at the opposite side of the causeway is found (Figure 3.5). This is because the length of the east causeway is shorter than the west causeway by one third.

Maximum layer thickness at day 5 ranges between 13 (5×10^{-4} in) and $390 \mu\text{m}$ (0.015 in), and is located at the release site. The thickest layer is found for the sediment source locates close to the east river shore with the causeways (scenario 1), followed by the scenario without the causeways (scenario 4), while the thinnest sedimentation observed at the release site is for scenario 3. A comparison from Table 3-4 indicates that higher sediment deposition in near field and larger longitudinal extent in far field are expected for the scenarios without the causeways than with the causeways.

In this deposition simulation study, one assumption is made which might lead to uncertainty in the sediment thickness. In the conversion to thickness, a value for the bulk density is $1.84 \times 10^{-9} \text{ mg/m}^3$ ($0.114 \times 10^{-15} \text{ lb/ft}^3$) of sand and it is commonly used for the three particles. However, actual bulk densities for silt and clay are $1.45 \times 10^{-9} \text{ mg/m}^3$ ($0.090 \times 10^{-15} \text{ lb/ft}^3$) and $1.10 \times 10^{-9} \text{ mg/m}^3$ ($0.068 \times 10^{-15} \text{ lb/ft}^3$) g/cm^3 , respectively (Saxton et al., 1986), which are smaller by about 20% for silt and 40% for clay than the sand density. Thus, the final result for the layer thickness should be correspondingly increased by a factor of 1.27 for silt and 1.67 for clay. However, the increase does not

Figure 3.5. Deposition distribution (μm) after 5-day simulation for scenario 1. This is a super position of the individually weighted results shown in Figures 3.4a, 3.4b and 3.4c. The sediment release site is south of the east causeway. Deposition units conversion is $1 \mu\text{m} = 0.00004 \text{ in.}$

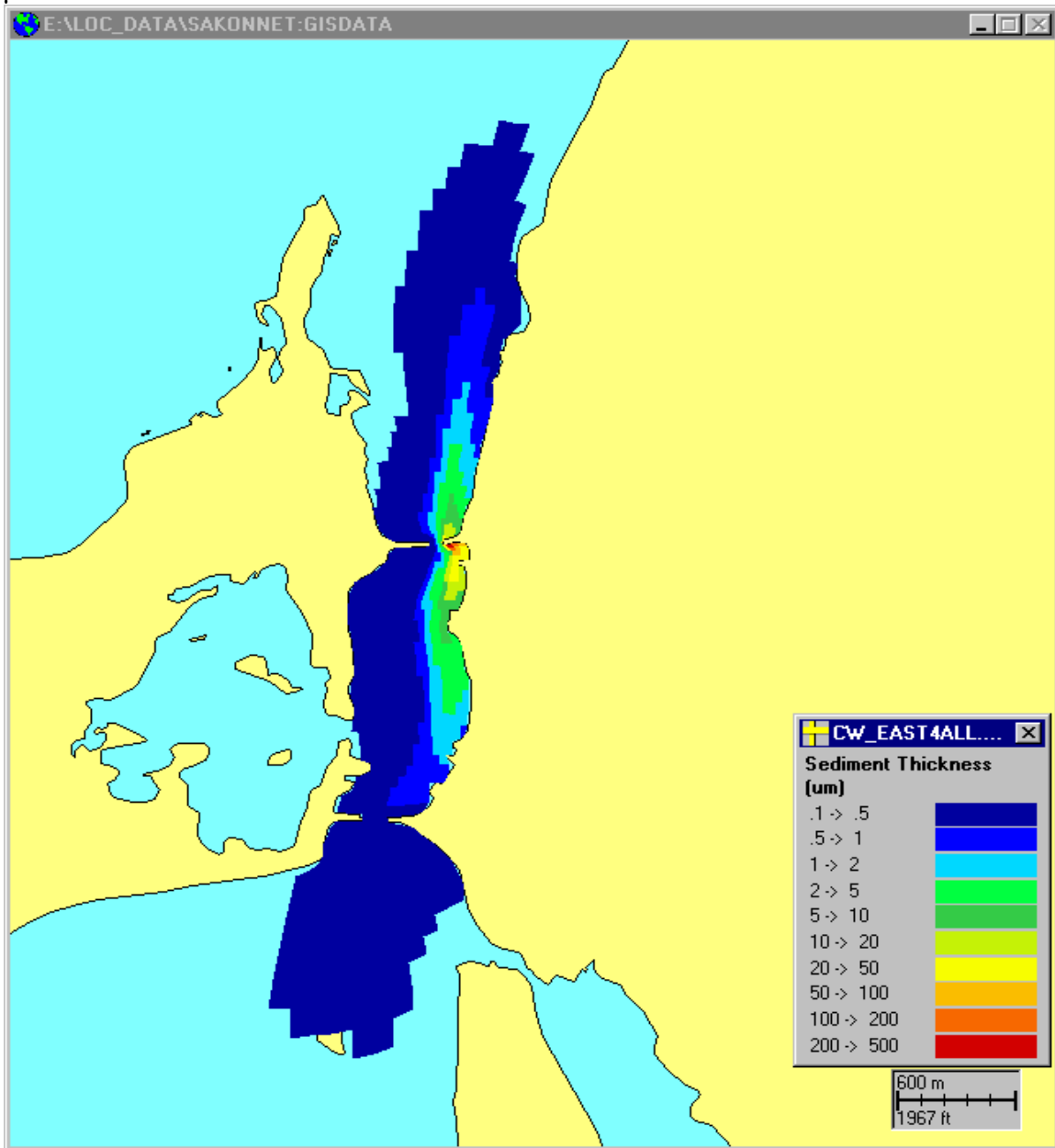


Figure 3.6. Deposition distribution (μm) after 5-day simulation for scenario 4. The sediment release site is at the east side of river. Deposition units conversion is $1 \mu\text{m} = 0.00004 \text{ in.}$

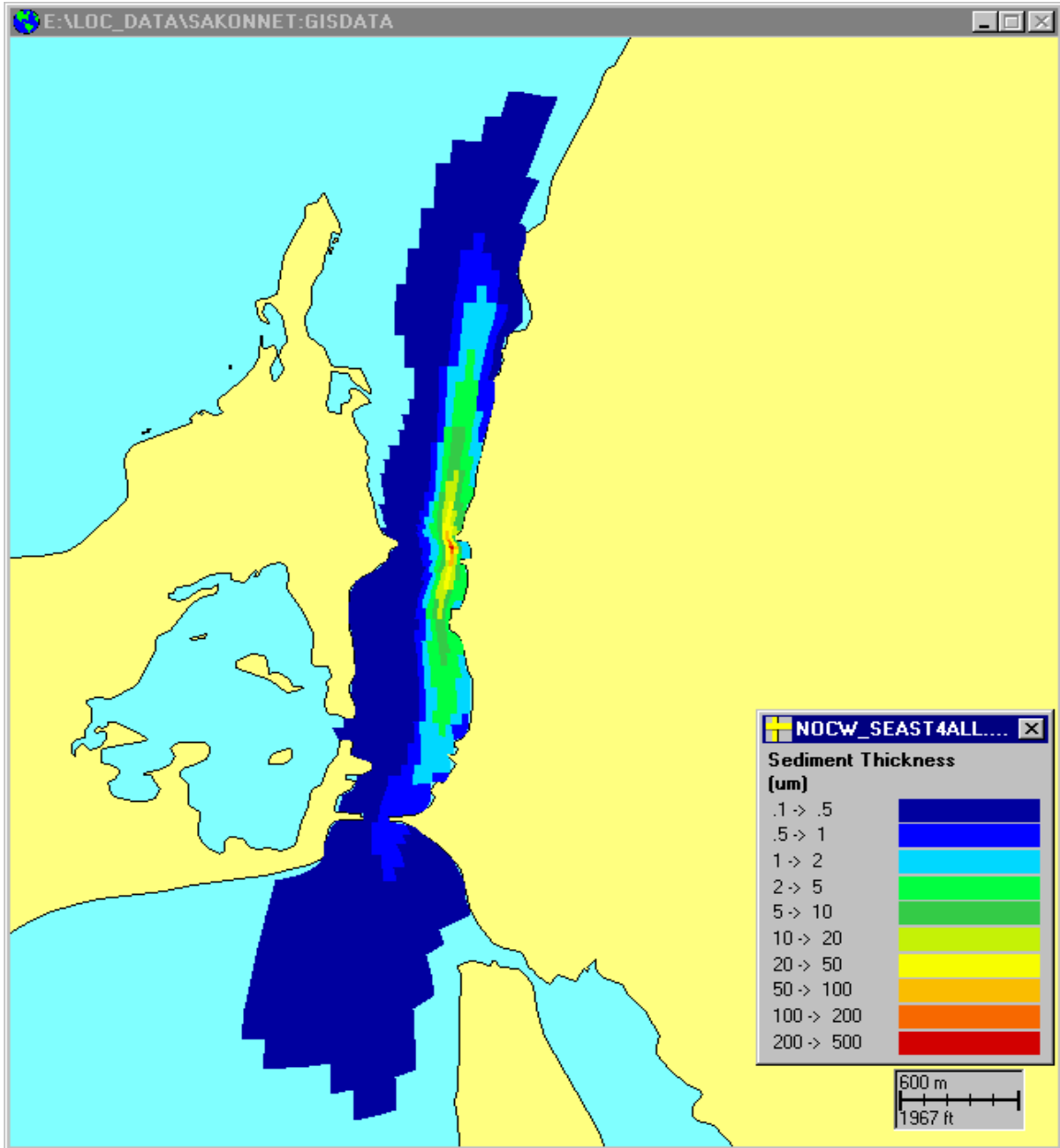


Figure 3.7. Deposition distribution (μm) after 5-day simulation for scenario 2. The sediment release site is north of the west causeway. Deposition units conversion is $1 \mu\text{m} = 0.00004 \text{ in.}$

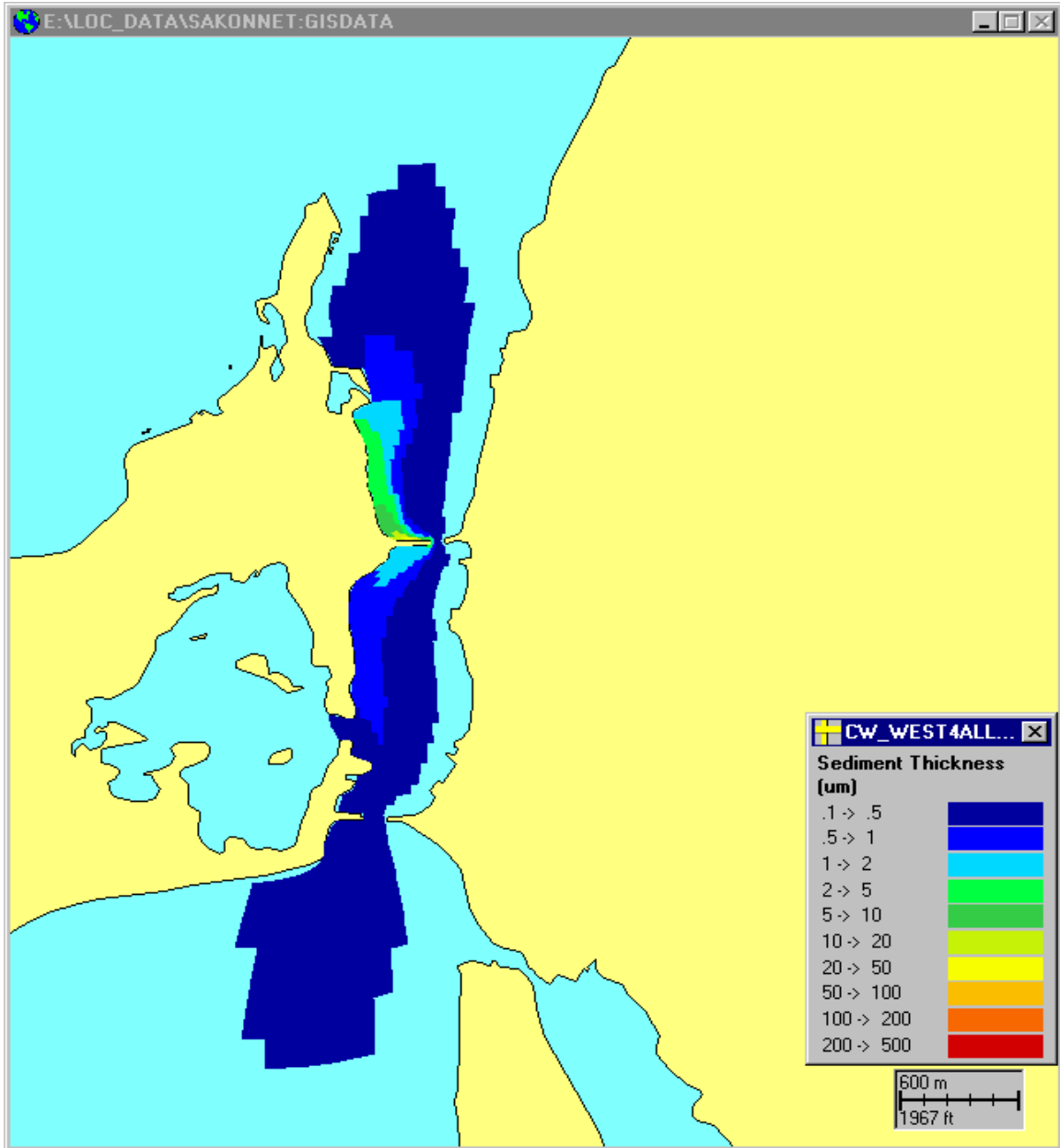


Figure 3.8. Deposition distribution (μm) after 5-day simulation for scenario 5. The sediment release site is at the west side of river. Deposition units conversion is $1 \mu\text{m} = 0.00004 \text{ in.}$

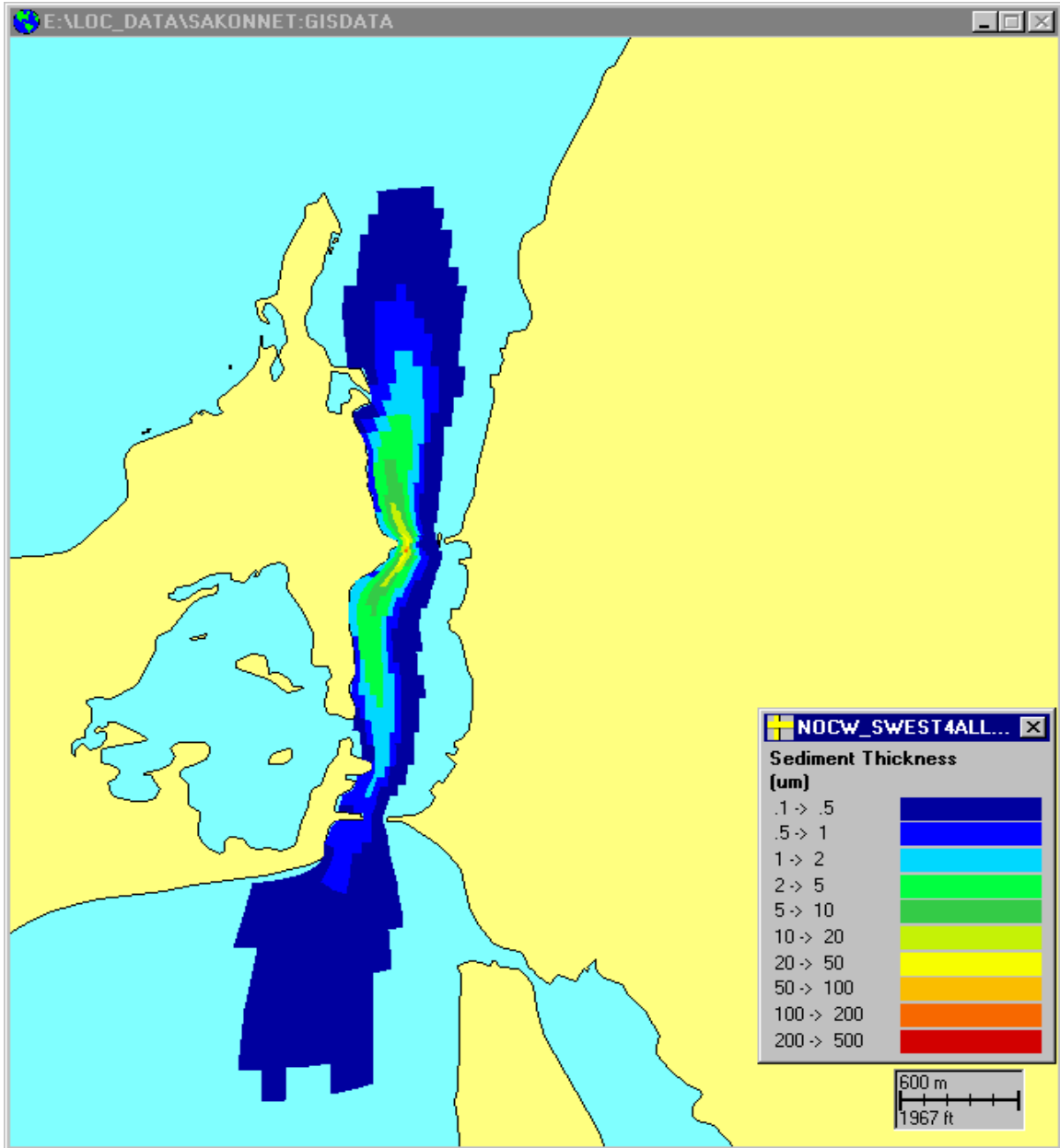
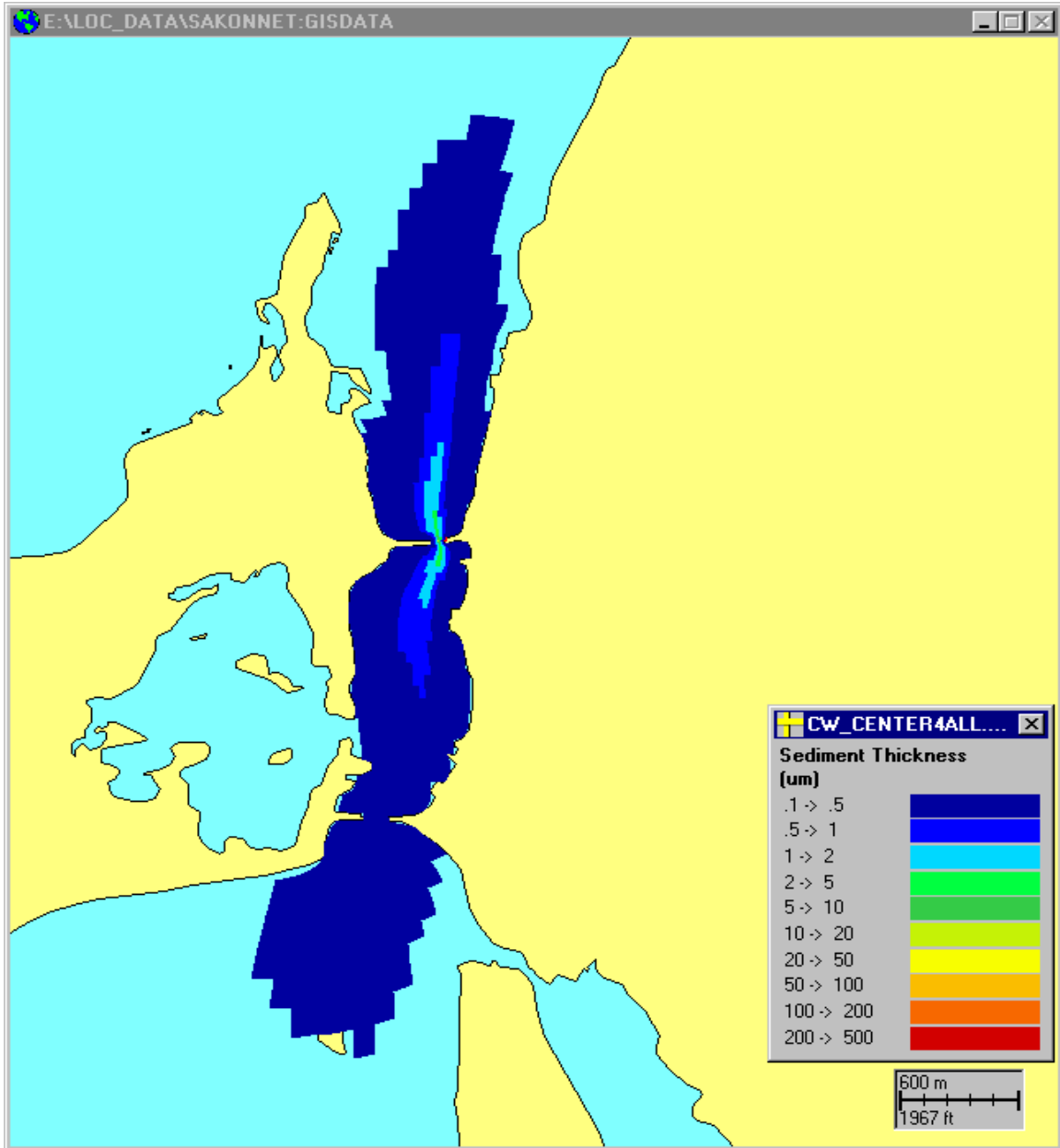


Figure 3.9. Deposition distribution (μm) after 5-day simulation for scenario 3. The sediment release site is at the opening waterway. Deposition units conversion is $1 \mu\text{m} = 0.00004 \text{ in.}$



make a significant difference to the results since the clay particles are a small fraction of the total composition and the total thicknesses are so small.

3.4 Sediment Transport

Since the semi-diurnal tides are dominant, the variation of suspended sediment concentration at a location would be expected to have the same period as the tides (12.42 hr). This is because the sediment particle is a passive tracer that moves in response only to the background hydrodynamic physics. As was done in the sediment deposition analysis, the transport simulations in the Sakonnet River are shown for the six scenarios: three different release sites and two different river configurations. Overall, maximum concentrations in the water column to the north and south of the release site are found at maximum flood and ebb currents, respectively. Figures 3.11 to 3.16 show distributions of the concentration in the water column at maximum flood and ebb. Each figure presents the two scenarios, with and without the causeways, for comparison. What is shown in the figure is the total concentration of three sediment particle fractions (silt, clay, and very fine sand). Coarse sand and gravel were not included because they do not remain in the water column but rapidly sink to the bottom.

The sediment transport shows similar distribution patterns for the configurations with and without the causeways except areal coverages and maximum water column concentrations are slightly different from scenario to scenario. During flood, when the release is close to the east river shore (Figures 3.11a and 3.11b), the coverage of concentrations greater than 0.1 mg/L is smaller with the causeways (scenario 1) than the area (0.065 km^2 [$0.704 \times 10^6 \text{ ft}^2$]) without the causeways (scenario 4) by about 26%. At maximum ebb (Figures 3.12a and 3.12b), the areal coverage is reversed. The areal coverage for the concentrations greater than 0.1 mg/L for scenario 1 is greater by 64% than the area (0.060 km^2 [$0.642 \times 10^6 \text{ ft}^2$]) for scenario 4. This is because the east causeway keeps the sediment from being transported to the south during ebb, whereas it keeps the sediment from being transported to the north during flood.

When a release is at the west side of the river (scenarios 2 and 5), the near field difference observed for the scenario 1 and 4 becomes more substantial. The west causeway becomes a barrier, playing the same role as the east causeway. However, the west causeway is as twice as long which makes the transport to the other side more difficult. The maximum concentration found during maximum flood (Figure 3.13a) is $520 \text{ } \mu\text{g/L}$ (Table 3-5). This is almost 1 times of the maximum value found in scenario 1, and 4 times of the value observed in scenario 5 (Figure 3.13b). During maximum ebb (Figures 3.14a and 3.14b), the maximum concentrations for scenarios 2 and 5 are 360 and $125 \mu\text{g/L}$, respectively, however the former scenario has a larger areal coverage than the latter.

When a sediment source is located at the middle of the river, the simulated distribution is an elongated plume shape as expected (Figures 3.15 and 3.16). The

Figure 3.11a. Sediment concentration in the water column at maximum flood for scenario 1. The sediment release site is south of the east causeway.

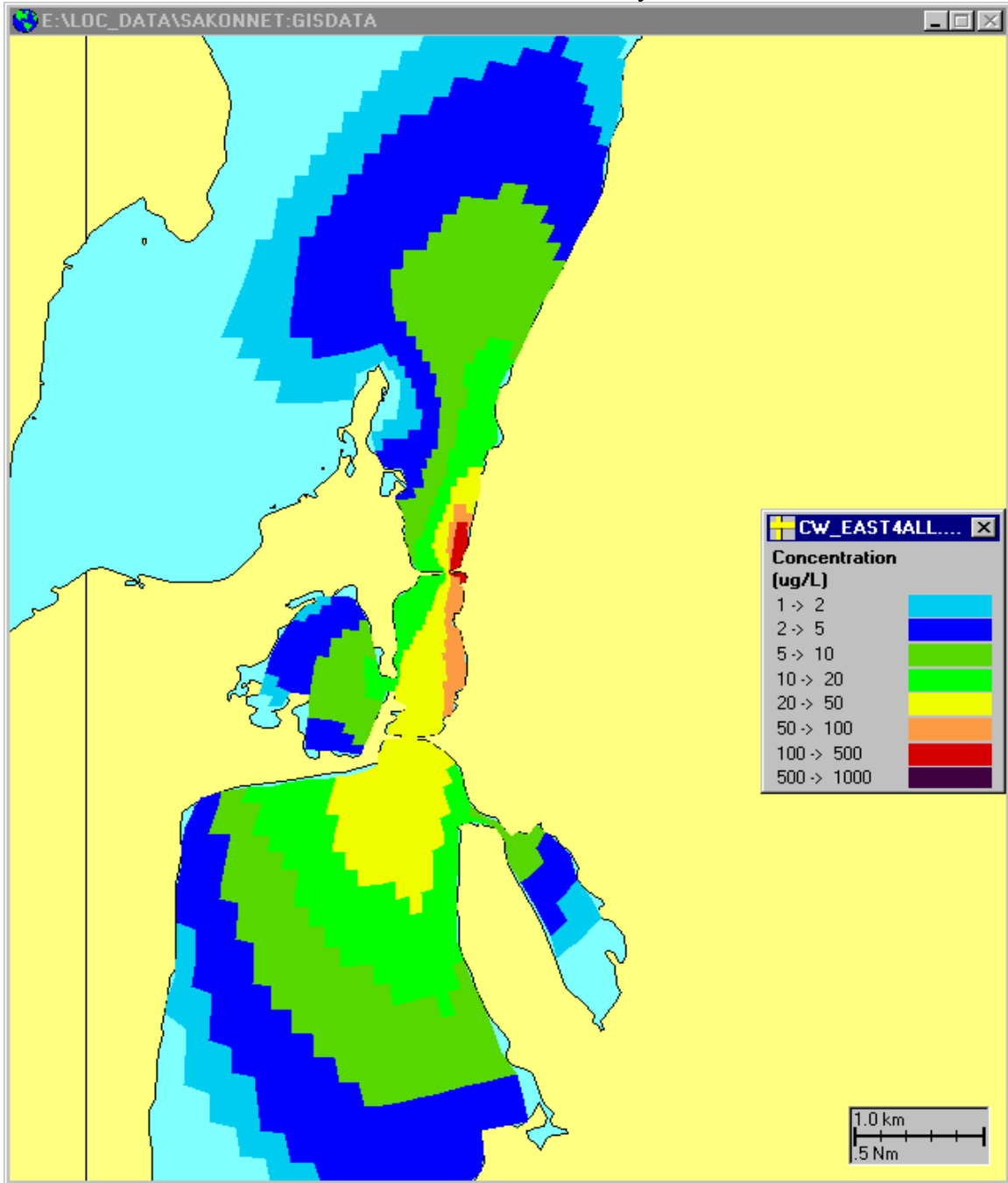


Figure 3.11b. Sediment concentration in the water column at maximum flood for scenario 4. The sediment release site is at the east side of river.

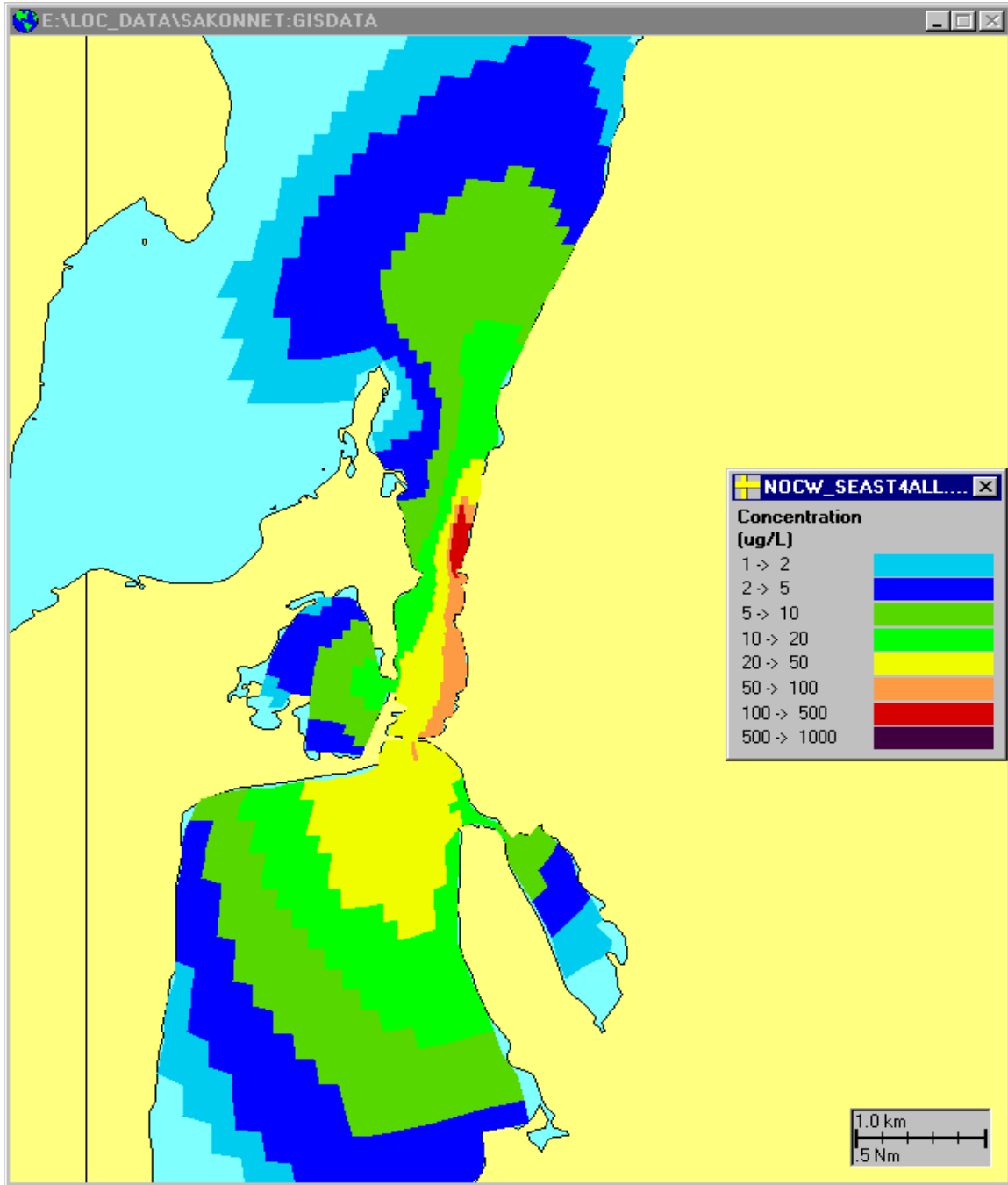


Figure 3.12a. Sediment concentration in the water column at maximum ebb for scenario 1. The sediment release site is south of the east causeway.

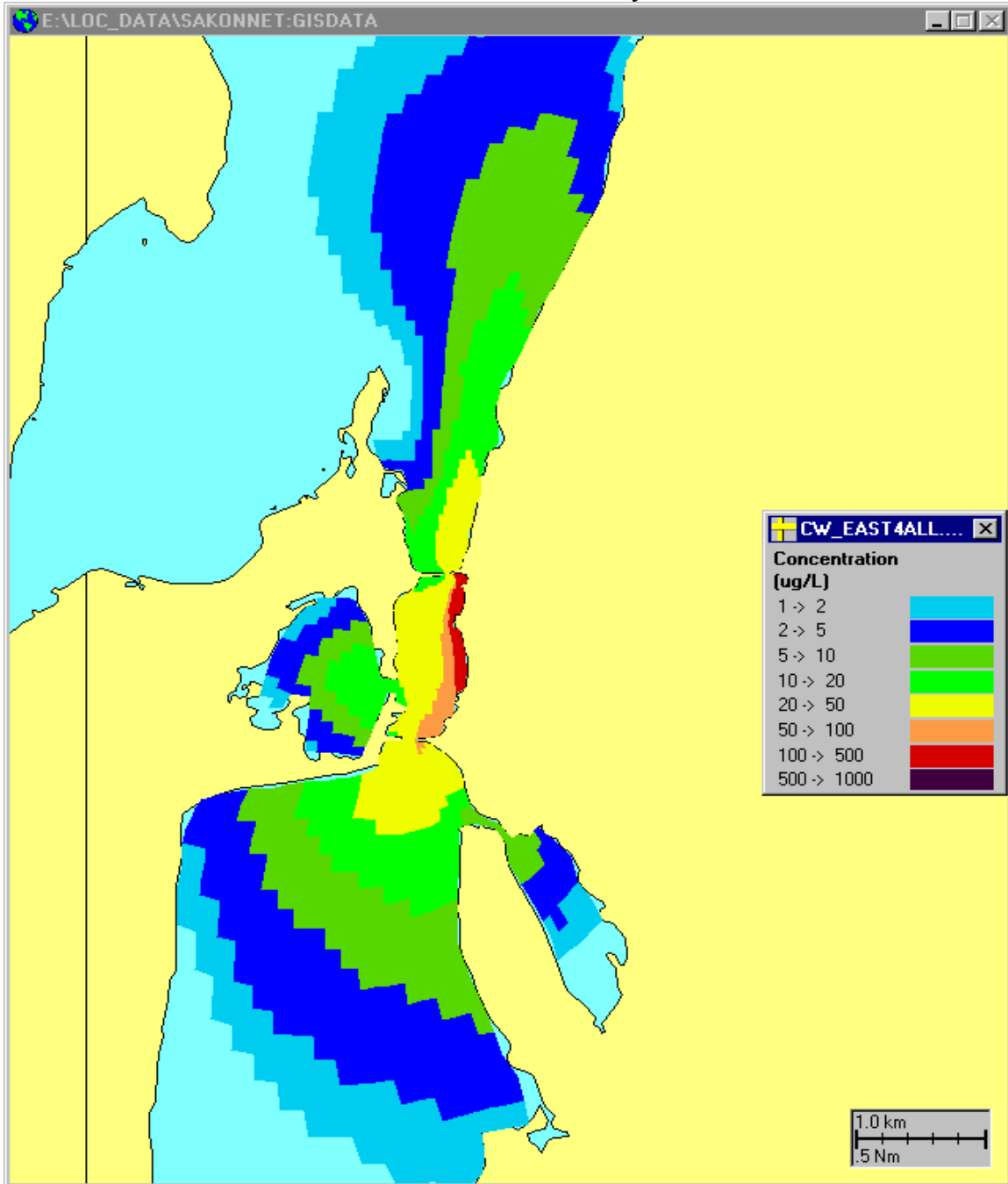


Figure 3.12b. Sediment concentration in the water column at maximum ebb for scenario 4. The sediment release site is at the east side of river.

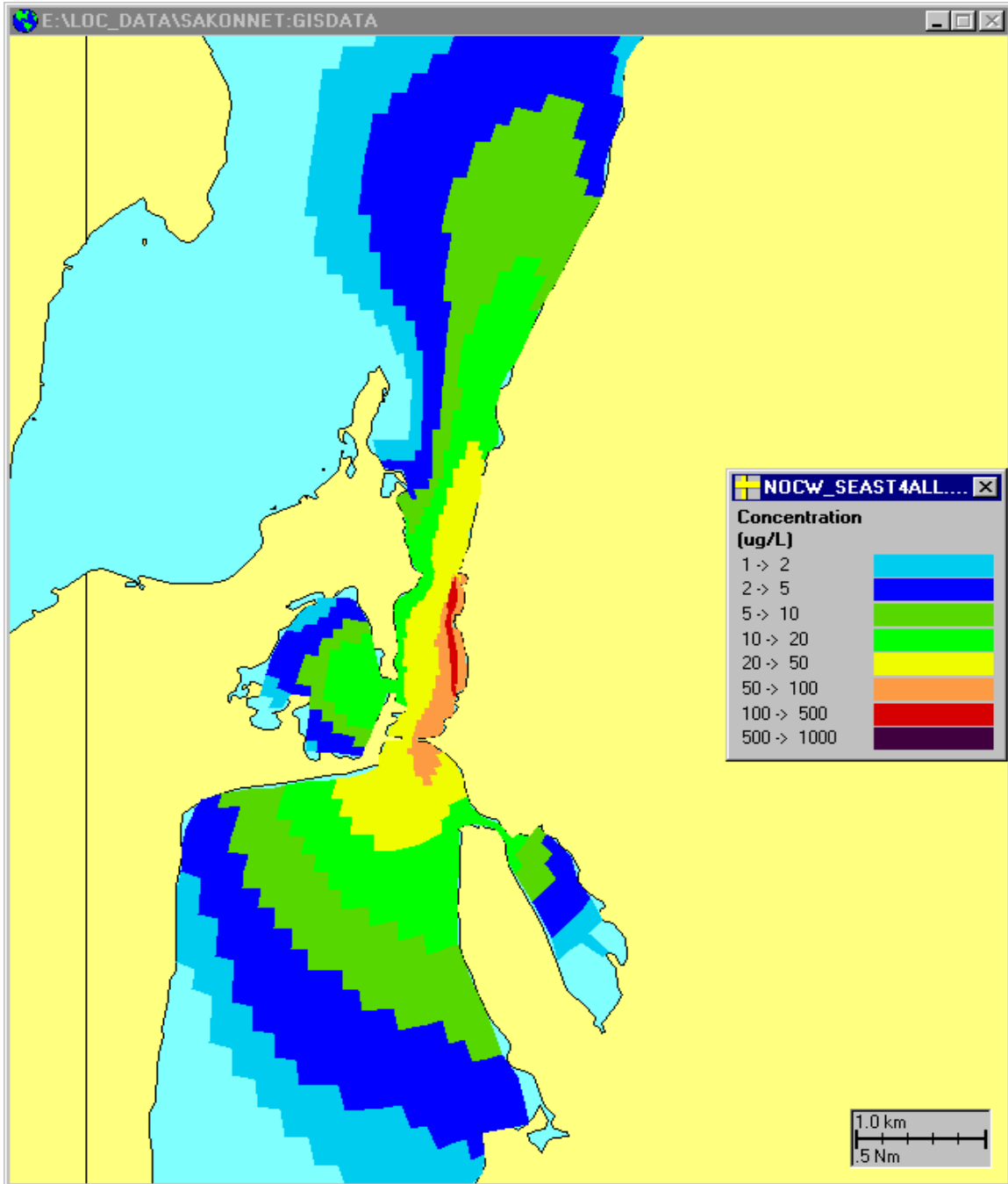


Figure 3.13a. Sediment concentration in the water column at maximum flood for scenario 2. The sediment release site is north of the west causeway.

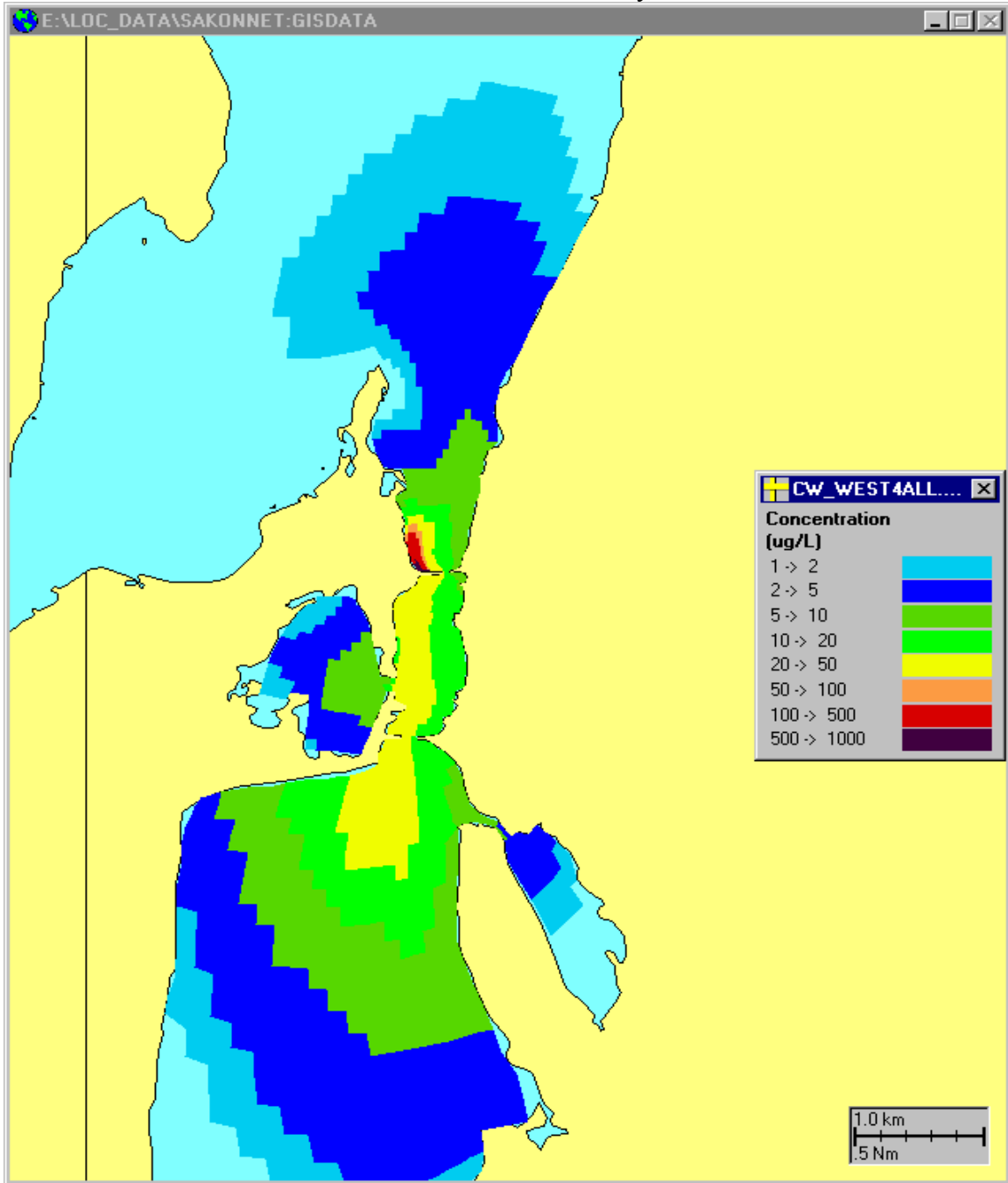


Figure 3.13b. Sediment concentration in the water column at maximum flood for scenario 5. The sediment release site is at the west side of river.

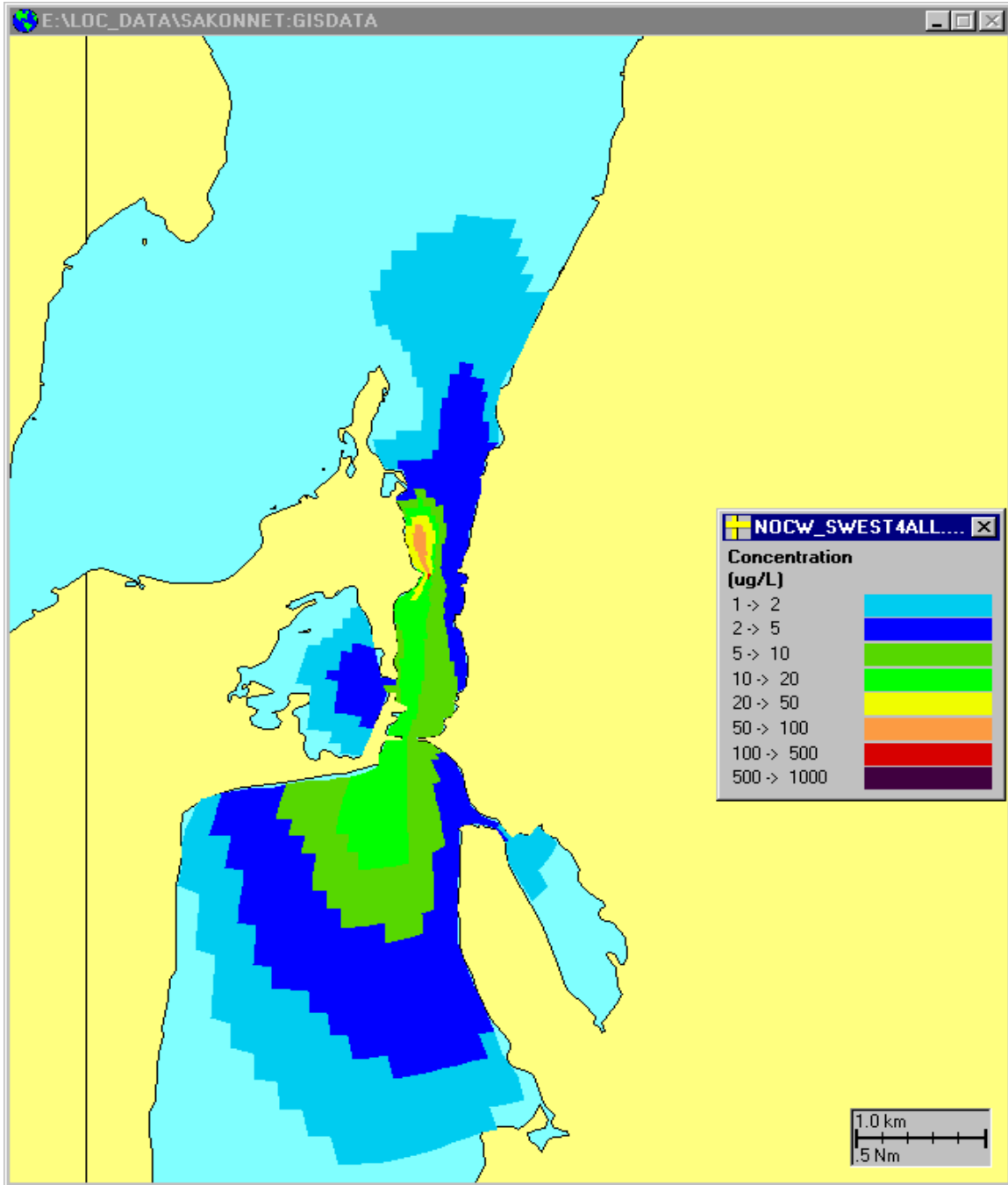


Figure 3.14a. Sediment concentration in the water column at maximum ebb for scenario 2. The sediment release site is north of the west causeway.

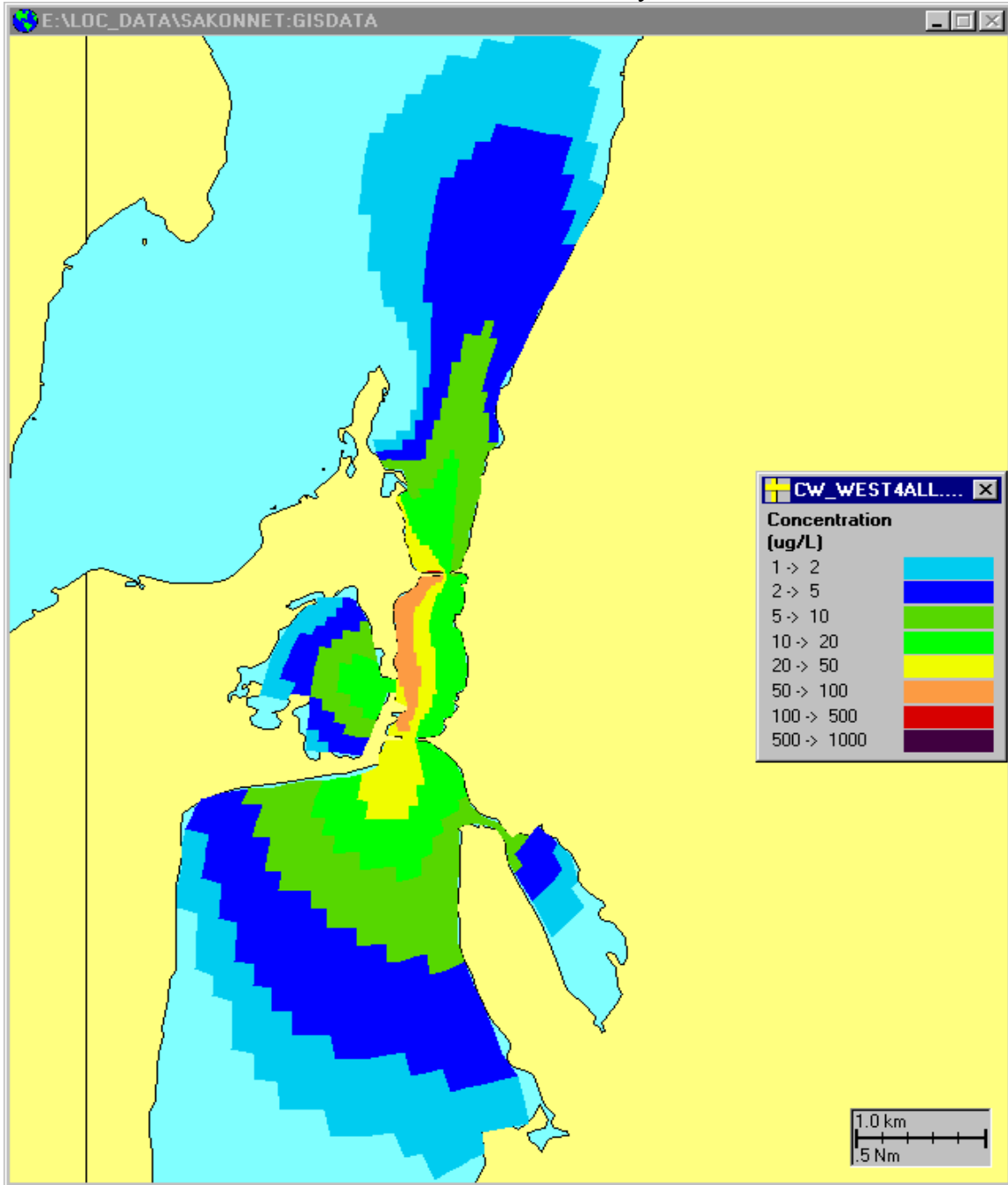


Figure 3.14b. Sediment concentration in the water column at maximum ebb for scenario 5. The sediment release site is at the west side of river.

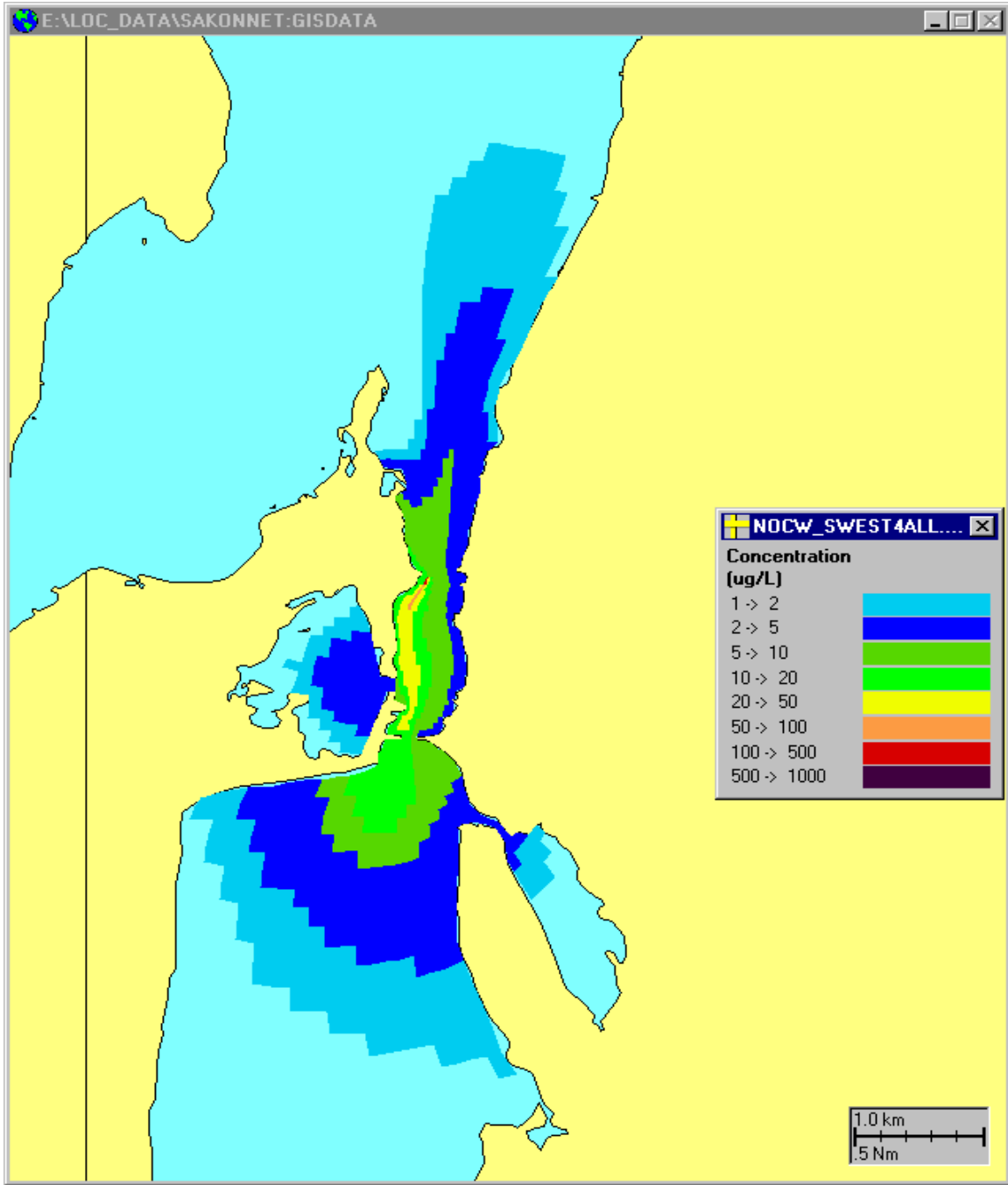


Figure 3.15a. Sediment concentration in the water column at maximum flood for scenario 3. The sediment release site is at the opening waterway.

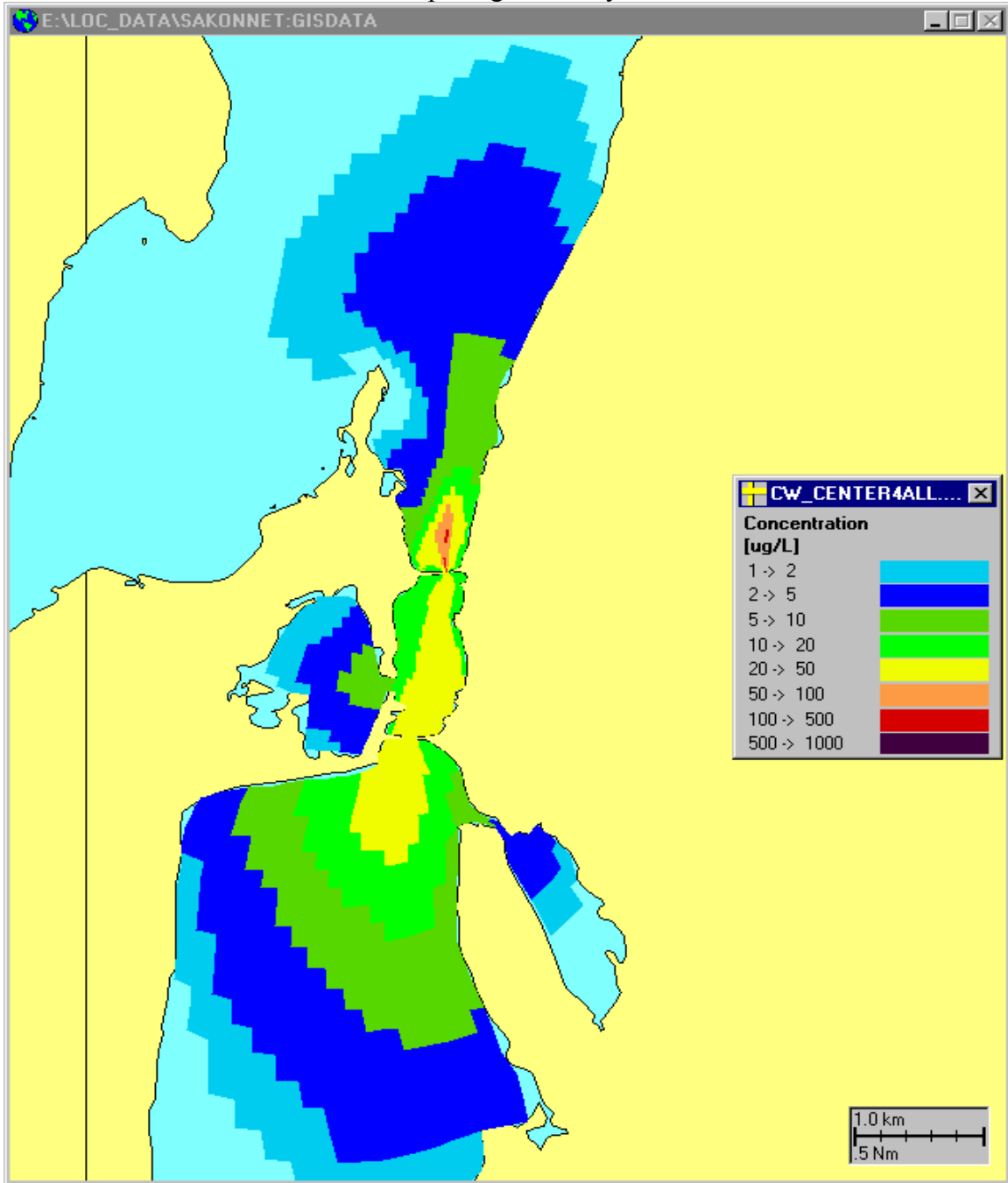


Figure 3.15b. Sediment concentration in the water column at maximum flood for scenario 6. The sediment release site is in the middle of river.

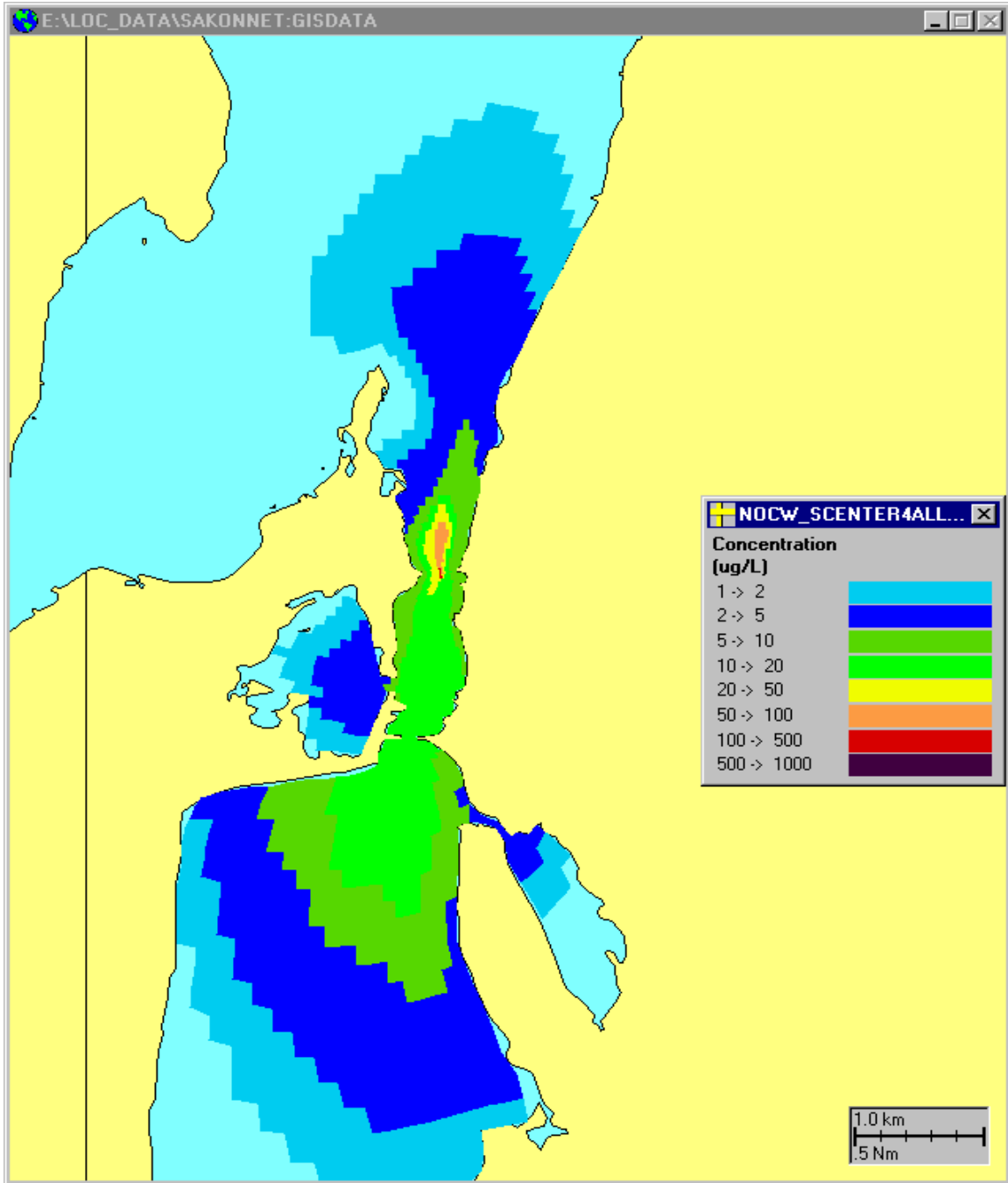


Figure 3.16a. Sediment concentration in the water column at maximum ebb for scenario 3. The sediment release site is at the opening waterway.

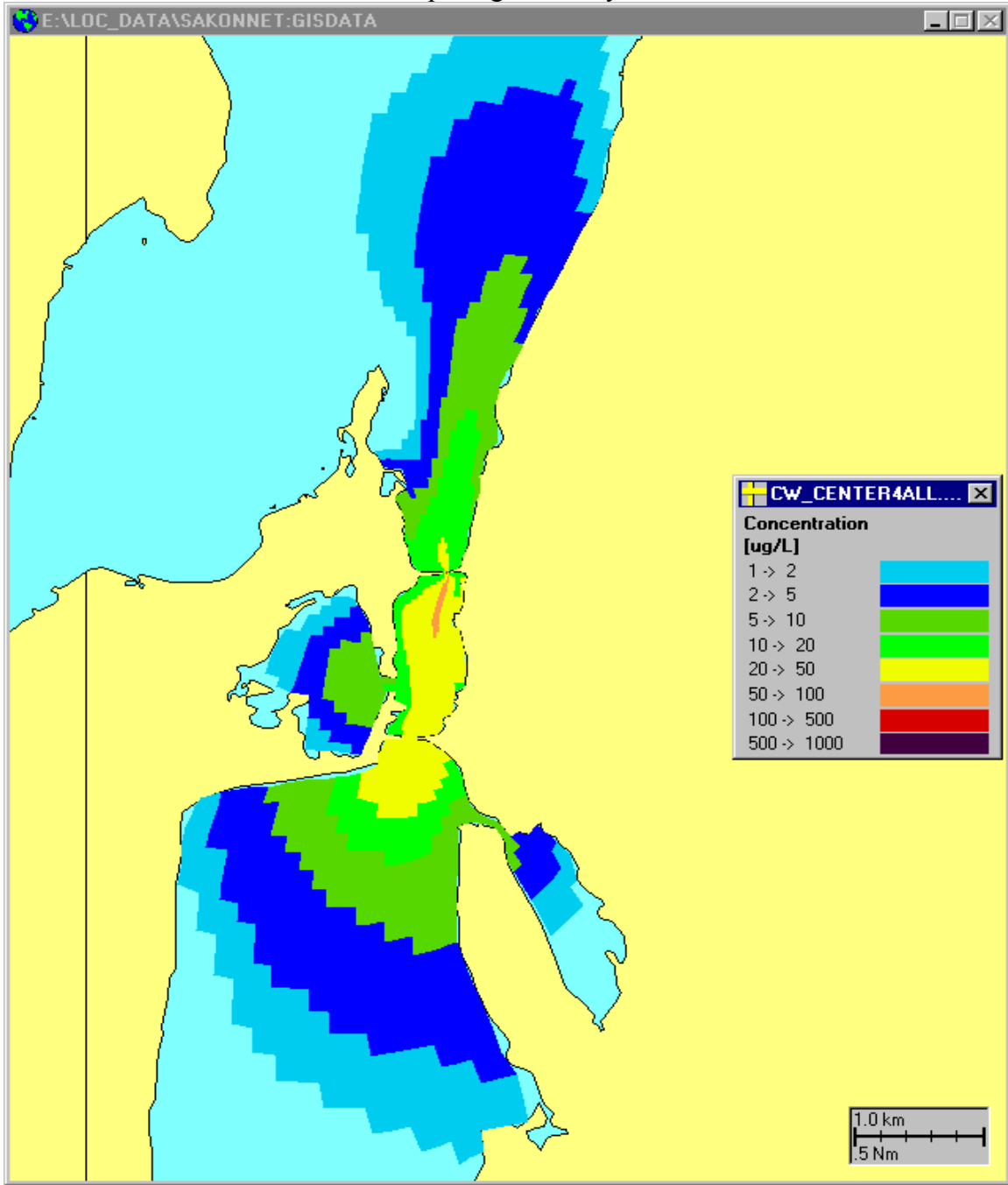
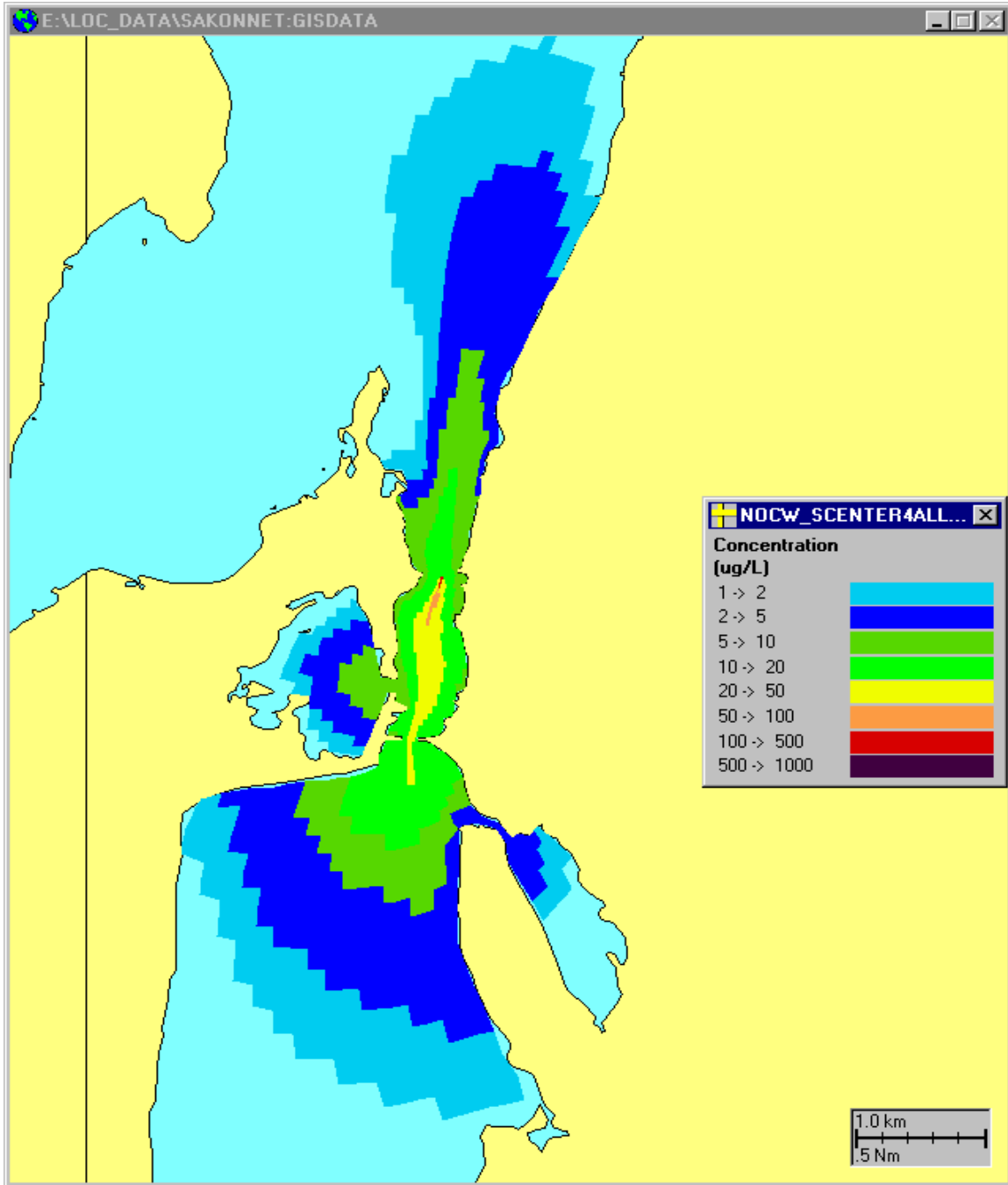


Figure 3.16b. Sediment concentration in the water column at maximum ebb for scenario 6. The sediment release site is at the middle of river.



difference first noticed between the scenarios is the maximum value and its areal coverage. Both are smaller for scenario 6 (without the causeways) than scenario 3 (with the causeways) during the flood (Figures 3.15a and 3.15b), similarly during the ebb (Figures 3.16a and 3.16b). This is because more sediment reaches the bottom, thus reducing water column concentration. The far field, however, is almost same for both the scenarios. A comparison of the simulation results for the center release versus the other release locations shows a smaller areal coverage of high concentration in the near field, but the same distribution in the far field.

Table 3-5 lists maximum suspended concentrations during flood and ebb. The values range between 0.12 and 0.55 mg/L for a unit load of 1-ton/day. With the causeways, the highest maximum concentration is found with a release site at the east river shore (scenario 1), followed by scenario 2, while low concentration is observed when the site is close to the west side of river (scenario 3). Without the causeways, high concentration is still found for the case with a release at the east (scenario 4). However, the lowest maximum value occurs when the release is at the west side of the river (scenario 5).

Table 3-5. Maximum suspended sediment concentrations (mg/L) at a release site and six sediment transport scenarios.

	Scenario 1	Scenario 2	Scenario 3	Scenario 4	Scenario 5	Scenario 6
flood	0.55	0.52	0.12	0.49	0.13	0.17
ebb	0.45	0.36	0.12	0.50	0.13	0.13

4. Conclusions and Summary

This study has evaluated potential impacts that five bridge construction alternatives will have on the hydrodynamics, sediment transport and deposition of the Sakonnet River and lower Mt. Hope Bay. The hydrodynamics were simulated with two representative scenarios using the ASA WQMAP BFHYDRO model, and the sediment transport and deposition modeling was performed for six different scenarios using the BFMASS model. The model grid was designed with various cell sizes, so that it resolves currents better in the narrow opening between the railroad causeways with fine cells, while it includes the bay-wide dynamics in the model system with coarse cells. The hydrodynamic scenarios were differentiated by the existence of the causeways, and the sediment transport scenarios were further discriminated by the locations of sediment release (east and west river shore, and middle of river).

The major result from the hydrodynamic simulations was the drastic decrease in speed if the causeways were removed. Under the present condition, *i.e.* with the causeways, the current speed ranged on average from 1.5 m/s (3.0 kt) at the open waterway between the causeways to 0.05 m/s (0.1 kt) as close to river shore. Without the

causeways, the mean speeds were in $O(0.25 \text{ m/s [0.5 kt]})$. The current pattern consisting of two floods and single ebb, however, was persistent for both the conditions.

The assessment of sediment transport and deposition focused on three grain sizes: very fine sand, silt and clay. The deposition and transport distributions both formed an elongated plume whose axis was almost aligned with the river axis. Over 5-day simulations with a continuous sediment release at a rate of 1 ton/day, the maximum sediment layer thickness was 0.01 - 0.4 mm ($5 \times 10^{-4} - 1.6 \times 10^{-2}$ in), and it was located either at the release site or close by in the near field. This estimate excluded the contribution by the larger grain sizes such as coarse sand or gravel, which fall almost immediately down to the bottom. The contribution by the larger grain sizes after 5 days increased the maximum thickness to 0.75 mm (~ 0.03 in) for a 1,620 m² area (17,400 ft²) area at the release site, for a release of 1-ton/day.

The range of deposition thickness and the distribution pattern varied depending on the location of the sediment release. Based on the six simulation results, higher accumulation to the north of the causeways was locally observed when the release was to the north of the west causeway. On the other hand, there was little accumulation south of the causeways. Similar results were observed for a scenario when the release was south of the east causeway. However, the areal coverage of the deposition was larger for the release at the east causeway than at the west causeway. Without the causeways, the release location made little difference on the resulting sediment deposition. Rather, the pattern was symmetric in longitudinal direction, and the extent to the north and south were similar.

Simulations of sediment transport showed that the suspended sediment was advected by the tidal currents in a form of an elongated plume, like the sediment deposition distribution. The maximum concentration of sediment was found in the near field (0.12 – 0.55 mg/L), with the value decreasing away from the release site. During the flood tide, high sediment concentrations in a range between (0.12 – 0.55 mg/L for a unit load of 1-ton/day) were observed to the north of the release site, similarly to the south during ebb tide. The finest grain (clay) particles could theoretically travel to Spar Island, 5.19 km (3.23 miles) to the north and Sapowet Point, 6.04 km (3.75 miles) to the south, but the concentrations at those locations were very small $O(1 \text{ } \mu\text{g/L})$. The range of more significant concentrations ($> 100 \text{ } \mu\text{g/L}$) are expected to be limited to the area adjacent to the release sites, or less than 640 m ($\sim 2,100$ ft) for the flood and 1.06 km (0.66 miles) for the ebb.

As part of combined sewer overflow facilities plan for City of Fall River in 1990, total suspended solids (TSS) were collected at a total of 8 stations in Mt. Hope Bay (Turner et al., 1990). The observations showed that the TSS concentration from two stations in the lower Mt. Hope Bay, closest to the Sakonnet River Bridge, ranged between 7 and 22 mg/L with an average of 9.75 mg/L and standard deviation of 5.36 mg/L, during dry weather. These values become higher during wet weather. The mean, standard deviation and range for the TSS during wet weather are 14.28 mg/L, 9.99 mg/L, and 0 - 61 mg/L, respectively. If we assume these observations are approximately valid at the

simulation study area and consider them as ambient conditions, the predicted concentrations varying from $O(1 \mu\text{g/L})$ to 0.55 mg/L range from 0.01% to 6% of the dry weather ambient at maximum. Accordingly, the sediment suspended by construction activities in the Sakonnet River Bridge area add a minor contribution to concentrations compared to the ambient.

The sediment suspended concentrations are observed to be, in general, lower without the causeways than with the causeways. The values may be further reduced, depending on the final bathymetry. The water depths with no causeways are defined at the same level as the surroundings, which resulted in a speed decrease of 40%. If dredging is required to open the navigation channel wider, the resultant current speed would be even smaller. The impact to sediment transport by the currents would therefore be less than the results that are presented in this study.

It should be noted that the estimate of transport and deposition is based on a hypothetical, unit load of 1-ton/day. Actual suspended volume is most likely going to be less than this amount. To obtain a corresponding estimate for the actual load, the simulation results can be scaled by a more definitive value of the load. Also, reduction of the load can be assumed if the construction work occurs only in daytime. The impact in far field can also be reduced if cofferdams are built to confine sediments near the construction area.

5. References

- Allen, J. R. L., 1985. Principles of Physical Sedimentology. *George Allen & Unwin*, pp272.
- Haight, F. J., 1936. Currents in Narragansett Bay Buzzards Bay, and Nantucket and Vineyard Sounds. *U.S. Department of Commerce, Coast and Geodetic Survey, Special Publication No. 208*, United States Government Printing Office, Washington. pp. 103.
- Isaji, T., H. M. Rines, C. Galagan, D. L. Mendelsohn, and S. Pratt, 1994. Field Investigations and Hydrodynamic and Sediment Modeling Study for Temporary Route 114 Bridges over the Barrington and Palmer Rivers. *ASA Report #93-097*, pp. 149.
- Muin, M. and M. L. Spaulding, 1996. Two-dimensional boundary fitted circulation model in spherical coordinates. In: *Journal of Hydraulic Engineering*, Vol. 122, No. 9, September 1996, p. 512-521.
- Muin, M. and M. L. Spaulding, 1997. Three-dimensional boundary fitted circulation model. In: *Journal of Hydraulic Engineering*, Vol. 123, No. 1, January 1997, p. 2-12.
- Saxton, K. E., W. J. Rawls, J.S. Romberger, R.I. Papendick, 1986. Estimating Generalized Soil-water Characteristics from Texture. *Soil Sci. Soc. Amer. J.*, 50(4), 1031-1036.
- Spaulding, M. L., and F. M. White, 1990. Circulation Dynamics in Mt. Hope Bay and the Lower Taunton River. *Coastal and Estuarine Studies*, Vol. 38, 494-510.
- Spaulding, M. L., D. Mendelsohn and J. C. Swanson, 1999. WQMAP: An integrated three-dimensional hydrodynamic and water quality model system for estuarine and coastal applications. *Marine Technology Society Journal*, Vol. 33, #3, Fall, 1999. 38-54.
- Turner, C., S. Asselin and S. Feng, 1990. Combined Sewer Overflow Facilities Plan: Receiving Water Impacts Field Measurement Program. *ASA Report #90-20*. pp.390.

APPENDIX A

RESULTS OF SEDIMENT SAMPLE ANALYSIS

SAK RIVER GRAIN SIZE

Sample SR-1

Sample SR-1

Wentworth class	Phi	mm	wt sample grams	cumulative wt grams	wt %	cum wt % coarser
granule	-1.5	3	0.544	0.544	3.35	3.35
granule	-1	2	0.255	0.799	1.57	4.92
vc sand	-0.5	1.41	0.196	0.995	1.21	6.13
vc sand	0	1	0.262	1.257	1.61	7.74
c sand	0.5	0.71	0.376	1.633	2.32	10.06
c sand	1	0.5	0.758	2.391	4.67	14.73
m sand	1.5	0.35	1.412	3.803	8.70	23.42
m sand	2	0.25	1.860	5.663	11.46	34.88
f sand	2.5	0.177	1.946	7.609	11.99	46.87
f sand	3	0.125	1.452	9.061	8.94	55.81
vf sand	3.5	0.088	1.009	10.07	6.21	62.03
vf sand	4	0.0625	0.665	10.735	4.10	66.12
c silt	4.5	0.044	0.550	11.285	3.39	69.51
c silt	5	0.031	0.300	11.585	1.85	71.36
c silt	5.5	0.021	0.300	11.885	1.85	73.21
m silt	6	0.0156	0.550	12.435	3.39	76.59
m silt	6.5	0.011	0.667	13.102	4.11	80.70
f silt	7	0.0078	0.533	13.635	3.29	83.99
f silt	7.5	0.006	0.473	14.108	2.91	86.90
vf silt	8	0.0039	0.427	14.535	2.63	89.53
vf silt	8.5	0.003	0.336	14.871	2.07	91.60
clay	9	0.002	0.364	15.235	2.24	93.84
clay	9.5	0.001	0.253	15.488	1.56	95.40
clay	10	0.0009	0.247	15.735	1.52	96.92
clay	>10	> 0.0009	0.500	16.235	3.08	100.00

Total Wt
SAMPLE

16.235

Wt GRAVEL % GRAV
0.544 3.35%

Wt SAND % SAND
10.191 62.77%

Wt SILT &
CLAY % SILT &
CLAY
5.500 33.88%

SAK RIVER GRAIN SIZE

Sample SR-2

Wentworth class	Phi	mm	wt sample grams	cumulative wt grams	wt %	cum wt % coarser
granule	-1.5	3	0.164	0.164	1.23	1.23
granule	-1	2	0.301	0.465	2.26	3.49
vc sand	-0.5	1.41	0.353	0.818	2.65	6.14
vc sand	0	1	0.277	1.095	2.08	8.23
c sand	0.5	0.71	0.246	1.341	1.85	10.07
c sand	1	0.5	0.253	1.594	1.90	11.97
m sand	1.5	0.35	0.289	1.883	2.17	14.14
m sand	2	0.25	0.456	2.339	3.43	17.57
f sand	2.5	0.177	1.008	3.347	7.57	25.14
f sand	3	0.125	1.100	4.447	8.26	33.40
vf sand	3.5	0.088	0.875	5.322	6.57	39.98
vf sand	4	0.0625	0.641	5.963	4.81	44.79
c silt	4.5	0.044	0.300	6.263	2.25	47.04
c silt	5	0.031	0.050	6.313	0.38	47.42
c silt	5.5	0.021	1.100	7.413	8.26	55.68
m silt	6	0.0156	1.550	8.963	11.64	67.33
m silt	6.5	0.011	0.596	9.559	4.47	71.80
f silt	7	0.0078	0.654	10.213	4.91	76.71
f silt	7.5	0.006	0.371	10.584	2.79	79.50
vf silt	8	0.0039	0.579	11.163	4.35	83.85
vf silt	8.5	0.003	0.299	11.462	2.25	86.10
clay	9	0.002	0.451	11.913	3.38	89.48
clay	9.5	0.001	0.215	12.128	1.62	91.10
clay	10	0.0009	0.485	12.613	3.64	94.74
clay	>10	> 0.0009	0.700	13.313	5.26	100.00

Sample SR-2

Total Wt
SAMPLE

13.313

Wt GRAVEL **% GRAV**
0.164 **1.23%**

Wt SAND **% SAND**
5.799 **43.56%**

Wt SILT & CLAY **% SILT & CLAY**
7.350 **55.21%**

SAK RIVER GRAIN SIZE

Sample SR-3

Wentworth class	Phi	mm	wt sample grams	cumulative wt grams	wt %	cum wt % coarser
granule	-2	4	0.97	0.97	1.78	1.78
granule	-1.5	3	0.520	1.49	0.95	2.73
granule	-1	2	0.500	1.99	0.92	3.65
vc sand	-0.5	1.41	0.480	2.47	0.88	4.53
vc sand	0	1	0.500	2.97	0.92	5.44
c sand	0.5	0.71	0.780	3.75	1.43	6.87
c sand	1	0.5	1.200	4.950	2.20	9.07
m sand	1.5	0.35	3.260	8.21	5.98	15.05
m sand	2	0.25	6.120	14.33	11.22	26.26
f sand	2.5	0.177	6.840	21.17	12.54	38.80
f sand	3	0.125	7.780	28.95	14.26	53.06
vf sand	3.5	0.088	4.920	33.87	9.02	62.08
vf sand	4	0.0625	3.340	37.21	6.12	68.20
c silt	4.5	0.044	2.150	39.36	3.94	72.14
c silt	5	0.031	7.850	47.21	14.39	86.53
c silt	5.5	0.021	1.850	49.06	3.39	89.92
m silt	6	0.0156	2.000	51.06	3.67	93.59
m silt	6.5	0.011	0.728	51.788	1.33	94.92
f silt	7	0.0078	0.622	52.410	1.14	96.06
f silt	7.5	0.006	0.022	52.432	0.04	96.10
vf silt	8	0.0039	0.178	52.610	0.33	96.43
vf silt	8.5	0.003	0.095	52.705	0.17	96.60
clay	9	0.002	0.205	52.910	0.38	96.98
clay	9.5	0.001	0.013	52.923	0.02	97.00
clay	10	0.0009	0.037	52.960	0.07	97.07
clay	>10	> 0.0009	1.600	54.560	2.93	100.00

Sample SR-3

Total Wt
SAMPLE

54.56

Wt GRAVEL	% GRAV
0.520	0.95%

Wt SAND	% SAND
35.720	65.47%

Wt SILT & CLAY	% SILT & CLAY
17.350	31.80%

SAK RIVER GRAIN SIZE

Sample SR-4

Wentworth class	Phi	mm	wt sample +beaker	wt beaker	wt sample	wt %	wt % coarser
pebble	-3	8					
pebble	-2.5	5.7					
pebble	-2	4	36.63	27.82	8.81	14.54	14.54
pebble	-1.5	2.85	28.97	28.02	1.15	1.90	16.44
granule	-1	2	26.78	26.31	0.47	0.78	17.21
vc sand	-0.5	1.42	28.12	27.58	0.54	0.89	18.10
vc sand	0	1	26.87	26.32	0.55	0.91	19.01
c sand	0.5	.71	27.56	26.86	0.70	1.16	20.17
c sand	1	.5	29.02	27.29	1.73	2.85	23.02
m sand	1.5	.35	30.52	26.36	4.16	6.86	29.88
m sand	2	.25	31.67	26.99	4.68	7.72	37.61
f sand	2.5	.177	30.93	25.51	5.42	8.94	46.55
f sand	3	.125	37.50	26.27	11.23	18.53	65.08
vf sand	3.5	.089	36.03	28.10	7.93	13.09	78.17
vf sand	4	.0625	33.59	27.19	6.40	10.56	88.73
<4	<0.625		33.73	26.90	6.83	11.27	100.00

Sample SR-4

Total Wt
SAMPLE

60.60

Wt GRAVEL

10.43

% GRAV

17.21%

Wt SAND

43.34

% SAND

71.52%

Wt SILT &
CLAY

6.83

**% SILT &
CLAY**

11.27%

SAK River Grain Size

Sample SR-5

Wentworth class	Phi	mm	wt sample grams	cumulative wt grams	wt %	cum wt % coarser
granule	-2	4				
granule	-1.5	3				
granule	-1	2	0.122	0.122	0.93	0.93
vc sand	-0.5	1.41	0.263	0.385	2.00	2.92
vc sand	0	1	0.394	0.779	2.99	5.92
c sand	0.5	0.71	0.468	1.247	3.55	9.47
c sand	1	0.5	0.620	1.867	4.71	14.18
m sand	1.5	0.35	0.572	2.439	4.34	18.53
m sand	2	0.25	0.480	2.919	3.65	22.17
f sand	2.5	0.177	0.484	3.403	3.68	25.85
f sand	3	0.125	0.887	4.290	6.74	32.59
vf sand	3.5	0.088	0.730	5.020	5.55	38.13
vf sand	4	0.0625	0.545	5.565	4.14	42.27
c silt	4.5	0.044	0.250	5.815	1.90	44.17
c silt	5	0.031	0.250	6.065	1.90	46.07
c silt	5.5	0.021	1.000	7.065	7.60	53.67
m silt	6	0.0156	0.550	7.615	4.18	57.84
m silt	6.5	0.011	0.969	8.584	7.36	65.20
f silt	7	0.0078	1.381	9.965	10.49	75.69
f silt	7.5	0.006	0.435	10.400	3.31	79.00
vf silt	8	0.0039	0.465	10.865	3.53	82.53
vf silt	8.5	0.003	0.273	11.138	2.07	84.60
clay	9	0.002	0.277	11.415	2.11	86.71
clay	9.5	0.001	0.170	11.585	1.29	88.00
clay	10	0.0009	0.180	11.765	1.37	89.37
clay	>10	> 0.0009	1.400	13.165	10.63	100.00

Sample SR-5

Total Wt
SAMPLE

13.165

Wt GRAVEL % GRAV

0.122 **0.93%**

Wt SAND % SAND

5.443 **41.34%**

Wt SILT &
CLAY % SILT &
CLAY

7.600 **57.73%**

SAK RIVER GRAIN SIZE

Sample SR-6

Wentworth class	Phi	mm	wt sample grams	cumulative wt grams	wt %	cum wt % coarser
granule	-1.5	3	4.000	4	8.19	8.19
granule	-1	2	1.650	5.65	3.38	11.57
vc sand	-0.5	1.41	2.540	8.19	5.20	16.77
vc sand	0	1	2.880	11.07	5.90	22.66
c sand	0.5	0.71	3.390	14.46	6.94	29.60
c sand	1	0.5	4.710	19.170	9.64	39.24
m sand	1.5	0.35	5.460	24.63	11.18	50.42
m sand	2	0.25	4.560	29.19	9.33	59.75
f sand	2.5	0.177	4.080	33.27	8.35	68.11
f sand	3	0.125	4.330	37.6	8.86	76.97
vf sand	3.5	0.088	2.010	39.61	4.11	81.08
vf sand	4	0.0625	1.340	40.95	2.74	83.83
c silt	4.5	0.044	0.900	41.85	1.84	85.67
c silt	5	0.031	0.150	42	0.31	85.98
c silt	5.5	0.021	0.800	42.8	1.64	87.62
m silt	6	0.0156	1.700	44.5	3.48	91.10
m silt	6.5	0.011	0.784	45.284	1.60	92.70
f silt	7	0.0078	1.266	46.550	2.59	95.29
f silt	7.5	0.006	0.102	46.652	0.21	95.50
vf silt	8	0.0039	1.098	47.750	2.25	97.75
vf silt	8.5	0.003	0.221	47.971	0.45	98.20
clay	9	0.002	0.279	48.250	0.57	98.77
clay	9.5	0.001	0.400	48.650	0.82	99.59
clay	10	0.0009	0.150	48.800	0.31	99.90
clay	>10	> 0.0009	0.050	48.850	0.10	100.00

Sample SR-6

Total Wt
SAMPLE

48.850

<u>Wt GRAVEL</u>	% GRAV
4.000	8.19%

<u>Wt SAND</u>	% SAND
36.950	75.64%

<u>Wt SILT & CLAY</u>	% SILT & CLAY
7.900	16.17%

SAK RIVER GRAIN SIZE

Sample SR-7

Wentworth class	Phi	mm	wt sample +beaker	wt beaker	wt sample	wt %	wt % coarser
pebble	-3	8					
pebble	-2.5	5.7					
pebble	-2	4					
pebble	-1.5	2.85	32.01	27.10	4.91	8.28	8.28
granule	-1	2	27.10	25.08	2.02	3.40	11.68
vc sand	-0.5	1.42	28.61	26.12	2.49	4.20	15.88
vc sand	0	1	31.06	27.94	3.12	5.26	21.14
c sand	0.5	.71	32.02	28.20	3.82	6.44	27.57
c sand	1	.5	32.74	27.34	5.40	9.10	36.68
m sand	1.5	.35	34.74	27.37	7.37	12.42	49.10
m sand	2	.25	34.92	27.23	7.69	12.96	62.06
f sand	2.5	.177	33.30	26.36	6.94	11.70	73.76
f sand	3	.125	33.87	27.25	6.62	11.16	84.91
vf sand	3.5	.089	30.02	27.19	2.83	4.77	89.68
vf sand	4	.0625	30.36	28.05	2.31	3.89	93.58
vf sand	<4	<0.625	31.74	27.93	3.81	6.42	100.00

Sample SR-7

Total Wt SAMPLE	
59.33	
<u>Wt GRAVEL</u>	% GRAV
6.93	11.68%
<u>Wt SAND</u>	% SAND
48.59	81.90%
<u>Wt SILT & CLAY</u>	% SILT & CLAY
3.81	6.42%

SAK RIVER GRAIN SIZE

Sample SR-8

Wentworth class	Phi	mm	wt sample +beaker	wt beaker	wt sample	wt %	wt % coarser
pebble	-3	8					
pebble	-2.5	5.7					
pebble	-2	4					
pebble	-1.5	2.85	31.34	26.96	4.38	8.22	8.22
granule	-1	2	29.76	26.90	2.86	5.36	13.58
vc sand	-0.5	1.42	31.28	27.32	3.96	7.43	21.01
vc sand	0	1	32.00	26.94	5.06	9.49	30.50
c sand	0.5	.71	32.52	27.69	4.83	9.06	39.56
c sand	1	.5	32.85	27.11	5.74	10.77	50.33
m sand	1.5	.35	35.23	27.37	7.86	14.74	65.07
m sand	2	.25	35.95	26.78	9.17	17.20	82.27
f sand	2.5	.177	32.12	27.18	4.94	9.27	91.54
f sand	3	.125	28.71	26.76	1.95	3.66	95.20
vf sand	3.5	.089	28.02	27.22	0.80	1.50	96.70
vf sand	4	.0625	26.65	25.97	0.68	1.28	97.97
vf sand	<4	<0.625	28.53	27.45	1.08	2.03	100.00

Sample SR-8

Total Wt
SAMPLE

53.31

Wt GRAVEL

7.24

% GRAV

13.58%

Wt SAND

44.99

% SAND

84.39%

Wt SILT &
CLAY

1.08

**% SILT &
CLAY**

2.03%